

FINAL REPORT

**Daily Dynamics of Grand Canyon Sandbars;
Monitoring With Terrestrial Photogrammetry**

Brian L. Cluer - Co Principal Investigator
Leland R. Dexter - Co Principal Investigator

With assistance from:

Mark F. Manone - Research Assistant
Robert M. Weber - Research Assistant
Glenn Dunno - Research Assistant
Randy Botts - Reserach Assistant
Merriane Etter - Research Assistant
Michael Applegarth - Student Assistant

Department of Geography
Northern Arizona University
Box 15016
Flagstaff, Arizona 86011

August 12, 1994

**GCES OFFICE COPY
DO NOT REMOVE!**

Sponsored by the
U. S. Department of the Interior
National Park Service
Cooperative Agreement # CA 8000-8-0002

Peter G. Rowlands, Technical Representative

Table of Contents

Abstract.....	iii
Introduction.....	1
Background.....	1
Hypothesis.....	5
Objectives.....	6
Methods.....	6
Site Description and Selection.....	6
Field Procedures.....	13
Image Processing.....	14
Results.....	18
Methodological Results.....	18
Environmental Results.....	25
Discussion and Conclusions.....	124
Magnitude of Erosional Events.....	124
Frequency Distribution of Sandbar Areas.....	124
Temporal Trends of Erosion.....	126
Spatial and Geomorphic Trends.....	136
Spatial and Temporal Relationships.....	137
Cumulative Effects.....	138
Processes of Adjustment.....	138
Success of the Interim Flows.....	145
Summary: Uniformitarianism or Catastrophism?.....	147
Recommendations.....	148
Value of the Technique.....	148
Management of the Sediment Resource.....	151
Monitoring Time Scales.....	152
Acknowledgments.....	153
References.....	154
Appendices.....	157

Abstract

This report presents a new technique developed to monitor fluvial sandbars along the highly regulated Colorado River in Grand Canyon National Park. Oblique photographs were taken daily, automatically, from 43 fixed position programmable cameras. Digital image processing techniques resulted in planimetric analyses of 20 sandbars for a period beginning in February 1991 through December 1993. The image processing technique can achieve spatial accuracy to within 1%. River stage variations decreased application accuracy depending on local site and camera-view geometry. The strength of the technique lies in daily sandbar area evaluation capability.

Spatial as well as temporal processes were observed at sites located within individual riffle-pool geomorphic units. Within the riffle-pool unit, multiple sequences of separation bar erosion, eddy bar deposition, and wholesale eddy bar erosion over 2-4 day periods occurred. Over 70% of the erosional events occurred during or within two days following a weekend low discharge period, suggesting that the weekend dam operation induces the driving forces. This is important because significant volumes of sand were found to cycle between storage and downstream transport during erosional events.

Sandbar area frequency was strongly bimodal with negative kurtosis, indicating that measurements taken at long time steps are not likely to document mean area but rather minima or maxima. Seasonality was also observed in area-frequency distribution related to seasonal adjustments in dam discharge patterns. This suggests that results from previous investigations require some new interpretation.

A conceptual model describes cyclic deposition and erosion. The driving processes are not clear but the temporal and spatial relations indicate feedback mechanisms operate between channel processes and channel margin storage processes. Recommendations include monitoring sandbars as daily frequency, reinterpreting results from previous investigations, and eliminating weekend discharge patterns.

Key words: sandbar, fluvial erosion, image analysis, Colorado River, Grand Canyon National Park, Glen Canyon Dam.

Introduction

Background

The construction and operation of Glen Canyon Dam has profoundly influenced the downstream riparian environment throughout Grand Canyon National Park (Dolan, Howard, and Gallenson 1974; Andrews 1991; Dawdy 1991; Johnson 1991). Until recently, water resource management policies in the west were not evaluated in terms of their impact on the downstream environment (Ingram et al. 1991). Since 1982, assessment of the types and magnitudes of changes downstream of Glen Canyon Dam has been coordinated by the U. S. Bureau of Reclamation's Glen Canyon Environmental Studies office (GCES).

Although the Colorado River flows in a bedrock gorge, the fluvial sediment resources of the system have been a major emphasis of the GCES investigations. The fluvial sediments serve as substrate for vegetation (Johnson, 1991), as water stilling structures and water warming structures for aquatic fauna (Valdez and Williams, 1993), and as camping sites for river runners (Dolan, Howard, and Gallenson, 1974). Not only is the morphology of sediment deposits important, but the amount of sediment in storage, delivery from tributaries, the dynamics of sediment transport and the sediment balance are all important components of the overall river ecosystem and its management. Indeed the Colorado River fluvial sediment resource is the first management priority of Grand Canyon National Park (River Management Plan, Grand Canyon National Park, 1994).

The fluvial sediment resources can be described by a simple categorization of three basic particle classes, made by Howard and Dolan (1981), that clarifies the importance of fluvial sediments in this bedrock gorge. Classification is based on probable time-scales of mobility. In this scheme, the largest category includes bedrock and large boulders which are considered mobile only during extreme floods or over geologic time-scales of tens or hundreds of thousands of years.

The intermediate category includes gravel and cobbles that are mobilized during floods that recurred frequently prior to dam construction but only rarely since then (i.e. the 1983 emergency releases that exceeded 90,000 cfs). The finest particle size category is sand. This particle size has been the focus of three decades of one-time studies as well as continuous and semi-continuous monitoring programs. Sand receives most attention because it is mobile, or potentially mobile, under all flow conditions. Sand responds to, and records, cause and effect relationships resulting from dam operations. Although the sand transport capacity of the Colorado River has been reduced mostly because of flood water storage behind Glen Canyon Dam, the supply of sand is also stored behind the dam. The post-dam supply of sand is limited to that in storage (which is poorly known) and by introduction from ephemeral tributaries. It has been calculated that the balance between sand supply and transport can be positive or negative depending on operation of the dam (Smillie, Jackson, and Tucker, 1993).

Many terms have been used to describe the sand deposits along the banks of the Colorado River. In this report, the fluvial sand deposits, regardless of geomorphic position or genesis, are referred to simply as sandbars in order to reduce confusion induced by terminology. Sand is deposited in zones of low velocity that are created by perturbations to the velocity profile, providing that a supply of sand is available. In the Grand Canyon, low velocity zones generally occur where the channel is constricted by rock outcrops or debris deposits. Constrictions of the channel cause local acceleration of flow velocity resulting in supercritical or shooting flow (of the rapids). The accelerated flow separates from the bank at the apex of the channel constriction and leaves a low velocity, recirculating eddy zone downstream and a bounding shear zone between the shooting flow and the eddy zone called the eddy fence (Kieffer, 1985). As the shooting flow of the rapid decelerates, flow reattaches to the bank at some point downstream (Kieffer, 1985).

Sandbars are persistent features over long time-scales (Webb, in press) and occur in predictable locations based on the interaction between river hydraulics and the less mobile controlling features such as bedrock or boulders (Schmidt, 1990).

The usual resulting sandbars are shown under low-stage conditions in Figure 1. Sandbars typically are found along the upstream face of channel constrictions (upper pool bars), along the downstream face of channel constrictions (separation bars), in the quiet water of the eddy center (eddy bars), and at the stagnation zone of the flow attachment (reattachment bars). Zones of low velocity are most commonly associated with debris deposits that form where tributaries and minor side channels introduce large quantities of particles of sizes not readily mobilized by the normal range of discharges. Uncommon depositional environments include point bars on the inside of meanders and thin channel margin sandbars between outcrops of bedrock or large boulders.

The Colorado River in Grand Canyon is entirely regulated by Glen Canyon Dam. The most notable difference in flow regime resulting from regulation is the change from an annual flow cycle (100,000 cfs - 2,000 cfs) dominated by a snowmelt flood occurring usually between late May and early June to a diurnal flow cycle (30,000 cfs - 8,000 cfs) optimized for electrical power generation based on peak electricity demand in the region. Discharges in excess of powerplant capacity (approximately 31,000 cfs) occur only during rare facilities tests or emergency conditions.

The mechanisms by which sandbars can change form and size are of interest to scientists as well as resource managers and planners especially because the flow regime of the post-dam Colorado River in Grand Canyon is so much different than in pre-dam times. Three major mechanisms seem to be active in the reworking of sandbars (Budhu, 1992):

1. seepage induced failure during low flow;
2. wave induced erosion from surface turbulence, wind, and boats; and
3. drag forces from bottom turbulence and downstream flow.

Initial effort of GCES Phase II research was directed at obtaining baseline volumetric estimates and short term volumetric changes of sandbars within Grand Canyon in response to a series of very specific controlled flow regimes (test flow program).

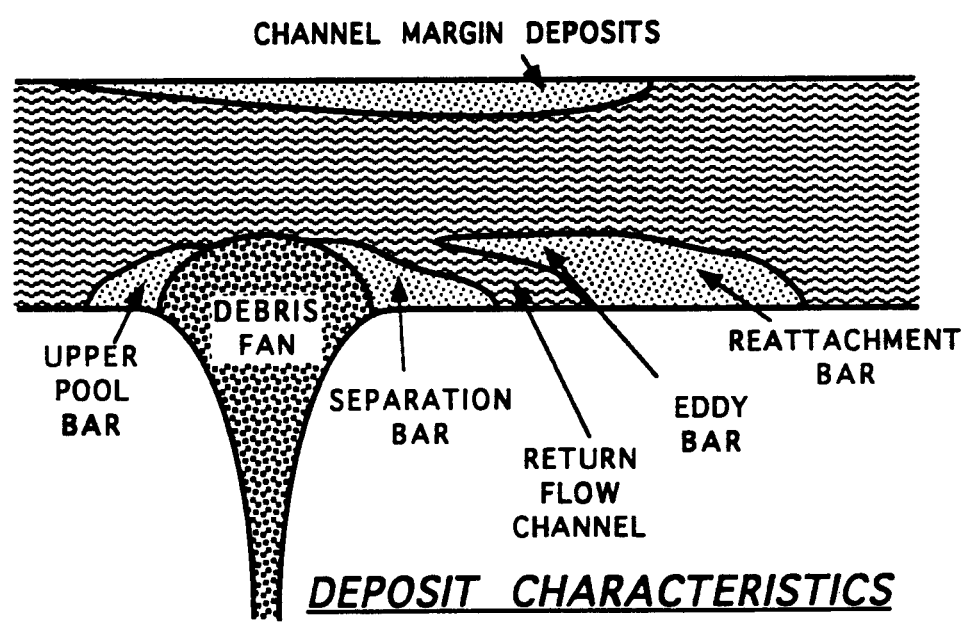
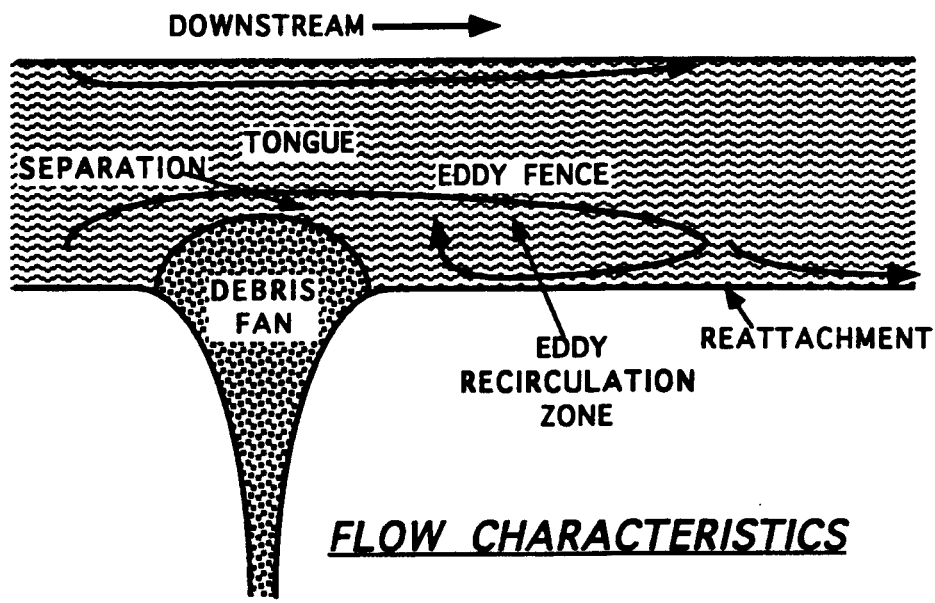


Fig. 1. The top panel illustrates the major hydraulic components of a Grand Canyon rapid and the bottom panel illustrates the resulting alluvial deposits shown at low water.

One early method involved inserting thin wire cables of known length vertically into sandbars at node points of precisely surveyed grids. In theory, the wires could be re-measured quickly on subsequent trips and supply data necessary for volumetric change estimates. Quite often, however, subsequent survey trips would find that sandbars had changed so much in just two weeks that large portions of the wire grids could not be found. This technique was replaced out of necessity by a much more labor intensive approach using total station plane surveying at biweekly intervals.

From these field observations, we felt that some form of short time interval sampling method of sandbar morphology was needed. Two traditional techniques that were technically possible and available were land surveying and aerial photography. Both techniques were considered to be excessively expensive and intrusive for the desired time step, thus were ruled out. An alternative method was developed to meet the technical criteria within the fiscal limitations.

Hypothesis

Volumetric survey data indicated that major changes in sandbar morphology occurred between surveys. General field observations of sandbars made while floating the Colorado River included occasionally seeing sandbar face calving, and the aftermath-vertical sandbar faces. These factors prompted the development of the hypothesis that some types of sandbar changes are neither uniform, nor consistent from sandbar to sandbar. The time between significant changes in sandbar morphology and volume was speculative. To test the hypothesis and determine timing, the following project objectives were set.

Objectives

The objectives of this project were to:

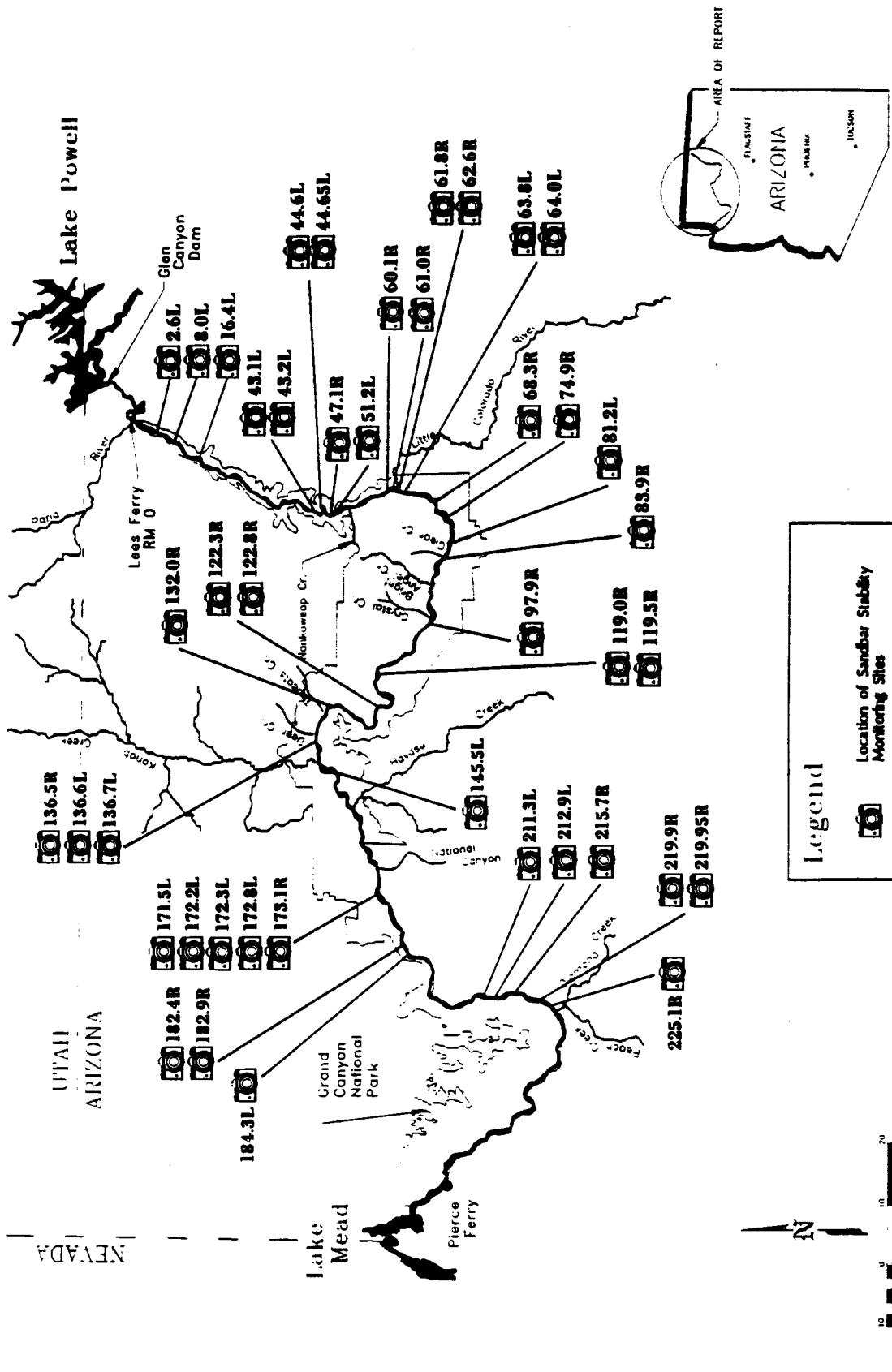
1. obtain daily photographs of 43 sandbars along the Colorado River between Lee's Ferry and Diamond Creek over a year or longer,
2. digitize selected photographs for analytical purposes,
3. rectify these images from oblique to planimetric views, and to develop procedures to assess the accuracy involved,
4. develop animated visualization to help assess short time step changes in sandbar morphology over the sampling period,
5. and use the results of the previous objectives to analyze the temporal and spatial characteristics of short term change in sandbar size and morphology, thus addressing the contract requirements to:
 - a. "determine if fluvial deposits have been stabilized by the interim flow prescription, and
 - b. compare fluvial deposit physical stability characteristics during the interim flow period to deposit dynamics observed during the test flow and pre-test flow periods."

Methods

Site Description and Selection

Forty three sandbars were selected for daily monitoring using oblique photography (Figure 2). From the forty three, a subset of twenty sandbars was selected for further image analysis using the techniques described below.

Location of Sandbar Stability Monitoring Sites



Legend

-  Location of Sandbar Stability Monitoring Sites
-  Colorado river mile 219.95 right

Scale of Miles

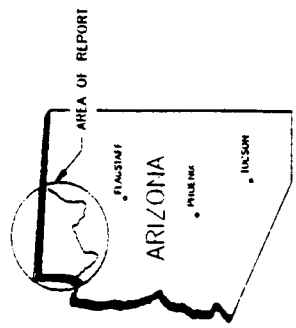
0 10 20

Scale of Kilometers

0 10 20

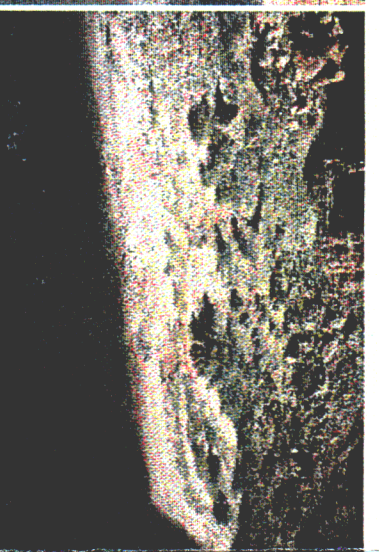
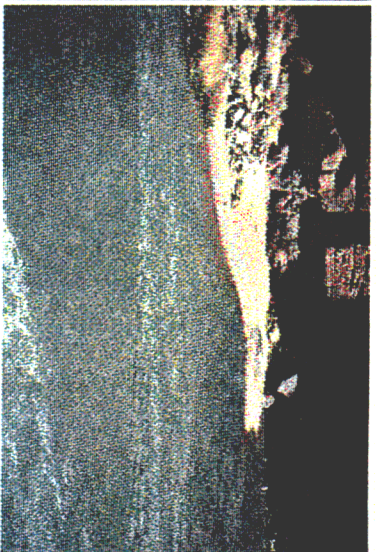
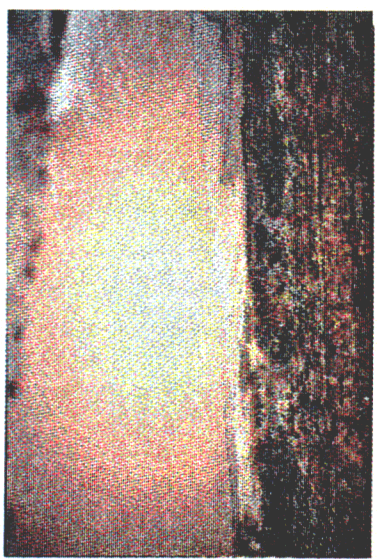
North Arrow

N



GLEN CANYON ENVIRONMENTAL STUDIES
 FLAGSTAFF, ARIZONA
 October, 1993

Fig. 2. Sandbar photography site index map.



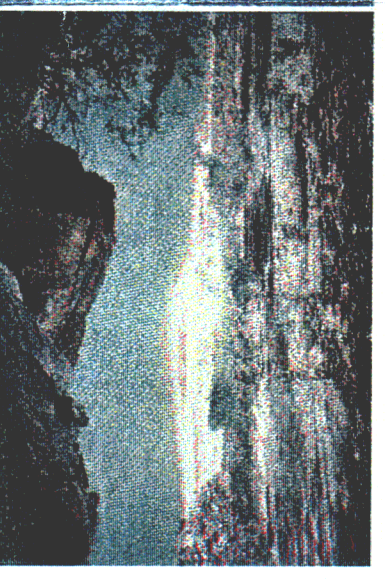
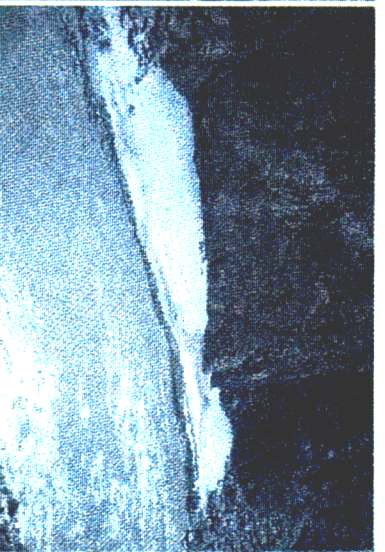
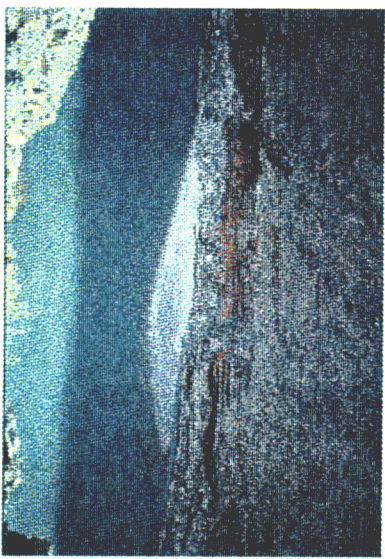
2.6 L

16.4 L

43.1 L

44.6 L

44.65 L



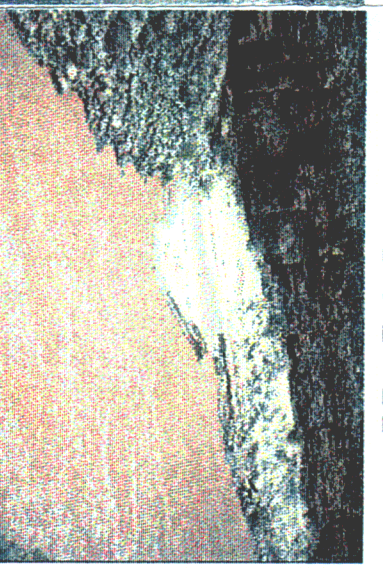
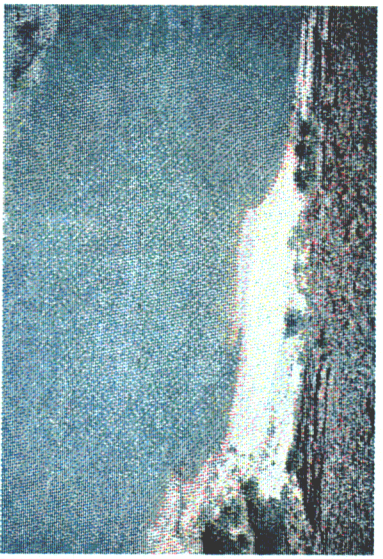
60.1 R

61.8 R

64.0 L

81.2 L

119.0 R



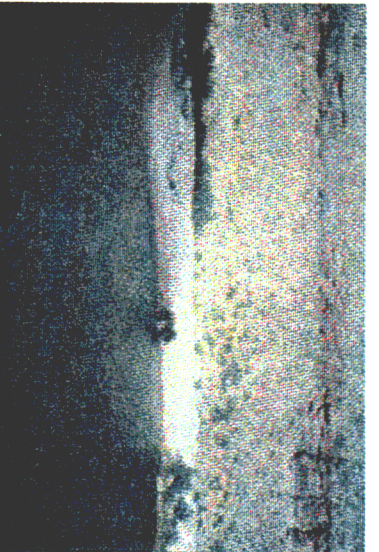
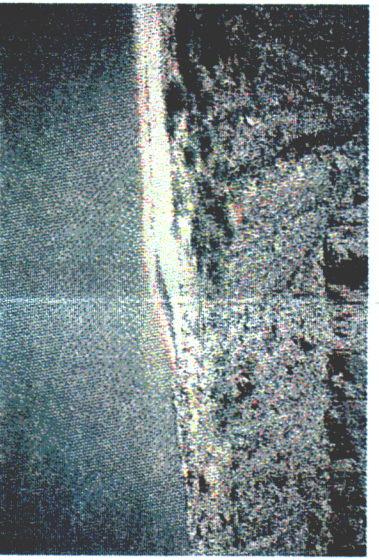
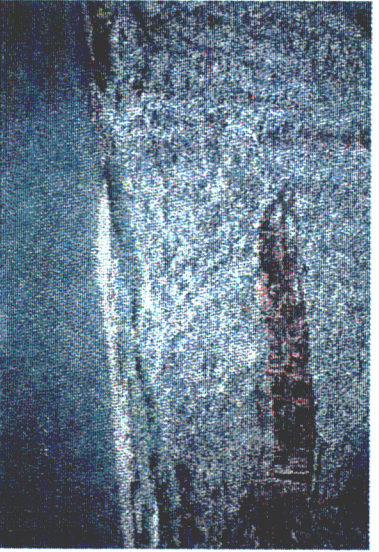
122.3 R

122.7 L

136.6 L

136.7 L

145.5 L



172.2 L

172.3 L

173.1 R

211.3 L

212.9 L

Figure 3 shows camera site views of each of the twenty sandbars that received planimetric rectification and quantitative area analysis. Descriptions of each site follow.

2.6L, Cathedral Wash Camp. This sandbar is formed downstream of several large blocky rocks and a mass of talus material. Hydraulic control is provided by a debris fan constriction approximately 0.1 mile downstream at Cathedral Wash. The sandbar studied is a reattachment bar with a bare sand eddy bar at the upstream end. The site was first measured in 1985 by Schmidt and Graf (1990) and subsequently monitored during the test flow period by Beus and Avery (1992). Daily photography began in March 1992. This site was selected for its proximity to the critical sediment delivery tributary, the Paria River, approximately 2.5 miles upstream.

16.4L, Hot Na Na. The sandbar consists of an eddy bar with high elevation separation deposits from prior high discharges. The river is characterized in this reach by narrow width constricted by the vertical walls of Marble Canyon. USGS benchmarks predate the first published measurements made on this sandbar by Beus and others in 1992. Daily photography began in March 1992. Hydraulic controls exist at the constriction which forms the deposit and 0.5 mile downstream at the Rider Canyon debris fan and House Rock Rapid. The site was selected to represent the narrow Marble Canyon reach and because of its proximity to the Paria River sediment supply.

43.1L, Anasazi Bridge. This is a large sandbar in an upper pool environment upstream of a debris fan channel constriction that provides hydraulic control. Its name is derived from the remains of a log structure that crosses a chimney along a South Rim/North Rim route presumed to be a foot bridge used by the Anasazi. The first published measurements are from Beus and Avery (1992) although USGS benchmarks predate this work. Photography began in November 1990 as one of seven original daily photography sites.

44.6L and 44.65L, Eminence Break. The separation sandbar is at the foot of the Eminence Break trail, just downstream of President Harding rapid. It was first surveyed in 1985 by Schmidt and Graf (1990).

Daily photography began in March 1992 at this sandbar and, simultaneously, at the reattachment sandbar immediately downstream within the riffle-pool unit. Surface waves continually rework the upstream half of the separation bar at all flow levels. The reattachment and eddy bars are the largest sampled due to its position on the outside of the meander bend called Point Hansbrough. The site was selected for its size and for coverage of the dual deposits within the riffle-pool unit.

60.1R. This sandbar is unlike most other monitoring sites in this or other studies and had not been measured prior to initiation of daily photography in March 1992. It is a low elevation eddy bar downstream of 60 Mile Rapid that is rarely visible at most discharges and, consequently, is not used for recreation. It is included in this project to monitor changes in sediment storage where the effects of higher elevation sand storage are not a factor. Typically, high elevation sand deposits result from prior high discharges and may supply sediment from above the zone of interim flow fluctuations. At this site, nearly vertical bedrock outcrops prevented deposition of sand at elevations exceeding the current maximum river stage. Hydraulic control is provided by the debris fan constriction of 60 Mile Rapid immediately upstream and downstream by gravel deposits of the LCR confluence.

61.8R. This is the first sandbar down stream of the LCR confluence and was first surveyed by Howard (1975). Daily photographic records began in March 1992. The field of view includes the separation and eddy bars formed by a debris cone on river right. The debris channel constriction forms a recirculation zone that is vertically confined by bedrock. The site was selected for its proximity to the LCR which provides ephemeral sediment laden discharges. At high discharge rates, the eddy covers about half of the downstream end of the sandbar. Surface waves continually rework the upstream part of the separation sandbar at all flow levels.

64.0L, Hopi Salt Mines. This reattachment bar is adjacent to the sacred Hopi Salt Mines. Since this site is closed for camping, it could be useful in the future as a control for camping impact assessment and monitoring.

Hydraulic controls are provided by an elongated debris constriction along the upstream left bank, and downstream by a debris fan constriction that forms a riffle. This site is included for its proximity to the LCR and, because of the desire to monitor a series of sites in spatial proximity. Daily photography began on March 1992.

81.2L, Grapevine. The Grapevine Camp is important because of its location in the Inner Gorge where few sandbars exist and campsites are widely spaced. It is a bare sandbar that is the result of flow deflection from the left bank by large rocks. The large rocks occurring at both the upstream and downstream ends of the sandbar create a low velocity zone along the left bank where the sandbar is formed. A long history of studies have included 81.2L beginning with Howard (1975). Daily photography began in June 1991. This site was selected to represent sandbars in the inner gorge reach and the somewhat unique hydraulic controls of channel margin deposits.

136.6L. This sandbar is located downstream of Deer Creek under an overhang known by river runners as Poncho's Kitchen. It is a channel margin sandbar, formed in a low velocity zone between rocks and bedrock at the upstream end and a debris fan at the downstream end. This site was first studied by Beus et al. (1991) beginning in 1990. Daily photographic records began in March 1992. The site was selected to represent the channel margin deposit type and to document spatial variability in conjunction with 136.7L.

136.7L. This sandbar is immediately downstream of 136.6L and is in the same riffle-pool unit. The deposit type is reattachment with a large eddy bar visible at low stages. The study history is the same as 136.6L with photography also beginning in March 1992. Hydraulic controls for both sandbars are at the upstream riffle and downstream pool. Both sandbars have extensive deposits at elevations several meters higher than stages from normal dam operations.

145.5L, above Olo Canyon. This sandbar is a narrow reattachment bar in a narrow reach downstream of Kanab Creek and upstream of Olo Canyon. It has the highest vertical relief of any sandbar in this study, probably due to a combination of flood discharges and aeolian processes.

The first measurements were made in 1990 by Beus and Avery (1992) and photography began in March 1992. The site was selected to represent the narrow Tapeats Sandstone reach and also because of its location downstream of a major ephemeral tributary, Kanab Creek.

172.2L, below Mohawk Canyon. A locally derived talus cone forms a channel constriction at this site. This sandbar is the separation bar that accompanies the large reattachment sandbar 172.3L. The separation sandbar was first studied beginning in March 1992 with daily photography.

172.3L. This reattachment and eddy bar completes the riffle-pool unit formed by channel constriction upstream at 172.2L. Hydraulic controls are provided by the upstream channel constriction and riffle, and downstream by a broad shallow riffle and minor channel constricting debris fan. The first study of this site was in 1990 by Beus and Avery (1992). It is one of the seven original time-lapse study sites, with daily photographic records beginning in February 1991. These sandbars were selected primarily to satisfy equal distance concerns between sites and to provide information for contemporary studies into bank-stored ground water (Carpenter, Carruth, and Cluer, 1991). The 172.2L camera was installed to provide coverage of the separation bar not visible by the 172.3L camera.

173.1R. This small sandbar was selected to provide information about the spatial and temporal migration of rapid erosion events known to occur upstream at 172.3L. It consists of a low elevation eddy deposit and remnant high elevation reattachment and eddy deposits. Hydraulic controls are provided upstream by the riffle that provides downstream control for 172.3L, and downstream by a channel constriction and riffle. Daily photography began in March 1992. The site was not measured previously.

211.3L. This is one of the seven original daily photography sites with the installation of the camera in December 1990. It consists of a large flat eddy bar and high elevation reattachment bar formed downstream of a debris fan. Hydraulic controls are provided upstream by the debris fan channel constriction and downstream by a wide riffle.

The sandbar was selected for its high elevation steep reattachment deposit that appeared to be actively slumping into the river and because recreational use was rare.

212.9L, Pumpkin Spring. This sandbar is adjacent to the travertine spring called Pumpkin Spring, in a zone of strong recirculating current between bedrock channel constrictions upstream and downstream. Recirculating current is unusually strong at this site, evident by the general arcuate shape of the sandbar. The original survey on this site was conducted in 1985 by Schmidt and Graf (1990). Daily photography began in March 1992. The site was selected because of its long history of investigations and for its unique hydraulic controls.

Field Procedures

A land-based time-lapse camera system was built from relatively inexpensive off-the-shelf products. The core of the system was the Pentax IQZ 105[®] programmable camera. The microprocessor controlled camera allowed the built-in timer to be set for repeat exposures once every 24 h at a pre-set time of day. Each camera was secured to an alignment base which was fastened snugly inside of a military ammunition can. A large, round hole was cut into the side of the box congruent with the position of the camera lens and fitted with glass. A small metal gable was fashioned to protect the glass from the elements. The boxes were painted in earth tones to make them inconspicuous.

At each sandbar site, a camera was located a sufficient distance away to photograph the entire subject and avoid interference by or with park visitors. Usually cameras were located across, and elevated above the river to provide an oblique view. Camera boxes were attached with silicon sealant to large boulders or to bedrock outcrops. Timers were set to expose the film daily at pre-determined times selected to take advantage of local low river stage and to avoid local shading. Each camera was loaded with 36 exposure, ASA 64, color slide film, attached to the base, and sealed in the box along with a packet of desiccant.

Forty three sandbars were included in the sample with each of the five major geomorphic reaches (Schmidt and Graf, 1988) well represented (Figure 2). Single cameras were used except at site 172.3L where two cameras were used to test oblique stereographic coverage.

Photo control techniques were developed to make the transition from semi-quantitative assessment used in the pilot study (Cluer, 1991) to a rigorous quantitative measurement program. While the cameras were being sited, aerial photography control panels were temporarily fixed at points around the field of view. A surveying crew then located the position coordinates of the panels and the camera lens/film plane using total station plane surveying techniques. Once the camera had photographed the area with the control panels in place, the panels were removed. Subsequently, the film was recovered approximately monthly. Virtually no mechanical failures occurred with the cameras during three years of service. However, a variety of operational errors occurred that occasionally reduced the image quality or resulted in gaps in the photographic records.

Image Processing

Film was processed conventionally and left in strips to facilitate scanning. A high resolution Nikon LS-3510AF[®] film scanner was used to convert the analog image to digital form. The digital Tagged Image Format File (TIFF) created by the scanner was controlled using Picture Publisher[®] software. The image was imported into ERDAS V.7.5[®] for image rectification and analysis (Figure 4; ERDAS 1992).

The image was subsequently rectified from an oblique view to a planimetric model (Figure 5). The pixel location of the control panels in the image were matched with the precisely surveyed coordinates of the same panels on the ground through a transformation equation. A variety of transformation equation orders or exponential powers may be applied. The benefit of higher order equations is a reduced RMS error between image and ground (Figure 6).

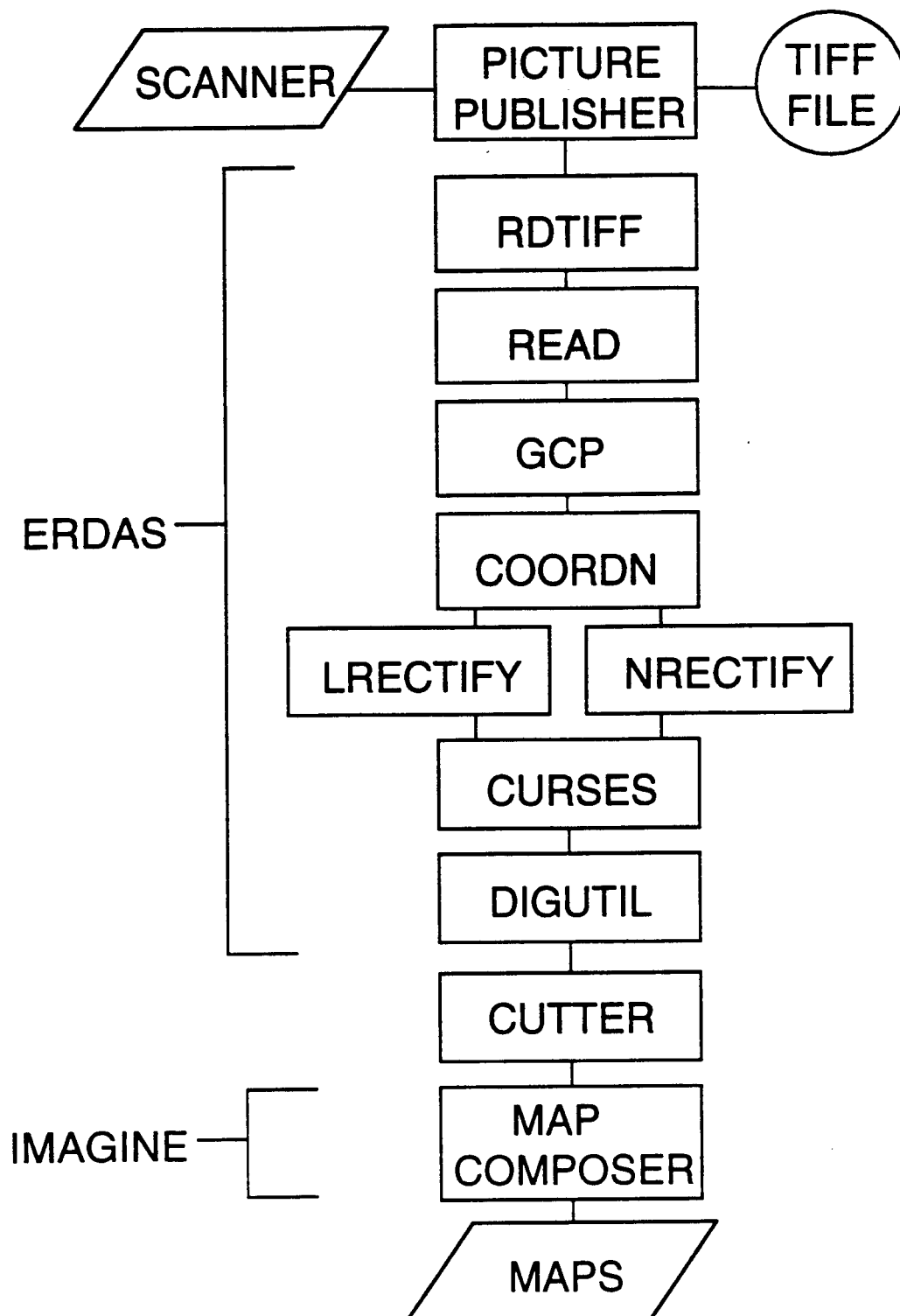


Fig. 4. Major image processing procedures and modules used in this study.

Sandbar 173.1R

11/16/92



Unrectified Surveyed Control Image



Rectified Control Image Employing a Second Order Transformation
Root Mean Square Error (pixels) = 1.86

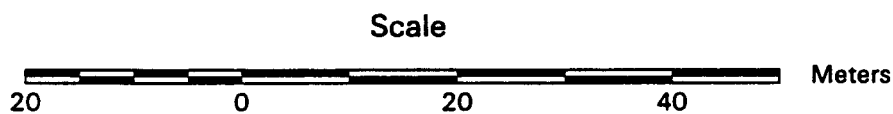


Fig. 5. Pre-transformation(top) and post-transformation (bottom) images in ERDAS of 173.1R showing control panels in place.

Each higher order equation requires an increase in the number of ground control points. Control panels were no longer necessary once the desired transformation equation had been established. Fixed natural features in the image were used to control subsequent transformations. Typically, these natural features were chosen from bedrock or debris fans surrounding the area of interest. Occasionally images were difficult to rectify due to poor exposure quality. We learned that the use of images reduced to only one or two of the primary color bands often eased the difficulty of pinpointing control features.

There are certain environmental factors (e.g. sun angle, steep cliffs) that sometimes result in film exposure problems. Several sandbars are prone to severe lighting contrasts and images may be over or under exposed, or both. We have developed a technique to enhance these difficult images. The Nikon scanner allows us to scan a number of different formats. These range from black and white positive to color negative. In addition, the scanner can separate color film into its three primary colors: red, green, and blue. This is extremely useful since ERDAS can view these spectral bandwidths individually. By manipulating the exposure time of each color we can bring out detail. For example, information within dark shadows is enhanced by increasing the amount of blue scanned. On the other hand, features washed out by over exposure is improved by decreasing the red. This procedure allows us to customize each image bringing out useful detail that would otherwise be unseen.

After image rectification, the resulting planimetric photo models were screen digitized using the DIGSCRN module. Screen digitizing the sandbars allowed approximate area and perimeter measurements to be determined from each photo (see the master data set in Appendix A) . These data were output as tabulated hard copy results using the DIGUTIL program. Lateral erosion or deposition rates were computed by comparing image pairs (e.g. Figures 41, 47, 48 and 53). Estimates of height change and sand volume cannot be made with single camera photogrammetry.

The DIGSCRN module also produced digital polygon files which enabled the rectified image of each sandbar to be extracted and placed into a map composition using ERDAS CUTTER and ERDAS-Imagine (V. 8.01) MAP COMPOSER modules respectively (see Figures 12 through 54). In addition to the measurements, the original oblique views or the rectified views were sequenced into high speed video loops for improved visualization and understanding of sandbar dynamics.

Results

Methodological

Analysis of Rectification Induced Error

One objective was analysis of the spatial accuracy of the techniques developed. The simplicity of the technique, and the ability to vary the repeat interval of the photography makes these methods usable in a wide variety of environmental assessments. Such information could be input into image analysis or GIS applications.

Possible sources of error accrued through the image capture and processing steps included: non-planar sandbar surfaces and abrupt changes in elevation, slight shifts in camera position during maintenance, diurnal environmental heat flux, scanning error (film curl etc.), manual identification of control points, and limitations in masking target image in batch processing.

To assess the cumulative spatial error involved in the procedures, three sandbars of about the same linear extent (approximately 100 m long) with different amounts of vertical relief were selected. The sandbars selected were 16.4L (Hot Na Na), 61.8R (first site below the Little Colorado River confluence), and 81.2L (Grapevine Camp). The sandbar at 61.8R was included because of its high relief while 16.4L and 81.2L represented more typical relief.

Several of the control panels were withheld from the test transformation. The transformation operation was run using the remaining control points. Finally, the transformed test image was queried for the location of the withheld panels. The resulting queried coordinates reflected accumulation of all errors propagated through the system when used in a likely manner for spatial analyses. These queried coordinates were obtained using the CURSES module of ERDAS (Figure 4). When the queried coordinates were compared to the surveyed coordinates for the panels, a Euclidean distance error could be computed for each panel withheld.

ERDAS internally computes a Root Mean Square (RMS) error for the transformed image compared to the control points used (Figure 5). It would be convenient if the transformation RMS value could be used as an estimate of error for any point on the transformed image. We set out to evaluate the validity of that possibility by comparing the RMS error to the Euclidean distance errors for the control points that were withheld. The salient statistics for the individual sandbar error analyses are illustrated in Table 1. While performing the error analysis, so many points must be withheld that third order transforms are not possible. Therefore, the results are derived using second order transforms and subsequently extrapolated to third order transforms (Table 2).

Results of the error analysis suggest that the RMS value is typically (but not always) a conservative estimation of the Euclidean distance error (Table 1), hence confidence intervals should be applied. Order three transforms are the optimal choice considering a balance between accuracy and surveying effort. Order three transform RMS suggest better than 1 in 100 spatial accuracy at an alpha level of 0.05 or 95% confidence (Table 2). Therefore, the techniques used here allow computation within +/- 1 meter of planimetric position for 95% of the point positions sampled.

Analysis of Stage Induced Error

One of the most persistent problems with interpretation of sandbar areas from any kind of imagery is the problem of water level.

Table 1. Point position error analysis for images of three Grand Canyon sandbars using second order transformations.

16.4L Hot Na Na (approximately 100 meters long)

Point #	Error in X (m)	Error in Y (m)	Z value (m)
5 (Front)	0.17	1.10	95.98
7 (Front)	0.72	0.11	96.00
F1 (Middle)	0.31	0.44	97.31
F2 (Middle)	0.74	2.28	97.62
RMS = 0.928	$\bar{X} = 0.49$	$\bar{Y} = 0.98$	$\Delta Z = 1.74$ $\Delta Z \text{ All} = 1.94$

61.8R first beach below the Little Colorado River (approximately 100 meters)

Point #	Error in X (m)	Error in Y (m)	Z value (m)
4 (Front)	0.21	0.16	101.29
7 (Back)	0.40	2.26	127.09
RMS = 4.78	$\bar{X} = 0.61$	$\bar{Y} = 1.21$	$\Delta Z = 25.8$
5 (Front)	0.23	0.31	110.17
9 (Middle)	0.00	1.95	128.89
10 (Back)	2.17	6.65	166.06
RMS = 4.68	$\bar{X} = 0.80$	$\bar{Y} = 2.97$	$\Delta Z = 55.89$ $\Delta Z \text{ All} = 77.14$

81.2l Grapevine Camp (approximately 100 meters long)

Point #	Error in X (m)	Error in Y (m)	Z value (m)
3 (Front)	0.95	0.68	95.00
9 (Back)	2.44	1.38	96.97
RMS = 3.9	$\bar{X} = 1.70$	$\bar{Y} = 1.03$	$\Delta Z = 1.97$
2 (Front)	1.61	0.61	95.07
7 (Back)	3.52	0.85	96.40
RMS = 1.83	$\bar{X} = 2.57$	$\bar{Y} = 0.73$	$\Delta Z = 1.33$ $\Delta Z \text{ All} = 3.40$

Table 2. Summary of point position error analysis for oblique single point photogrammetry as used in this study.

A summary of the RMS curves presented earlier is given as:

First order	20.39 meters
Second order	4.44 meters
Third order	0.41 meters

Results of point position tests on the second order transforms from three beaches yield the following values:

	Mean (m)	Standard Deviation (m)
$\Delta Z < 60.0$ m	1.99	1.81
$\Delta Z < 5.0$ m	1.76	1.08

Compared to the equivalent RMS values for the associated transformation:

	Mean (m)	Standard Deviation (m)
$\Delta Z < 60.0$ m	4.37	1.73
$\Delta Z < 5.0$ m	2.21	1.52

Applying confidence intervals to the reported RMS Values:

Confidence	Order 2 RMS (m)	Order 3 RMS (m)
80 % ($\alpha = 0.2$)	6.15	0.75
90 % ($\alpha = 0.1$)	7.04	0.92
95 % ($\alpha = 0.05$)	7.78	1.07

Table 3. Hypsometric (elevation-area) index for determining susceptibility of sandbars to stage induced area error. Class 1 sandbars exhibit large changes in area with respect to changes in river stage. Class 2 sandbars exhibit moderate changes in area with respect to changes in river stage. Class 3 sandbars exhibit small changes in area with respect to changes in river stage.

Sandbar	Elevation-Area Class
2.6L	1
16.4L	2
43.1L	3
44.6L	3
44.65L	2
60.1R	1
61.8R	2
64.0L	1
81.2L	3
119.0R	3
122.3R	2
122.7L	2
136.6L	3
136.7L	2
145.5L	3
172.2L	3
172.3L	2
173.1R	2
211.3L	2
212.9L	2

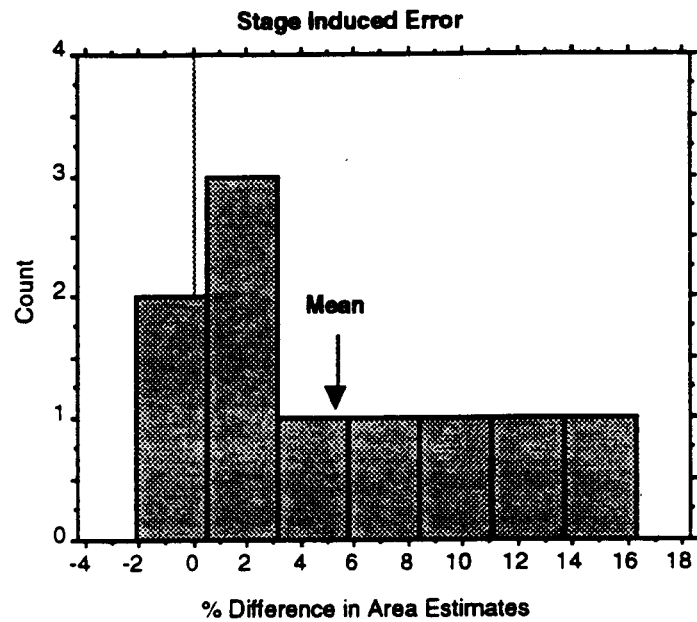


Fig. 7. Frequency distribution of stage induced error estimates.

Table 4. Summary statistics for stage induced error estimates.

Mean:	Std. Dev.:	Std. Error:	Variance:	Coef. Var.:	Count:
5.296	5.956	1.883	35.473	112.46	10
Minimum:	Maximum:	Range:	Sum:	Sum of Sqr.:	# Missing:
-2.18	15.29	17.47	52.96	599.731	0
t 95%:	95% Lower:	95% Upper:	# < 10th %:	10th %:	25th %:
4.261	1.035	9.557	1	-.88	.88
50th %:	75th %:	90th %:	# > 90th %:	Mode:	Geo. Mean:
3.285	10.05	14.325	1	•	•
Har. Mean:	Kurtosis:	Skewness:			
•	-1.114	.501			

Different stage levels expose different areas of alluvial deposits without any true aerial modification of the deposit. The problem becomes even more difficult when the sub-aqueous channel configurations change along with the exposed portion of the deposit. Stage-discharge relations established on transient deposit material will not hold. One of our future objectives is to establish stage-discharge relations at each of the monitored sandbars using "hard" or bedrock derived control points.

For the work presented here, poorly defined discharge-to-stage-to-area relations were constantly problematic. Most cameras are set to trigger for local low flows at each sandbar. Whenever possible, comparable discharge days were used as a selection criterion for images. We further categorized each deposit in terms of its hypsometry (area-elevation relationship) in effort to isolate less reliable results (see Table 3). Problems arose over long-term (seasonal) changes in stage and even in analysis of images taken before and after short term erosional events.

To assess the effect of misinterpreted stage levels on subsequent area calculations, we preserved varying area estimates made on the same deposit at the same time. Results are presented in Figure 7 and Table 4. Generally stage errors averaged five percent total area but were skewed by occasional high values as much as 17 percent total area.

Environmental

Hydrologic Inputs

Glen Canyon Dam Discharges. Since August 1991, and during the course of this project, Glen Canyon Dam has been operating under interim flow operating criteria. The specific criteria for interim flow releases are as follows:

- Maximum flow: 20,000 cfs
- Minimum flow: 5,000 cfs (up to 6 hours at night)
8,000 cfs (7 a.m. to 7 p.m.)

Change per day: 5,000 cfs for low volume months
6,000 cfs for medium volume months
8,000 cfs for high volume months

Ramping rates: upramp, no greater than 8,000 over 4
hours with a maximum of 2,500 cfs/h
downramp, no greater than -2,500 cfs/h

We have included daily maximum, mean, and minimum discharge values in graphical form as part of each sandbar time series plot (figures 60 through 79). Figures 8 and 9 show maximum, mean and minimum daily discharge frequency along with estimated daily upramp and downramp frequencies derived from the daily maximum and minimum discharge values (summary statistics provided in Appendix D).

Figure 10 indicates maximum, mean and minimum daily discharge frequency for all days where oblique photography was rectified. The similarity in frequency distributions suggests we have area estimates from a representative set of flow conditions.

Figure 11 is a series of correlograms (autocorrelation plots) for daily maximum, mean and minimum flows. Note the pronounced seven day lag positive peak (and successive seven day harmonics positive peaks) in the maximum and mean discharge. These peaks are a product of periodic weekend low flows.

Little Colorado River Peak Flood Discharges. Figure 92 shows the hydrograph for the Little Colorado River as gauged at Cameron, Arizona for the month of January 1993. The hydrograph captures the two main peaks of a snowmelt/rain driven flood. The first peak crests at 13,8000 cfs on January 12 and the second peak crests at 10,600 cfs on January 21. A subsequent flood event also occurred in March 1993. These flood events are significant inputs to mainstem sandbar dynamics as the Little Colorado River is now (post Glen Canyon Dam) the largest single supplier of sediment to the Colorado River in Grand Canyon.

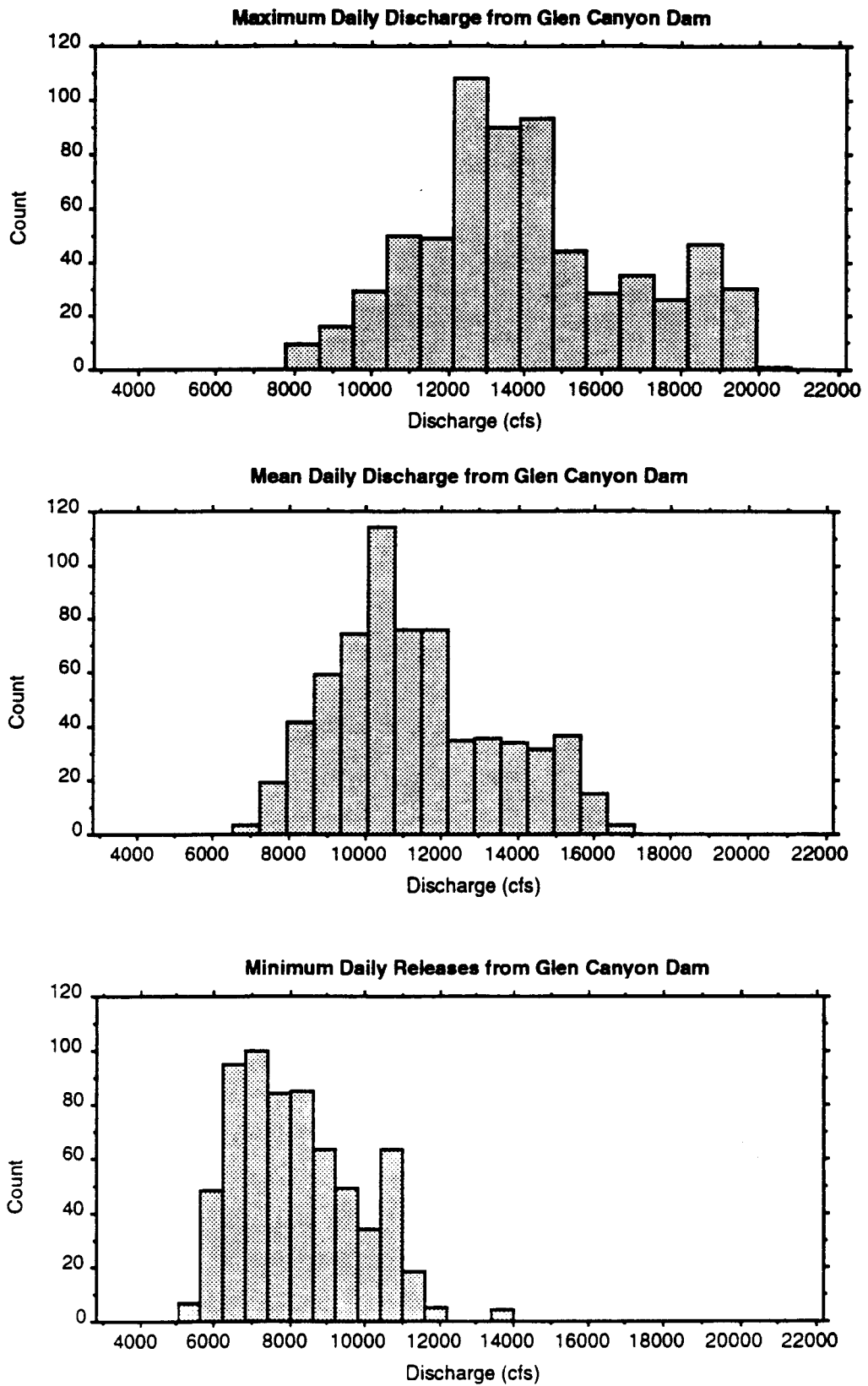


Fig. 8. Frequency distributions of maximum, mean and minimum discharge from Glen Canyon Dam, March 15, 1992 through December 31, 1993.

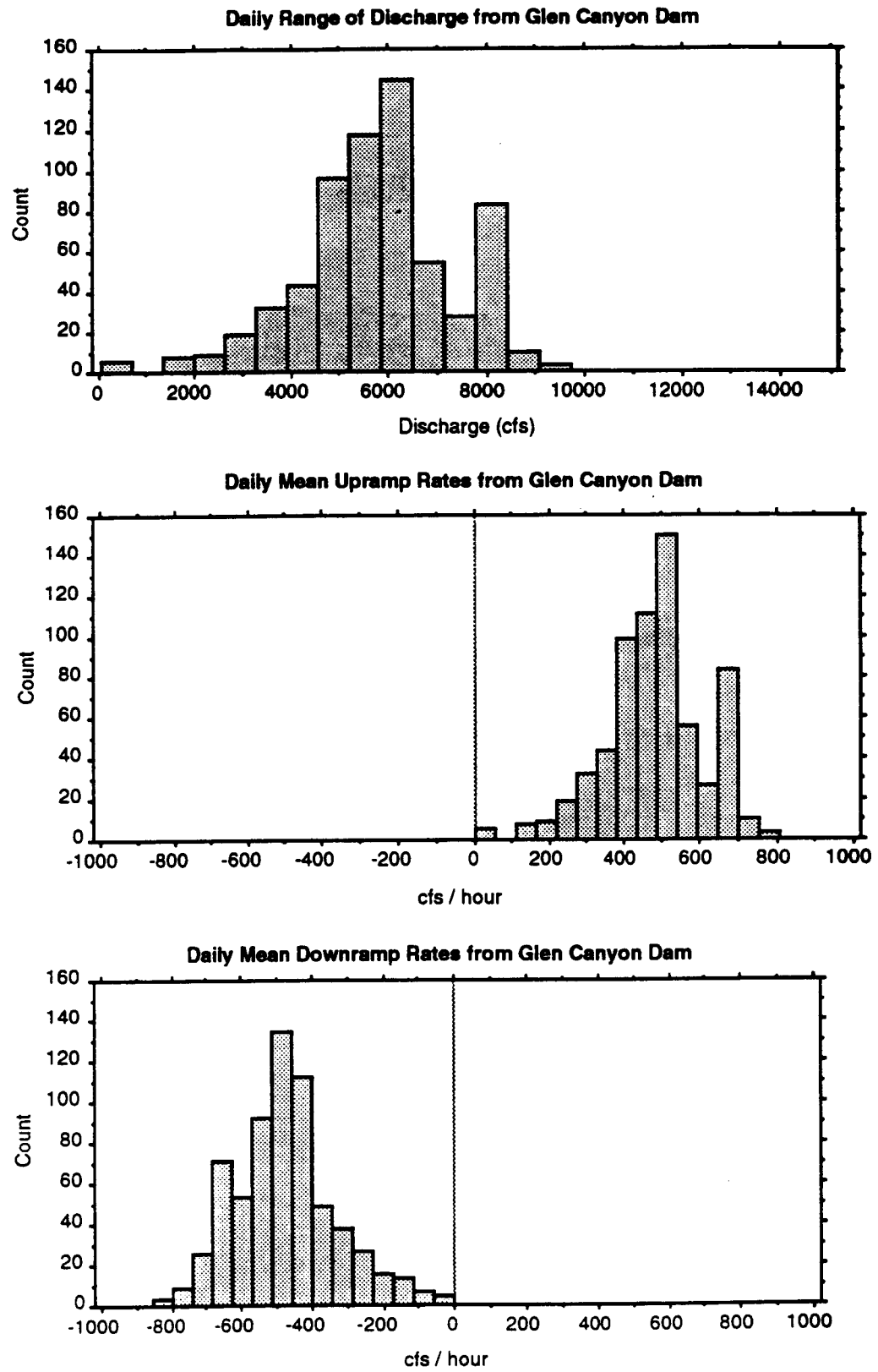


Fig. 9. Frequency distributions of discharge range and mean ramping rates from Glen Canyon Dam, March 15, 1992 through December 31, 1993.

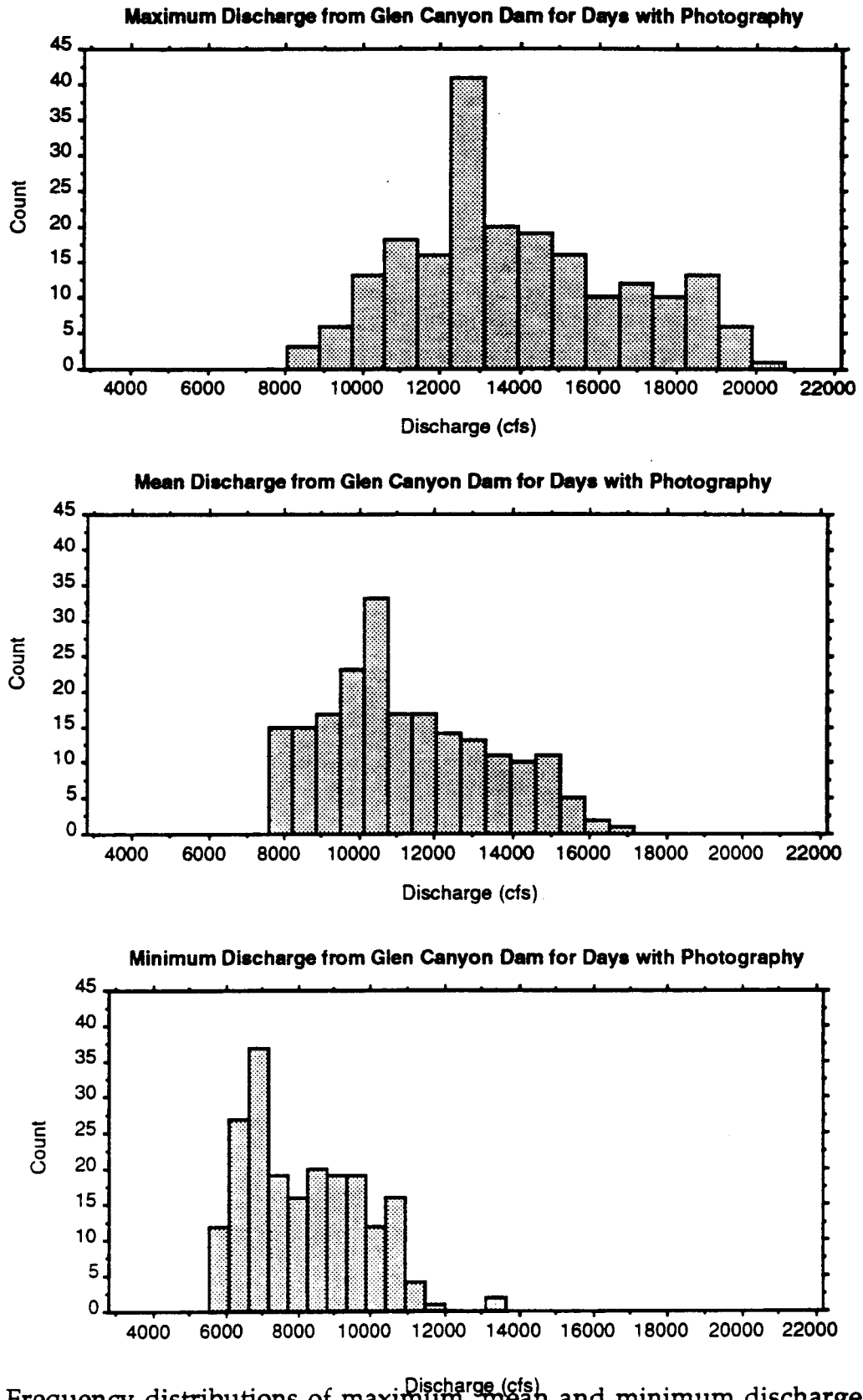


Fig. 10. Frequency distributions of maximum, mean and minimum discharge from Glen Canyon Dam for all days with rectified imagery from March 15, 1992 through December 31, 1993.

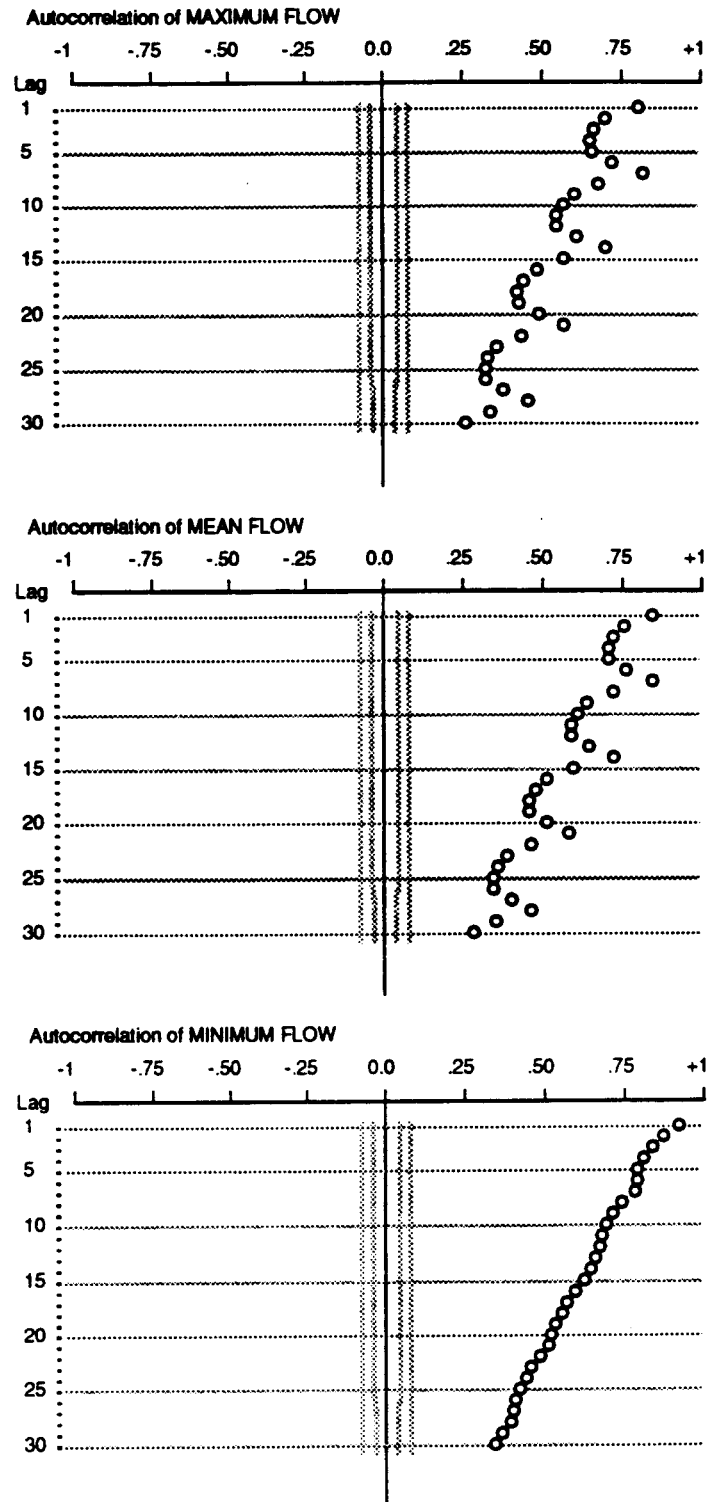


Fig. 11. Correlograms (autocorrelation plots) of maximum, mean and minimum discharge from Glen Canyon Dam, March 15, 1992 through December 31, 1993. The positive peak at the seven day lag (and subsequent seven day harmonics) shows the periodicity introduced by weekend low flows.

The winter 1993 flood was opportune in terms of this study because it allows for an evaluation of flood-driven sedimentation downstream from the LCR-Colorado confluence while leaving a control reach upstream from the LCR-Colorado confluence to Glen Canyon Dam.

Analysis of Site Responses Using Oblique and Rectified Image Photogrammetry

Rectified Image Photogrammetry. Results of the ERDAS derived area determinations for twenty sandbars rectified from oblique color photographs exposed between March 15, 1992 to December 31, 1993 are presented in maps (Figures 12 through 54) and time-series plots (Figures 60 through 79). Detailed analyses of these twenty sandbars are presented in the following section. In this report we provide a routine rectified area measurement approximately every 30 days and rectified area measurements before and after notable erosion events. These measurements were made during the low constant 8,000 cfs discharges and during weekend low flows approximating the stage of 8,000 cfs constant flows. Additional evaluations of sandbar areas were qualitatively determined by inspecting daily oblique photographs, noting area increase, decrease, or no change, and noting the location on the sandbar where changes were occurring. Consequently, the time scale of evaluation is daily. Some of the details of geomorphic activities not apparent in the rectified images but obvious in the original color slides are also discussed.

Extending Site Responses by Including Pilot Study Photography. By combining the results of photography and photogrammetry from this investigation with those of an earlier pilot project (Cluer, 1992), the length of record for selected sandbars is extended from August 1990 to December 1993. Photos from 172.3L obtained during the test flow period were rectified by methods described in this report. For the other sites in the pilot study, photographs were used in original oblique view form for the purpose of determining event timing, qualitative assessments of morphological change, and semi-quantitative estimation of size change (see Figures 81 through 88 for examples). The results are summarized in Table 10.

Magnitude and Frequency Results. Table 5 presents overall summary statistics for the twenty sandbars included in this study. Full summary statistical tables are included in Appendix B and C. Time is constrained between March 15, 1992 and December 21, 1993 to provide consistent statistical comparisons.

A Tukey box and whisker plot (Tukey, 1988) is provided (Figure 55) to give a quick visual overview of area-distribution relations by sandbar. This plot is organized on a downstream basis but no relation to true downstream scale exists on this plot. Other time series graphs (Figures 56 and 57) are provided to show true downstream scale.

Individual frequency histograms for each sandbar are presented in the composite Figure 58. Each histogram is divided into fifteen class intervals with the number of occurrences of measured areas (see the master rectified image data set in Appendix A) plotted against the area class. Three summary tables have been derived from these frequency analyses.

Table 6 is a listing of important distribution characteristics which are often used in assessing the normality of any frequency distribution. Kurtosis, skewness and visual assessment of distribution type are listed in the right three columns, while frequency class membership is summarized in the left three columns. The frequency class membership is based on 3 categories, number of deposit areas falling in the 3 middle classes of the fifteen class distribution, number of sandbar areas falling in the upper tail, and the number of sandbar areas falling in the lower tail.

A normally distributed "synthetic" sandbar was numerically generated to have the same approximate area values and the same sample size as a typical Grand Canyon sandbar (see Figure 59 for a frequency histogram and Table 7 for statistical characteristics and appendix E for the data set). In summary, the synthetic sandbar has 14 percent of its population in the middle three classes, and 43 percent of its population in each of the tail classes. This synthetic normal sandbar can be used to compare distribution characteristics of the twenty real sandbars.

Two further analyses were conducted to investigate seasonal and sub-seasonal distribution characteristics. Table 8 brings out seasonal trends in sandbar area. Areas for each deposit are averaged by season over the seven study seasons. The resulting time-series plot of the seasonally averaged areas for each sandbar is categorized relative to the mean area for the deposit. Each mean area is given a rank with one being smaller than average, two being about average and three being larger than average. Each class covers about one third the total range between maximum and minimum mean areas. These ranks are arranged by season with summary statistics presented. Seasons with relatively small sandbars compared to their individual means will sum up to lower values, while seasons with relatively large sandbars compared to their individual means will sum up to higher values. Results of this analysis are quite consistent and were easily related to dam discharge.

Table 9 is similar to Table 6 in that it summarizes frequency distributions for normality. The difference is that the time step is divided seasonally so that resulting distribution characteristics are made free of the seasonal cycling which was emphasized in Table 8. It is important to note that the bimodal and tail heavy distribution of sandbar areas obviously persists into sub-seasonal time steps.

Time-Series Results. Figures 60 through 79 contain the time sequenced results of sandbar area measurements both for routine sampling intervals and for significant failure events. Significant erosional events are highlighted and eroded areas listed alongside each event.

Individual correlograms (autocorrelation plots) for each deposit are presented in the composite Figure 80. These plots are derived by calculating a correlation coefficient for a time-series compared first to itself. This first comparison will always yield a correlation coefficient of 1.0 and is an implied value at lag zero on the correlogram figures. Subsequent correlation coefficients are derived by successively offsetting the time-series by one time increment (called the lag) and computing a new correlation coefficient at that lag. This process is repeated until too few data points remain for further comparison. These autocorrelation plots are useful for identification of cyclic trends in the time domain.

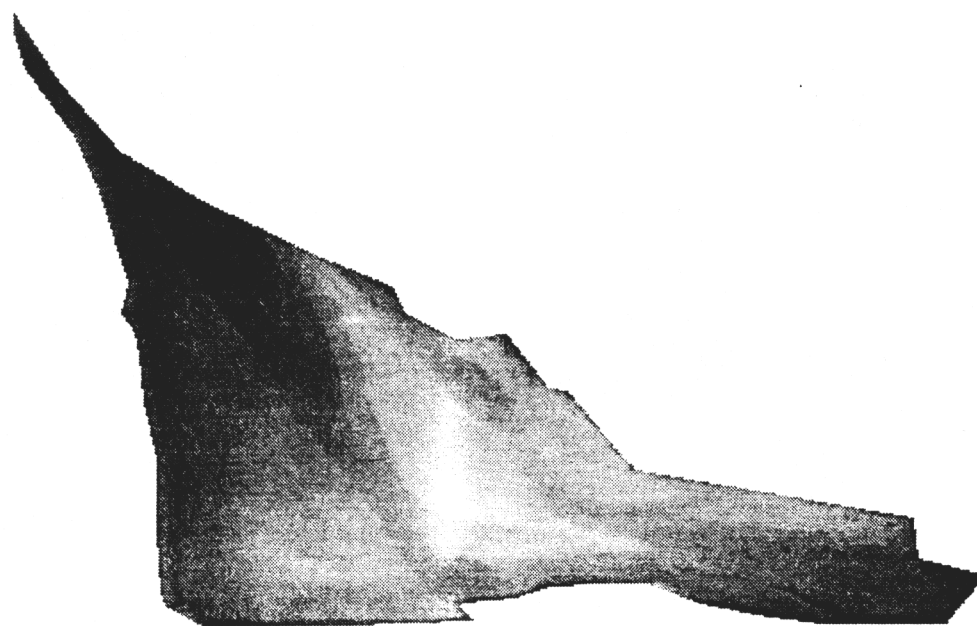
A subset of the standard time-series deposit area plots is included in Figure 93 to focus on the effects of the LCR flood event described earlier. The figure contains four panels divided by distance downstream. The first panel shows responses of deposits upstream from the LCR and is largely free from flood influence. Subsequent panels show responses of deposits successively further downstream.

Short time step (daily to weekly) area changes (rapid erosional events) have been extracted from the master data set (Appendix A) and compiled into Table 10. A three-way time-space plot (Figure 89) and a hydrology vs. event time-series plot (Figure 90) focuses on the characteristics of these events.

Sandbar 2.6L

Grand Canyon, Arizona

10/12/92



River Flow →

Scale



Area (sq. m) = 2365
Perimeter (m) = 304.25
Ave. Input Pixel Size (sq. m) = 0.23
Total RMS Error (pix) = 3.83

Northern Arizona University
Department of Geography, GIS Lab
Sandbar Photogrammetry Project

Fig. 12. Rectified image map of sandbar 2.6L, 10/12/92.

Sandbar 16.4L

Grand Canyon, Arizona

10/11/92



River Flow →

Scale



Area (sq. m) = 1448
Perimeter (m) = 162.64
Pixel Size (sq. m) = 0.14
Total RMS Error (pix) = 5.38

Northern Arizona University
Department of Geography, GIS Lab
Sandbar Photogrammetry Project

Fig. 13. Rectified image map of sandbar 16.4L, 10/11/92.

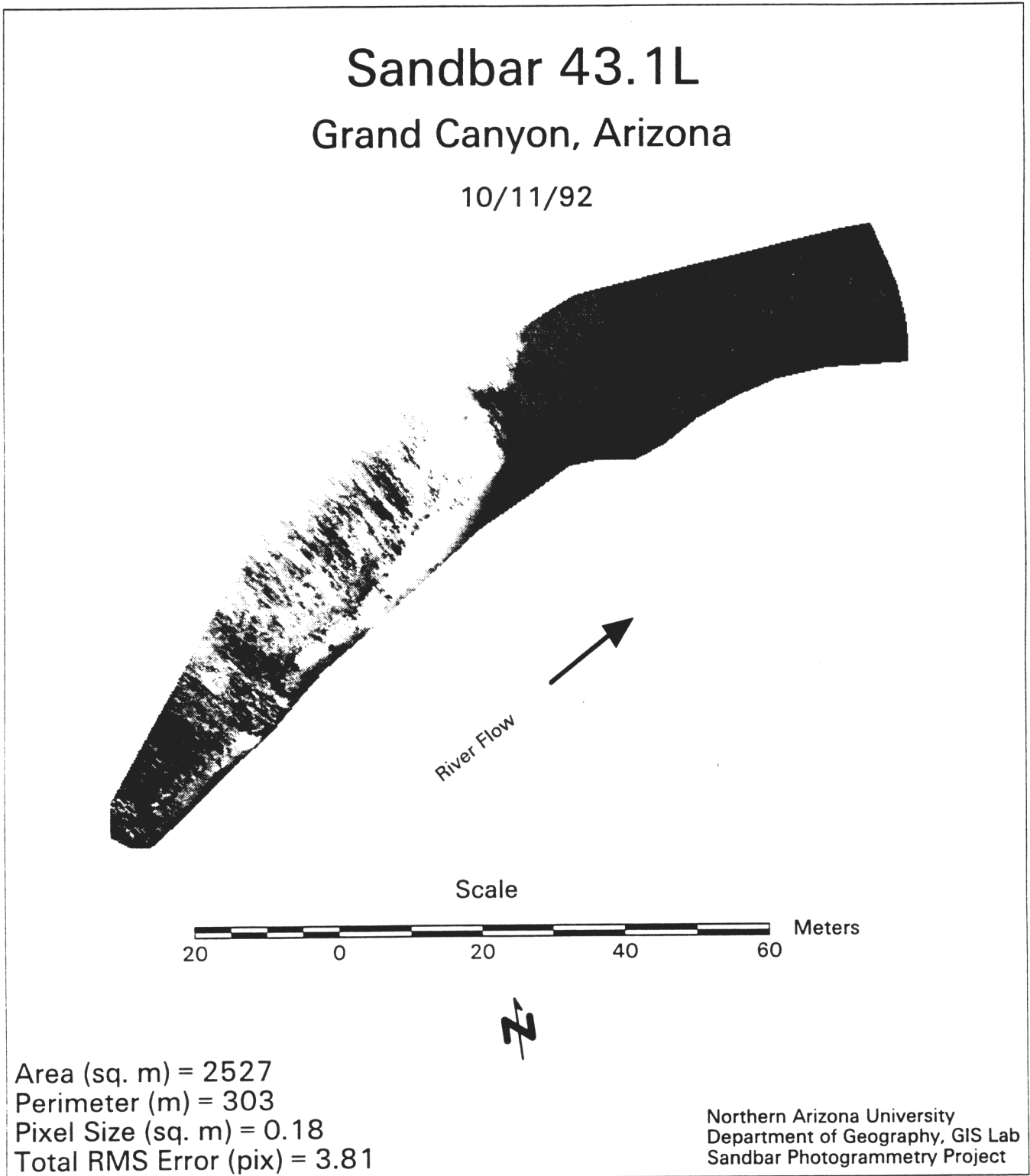


Fig. 14. Rectified image map of sandbar 43.1L, 10/11/92.

Sandbar 44.6L

Grand Canyon, Arizona

10/12/92



River Flow



Scale



Area (sq. m) = 782
Perimeter (m) = 182.47
Ave. Input Pixel Size (sq. m) = 0.22
Total RMS Error (pix) = 3.27

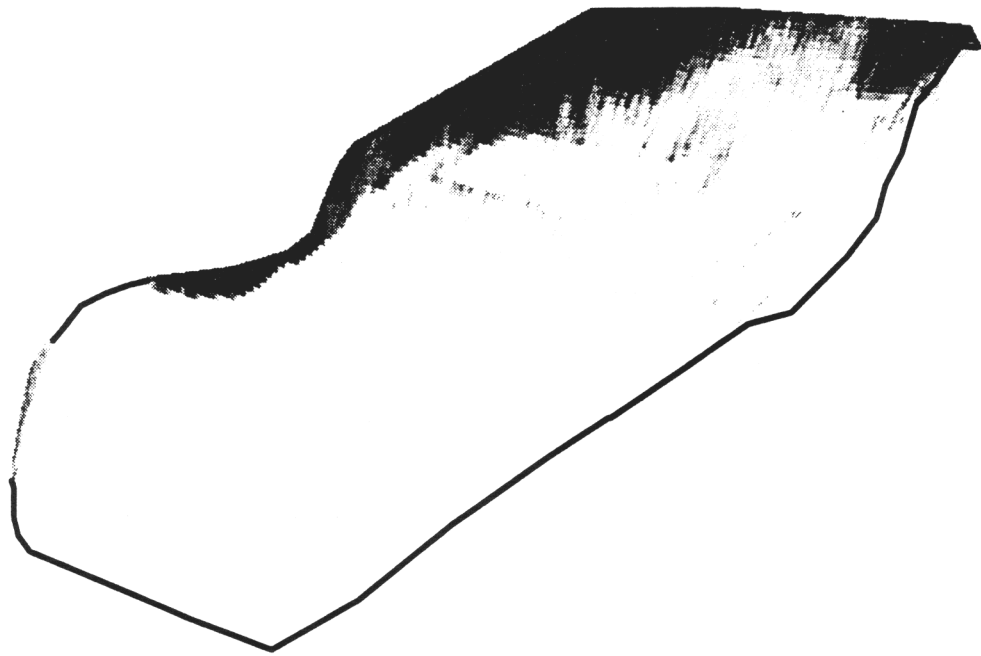
Northern Arizona University
Department of Geography, GIS Lab
Sandbar Photogrammetry Project

Fig. 15. Rectified image map of sandbar 44.6L, 10/12/92.

Sandbar 44.65L

Grand Canyon, Arizona

10/11/92



River Flow →

Scale



Area (sq. m) = 5580
Perimeter (m) = 336
Pixel Size (sq. m) = 0.43
Total RMS Error (pix) = 3.56

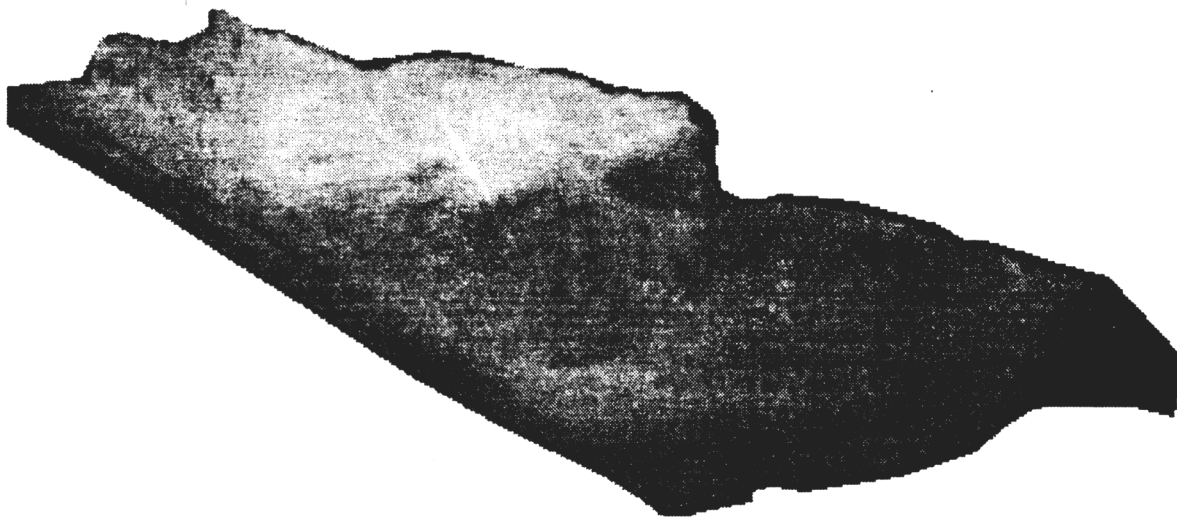
Northern Arizona University
Department of Geography, GIS Lab
Sandbar Photogrammetry Project

Fig. 16. Rectified image map of sandbar 44.65L, 10/11/92.

Sandbar 60.1R

Grand Canyon, Arizona

10/13/92



River Flow ←

Scale



Area (sq. m) = 1797
Perimeter (m) = 217.28
Ave. Input Pixel Size (sq. m) = 0.19
Total RMS Error (pix) = 6.50

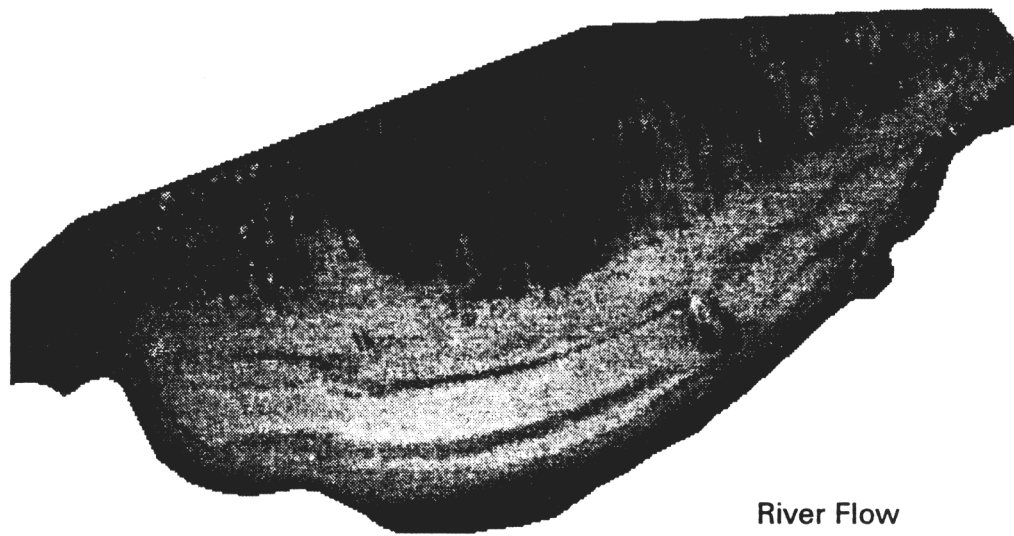
Northern Arizona University
Department of Geography, GIS Lab
Sandbar Photogrammetry Project

Fig. 17. Rectified image map of sandbar 60.1R, 10/13/92.

Sandbar 61.8R

Grand Canyon, Arizona

10/12/92



River Flow



Scale



Area (sq. m) = 3753
Perimeter (m) = 271
Ave. Input Pixel Size (sq. m) = 0.21
Total RMS Error (pix) = 2.77

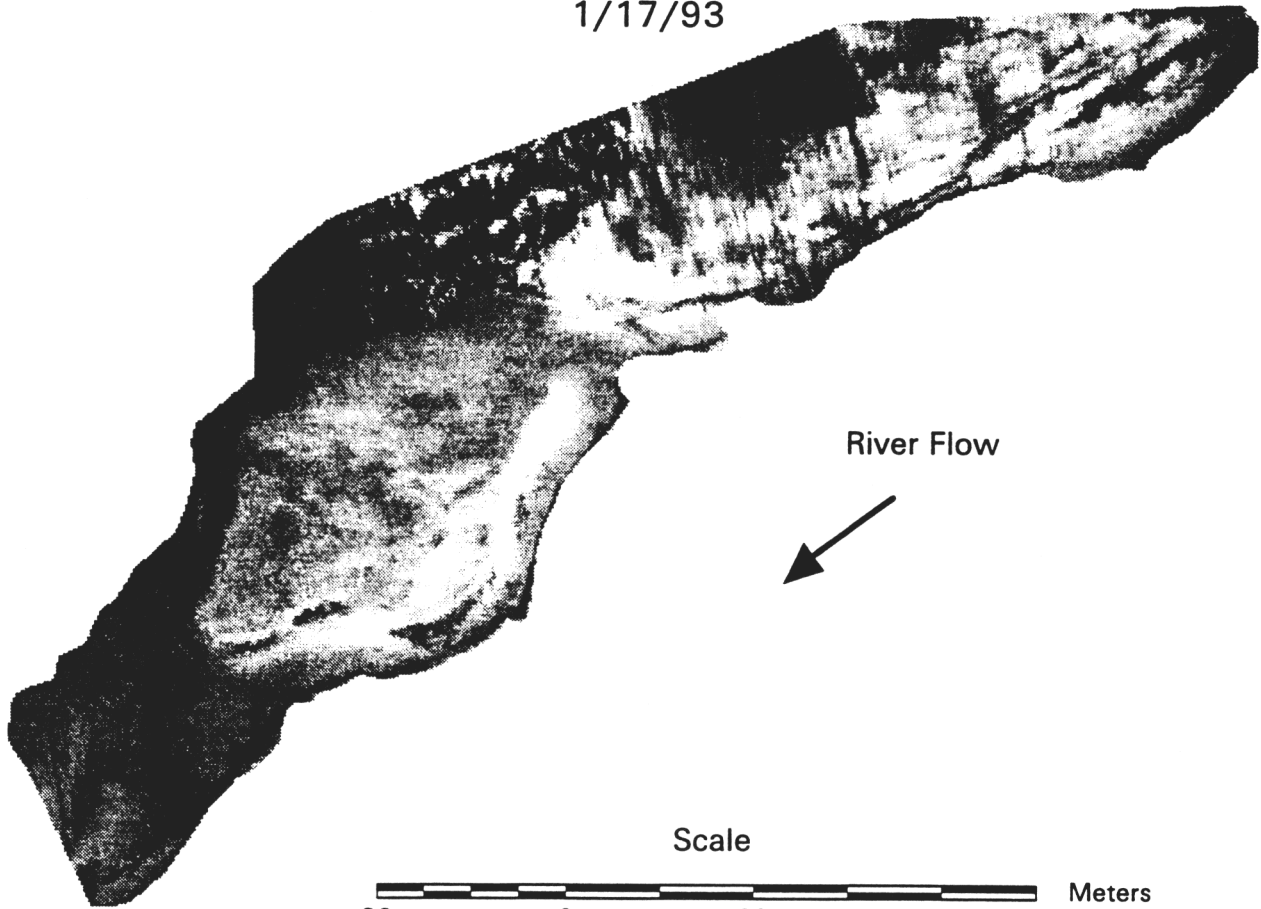
Northern Arizona University
Department of Geography, GIS Lab
Sandbar Photogrammetry Project

Fig. 18. Rectified image map of sandbar 61.8R, 10/12/92.

Sandbar 61.8R

Grand Canyon, Arizona

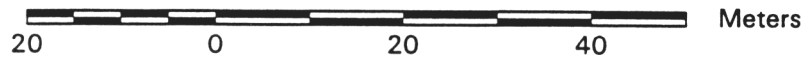
1/17/93



River Flow



Scale



Area (sq. m) = 4006
Perimeter (m) = 375
Ave. Input Pixel Size (sq. m) = 0.21
Total RMS Error (pix) = 2.77

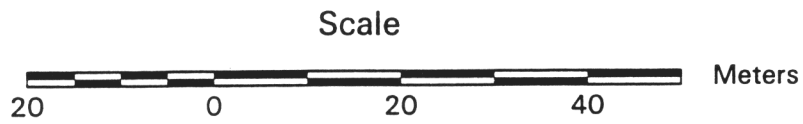
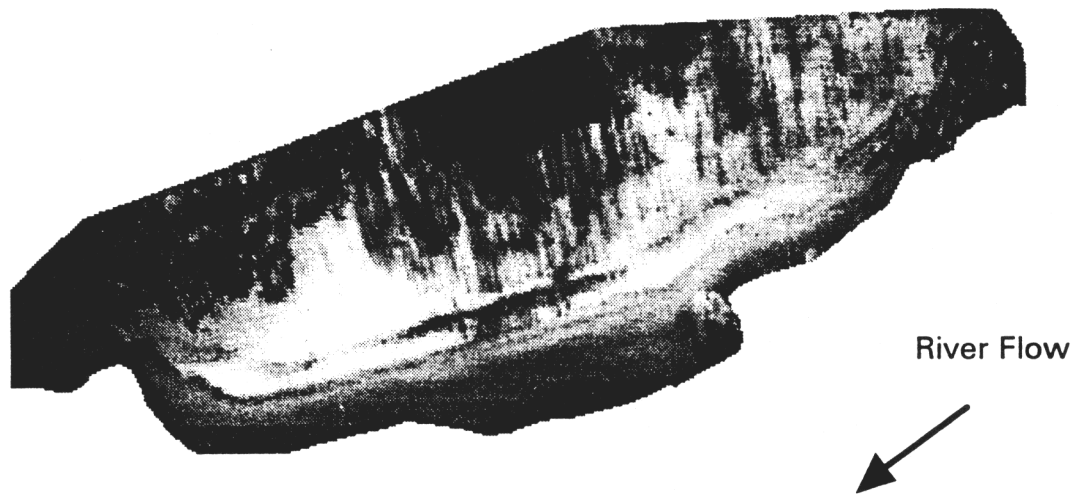
Northern Arizona University
Department of Geography, GIS Lab
Sandbar Photogrammetry Project

Fig. 19. Rectified image map of sandbar 61.8R, 1/17/93.

Sandbar 61.8R

Grand Canyon, Arizona

3/14/93



Area (sq. m) = 3055
Perimeter (m) = 265
Ave. Input Pixel Size (sq. m) = 0.21
Total RMS Error (pix) = 2.77

Northern Arizona University
Department of Geography, GIS Lab
Sandbar Photogrammetry Project

Fig. 20. Rectified image map of sandbar 61.8R, 3/14/93.

Sandbar 61.8R

Grand Canyon, Arizona

4/18/93



Scale



Area (sq. m) = 4628
Perimeter (m) = 344
Ave. Input Pixel Size (sq. m) = 0.21
Total RMS Error (pix) = 2.77

Northern Arizona University
Department of Geography, GIS Lab
Sandbar Photogrammetry Project

Fig. 21. Rectified image map of sandbar 61.8R, 4/18/93.

Sandbar 61.8R

Grand Canyon, Arizona

6/7/93



Area (sq. m) = 3418
Perimeter (m) = 268
Ave. Input Pixel Size (sq. m) = 0.21
Total RMS Error (pix) = 2.77

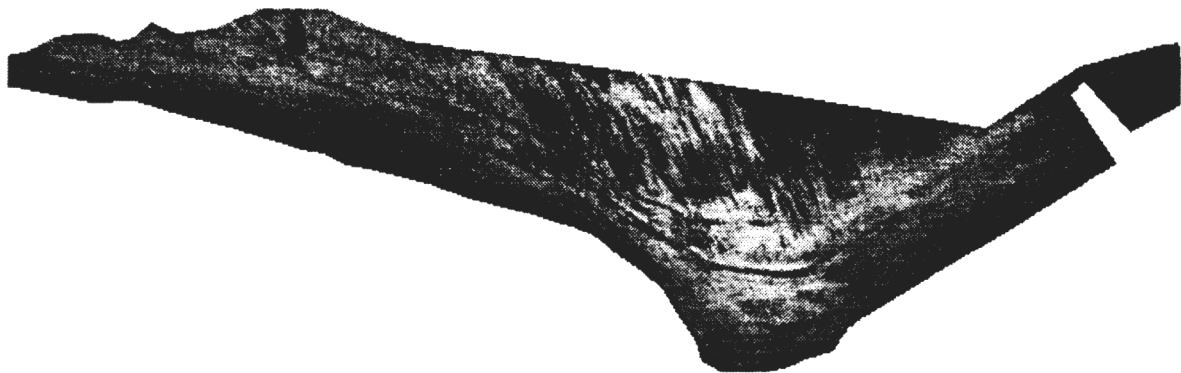
Northern Arizona University
Department of Geography, GIS Lab
Sandbar Photogrammetry Project

Fig. 22. Rectified image map of sandbar 61.8R, 6/7/93.

Sandbar 64.0L

Grand Canyon, Arizona

10/13/92



River Flow →

Scale



Area (sq. m) = 3027
Perimeter (m) = 375
Ave. Input Pixel Size (sq. m) = 0.18
Total RMS Error (pix) = 3.91

Northern Arizona University
Department of Geography, GIS Lab
Sandbar Photogrammetry Project

Fig. 23. Rectified image map of sandbar 64.0L, 10/13/92.

Sandbar 64.0L

Grand Canyon, Arizona

11/14/92



River Flow 

Scale



Area (sq. m) = 2642
Perimeter (m) = 368
Ave. Input Pixel Size (sq. m) = 0.18
Total RMS Error (pix) = 3.91

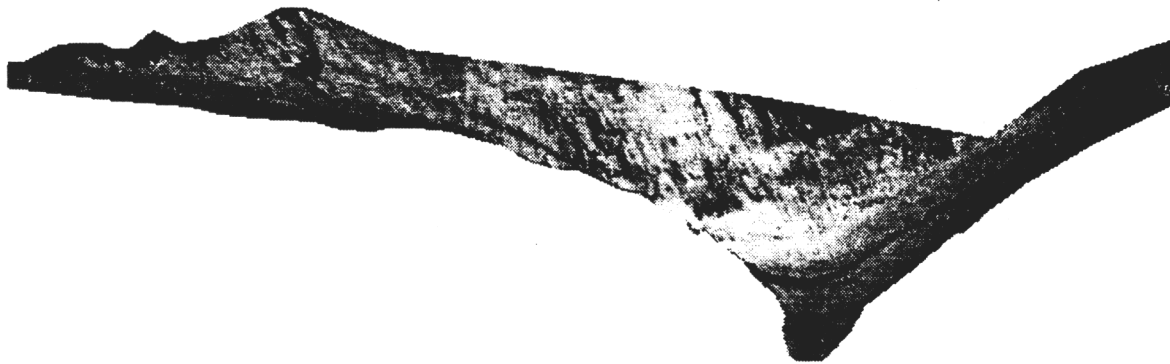
Northern Arizona University
Department of Geography, GIS Lab
Sandbar Photogrammetry Project

Fig. 24. Rectified image map of sandbar 64.0L, 11/14/92.

Sandbar 64.0L

Grand Canyon, Arizona

12/11/92



River Flow →

Scale



Area (sq. m) = 2153
Perimeter (m) = 358
Ave. Input Pixel Size (sq. m) = 0.18
Total RMS Error (pix) = 3.91

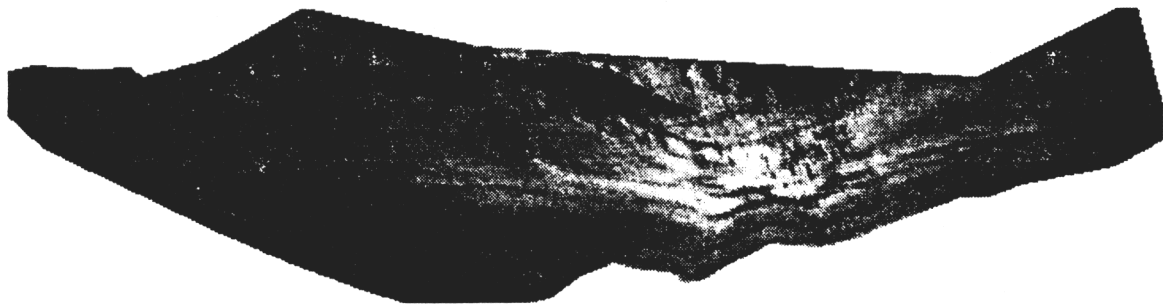
Northern Arizona University
Department of Geography, GIS Lab
Sandbar Photogrammetry Project

Fig. 25. Rectified image map of sandbar 64.0L, 12/11/92.

Sandbar 64.0L

Grand Canyon, Arizona

1/15/93



River Flow →

Scale



Area (sq. m) = 3757
Perimeter (m) = 349
Ave. Input Pixel Size (sq. m) = 0.18
Total RMS Error (pix) = 5.86

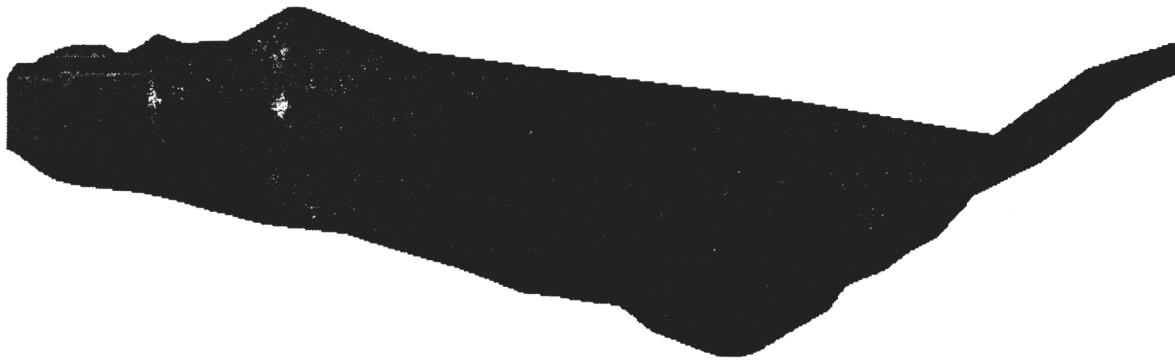
Northern Arizona University
Department of Geography, GIS Lab
Sandbar Photogrammetry Project

Fig. 26. Rectified image map of sandbar 64.0L, 1/15/93.

Sandbar 64.0L

Grand Canyon, Arizona

3/15/93



River Flow →

Scale



Area (sq. m) = 3454
Perimeter (m) = 353
Pixel Size (sq. m) = 0.18
Total RMS Error (pix) = 3.91

Northern Arizona University
Department of Geography, GIS Lab
Sandbar Photogrammetry Project

Fig. 27. Rectified image map of sandbar 64.0L, 3/15/93.

Sandbar 64.0L

Grand Canyon, Arizona

4/11/93



River Flow 

Scale



Area (sq. m) = 3043
Perimeter (m) = 358
Pixel Size (sq. m) = 0.18
Total RMS Error (pix) = 3.91

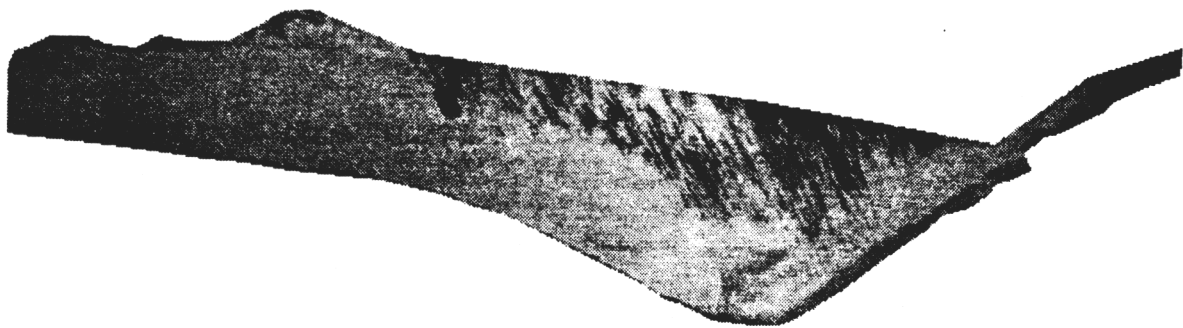
Northern Arizona University
Department of Geography, GIS Lab
Sandbar Photogrammetry Project

Fig. 28. Rectified image map of sandbar 64.0L, 4/11/93.

Sandbar 64.0L

Grand Canyon, Arizona

5/31/93



River Flow →

Scale



Area (sq. m) = 2678
Perimeter (m) = 351
Ave. Input Pixel Size (sq. m) = 0.18
Total RMS Error (pix) = 3.91

Northern Arizona University
Department of Geography, GIS Lab
Sandbar Photogrammetry Project

Fig. 29. Rectified image map of sandbar 64.0L, 5/31/93.

Sandbar 81.2L (Grapevine)

Grand Canyon, Arizona

10/12/92



River Flow 

Scale



Area (sq. m) = 1947
Perimeter (m) = 230
Ave. Input Pixel Size (sq. m) = 0.19
Total RMS Error (pix) = 3.88

Northern Arizona University
Department of Geography, GIS Lab
Sandbar Photogrammetry Project

Fig. 30. Rectified image map of sandbar 81.2L, 10/12/92.

Sandbar 81.2L (Grapevine)

Grand Canyon, Arizona

11/11/92



River Flow →

Scale



Area (sq. m) = 1753
Perimeter (m) = 226
Ave. Input Pixel Size (sq. m) = 0.19
Total RMS Error (pix) = 3.88

Northern Arizona University
Department of Geography, GIS Lab
Sandbar Photogrammetry Project

Fig. 31. Rectified image map of sandbar 81.2L, 11/11/92.

Sandbar 81.2L (Grapevine)

Grand Canyon, Arizona

1/25/93



River Flow 

Scale



Area (sq. m) = 1787
Perimeter (m) = 230
Ave. Input Pixel Size (sq. m) = 0.19
Total RMS Error (pix) = 3.88

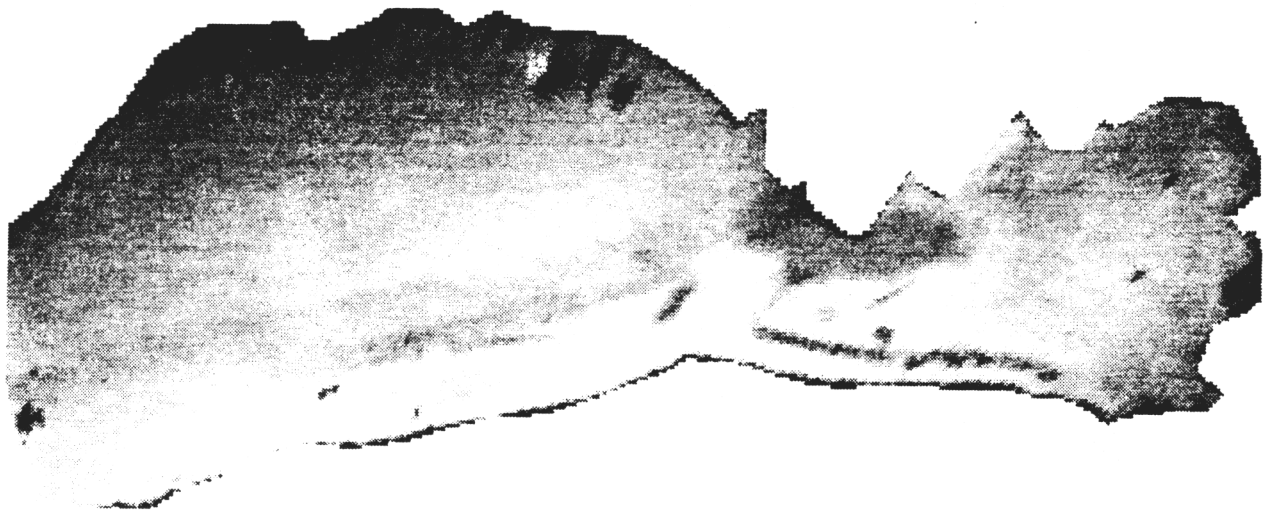
Northern Arizona University
Department of Geography, GIS Lab
Sandbar Photogrammetry Project

Fig. 32. Rectified image map of sandbar 81.2L (Grapevine), 1/25/93.

Sandbar 81.2L (Grapevine)

Grand Canyon, Arizona

3/15/93



River Flow →

Scale



Area (sq. m) = 1757
Perimeter (m) = 234
Ave. Input Pixel Size (sq. m) = 0.19
Total RMS Error (pix) = 3.88

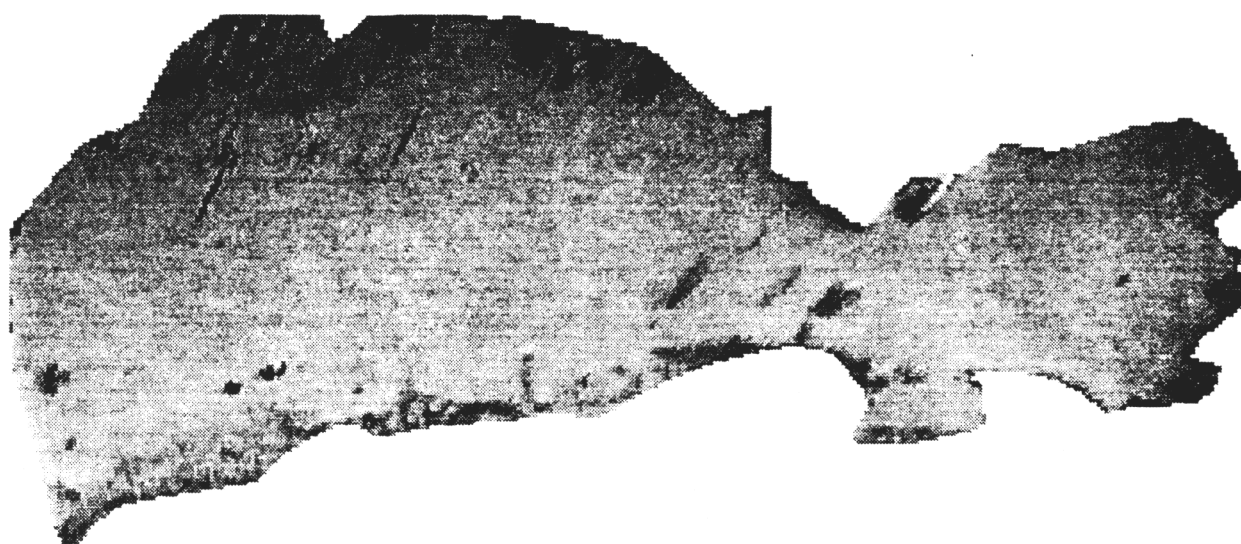
Northern Arizona University
Department of Geography, GIS Lab
Sandbar Photogrammetry Project

Fig. 33. Rectified image map of sandbar 81.2L (Grapevine), 3/15/93.

Sandbar 81.2L (Grapevine)

Grand Canyon, Arizona

5/31/93



River Flow →

Scale



Area (sq. m) = 1740
Perimeter (m) = 238
Ave. Input Pixel Size (sq. m) = 0.19
Total RMS Error (pix) = 3.88

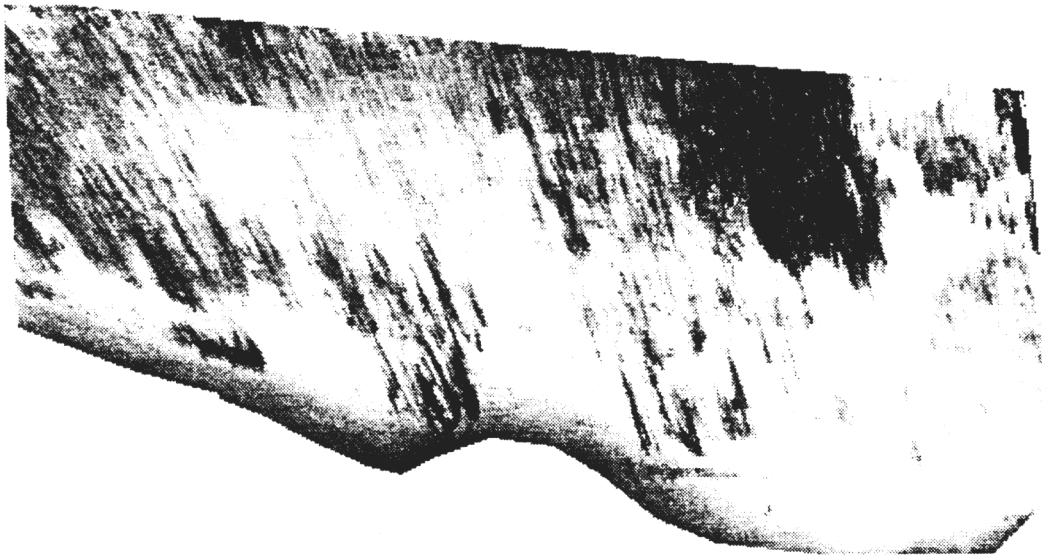
Northern Arizona University
Department of Geography, GIS Lab
Sandbar Photogrammetry Project

Fig. 34. Rectified image map of sandbar 81.2L (Grapevine), 5/31/93.

Sandbar 119.0R

Grand Canyon, Arizona

10/12/92



River Flow



Scale



Area (sq. m) = 3394
Perimeter (m) = 256
Pixel Size (sq. m) = 0.22
Total RMS Error (pix) = 8.78

Northern Arizona University
Department of Geography, GIS Lab
Sandbar Photogrammetry Project

Fig. 35. Rectified image map of sandbar 119.0R, 10/12/92.

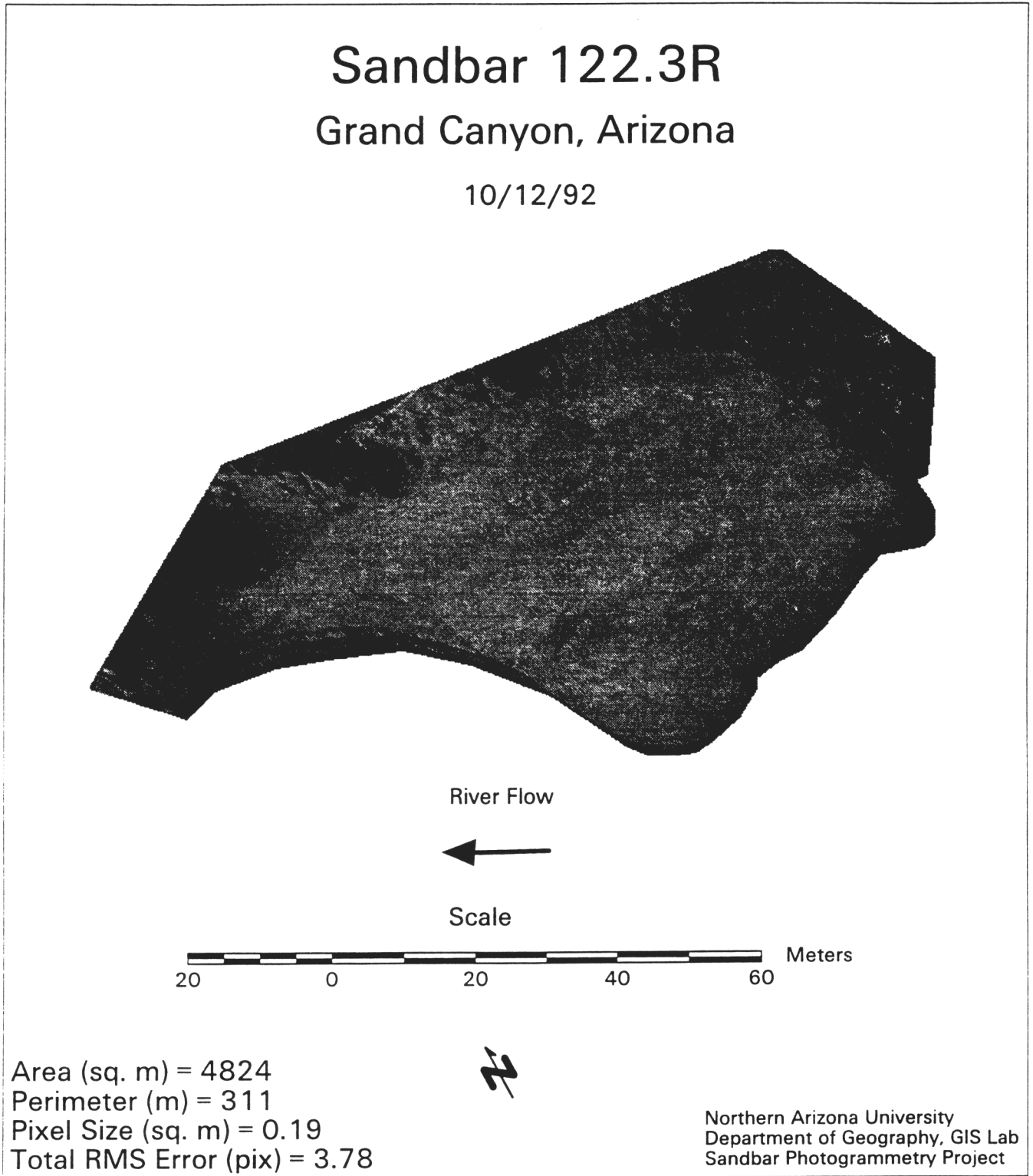
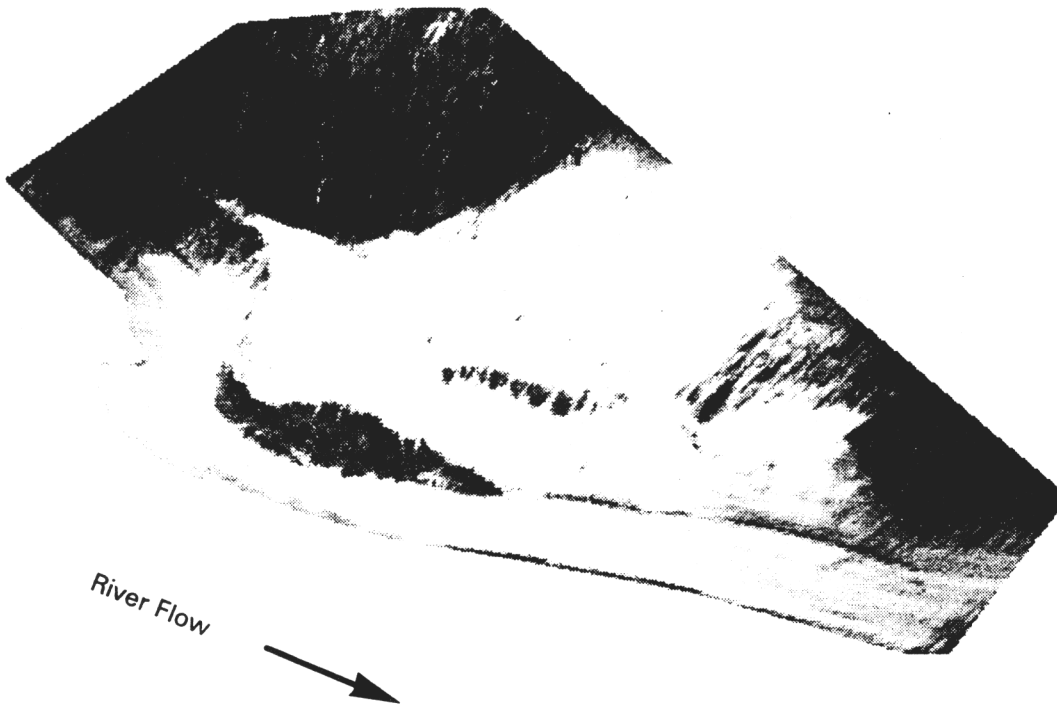


Fig. 36. Rectified image map of sandbar 122.3R, 10/12/92.

Sandbar 122.7L

Grand Canyon, Arizona

5/31/93



River Flow
↓

Scale



Area (sq. m) = 3553
Perimeter (m) = 262
Ave. Input Pixel Size (sq. m) = 0.09
Total RMS Error (pix) = 1.27



Northern Arizona University
Department of Geography, GIS Lab
Sandbar Photogrammetry Project

Fig. 37. Rectified image map of sandbar 122.7L, 5/31/93.

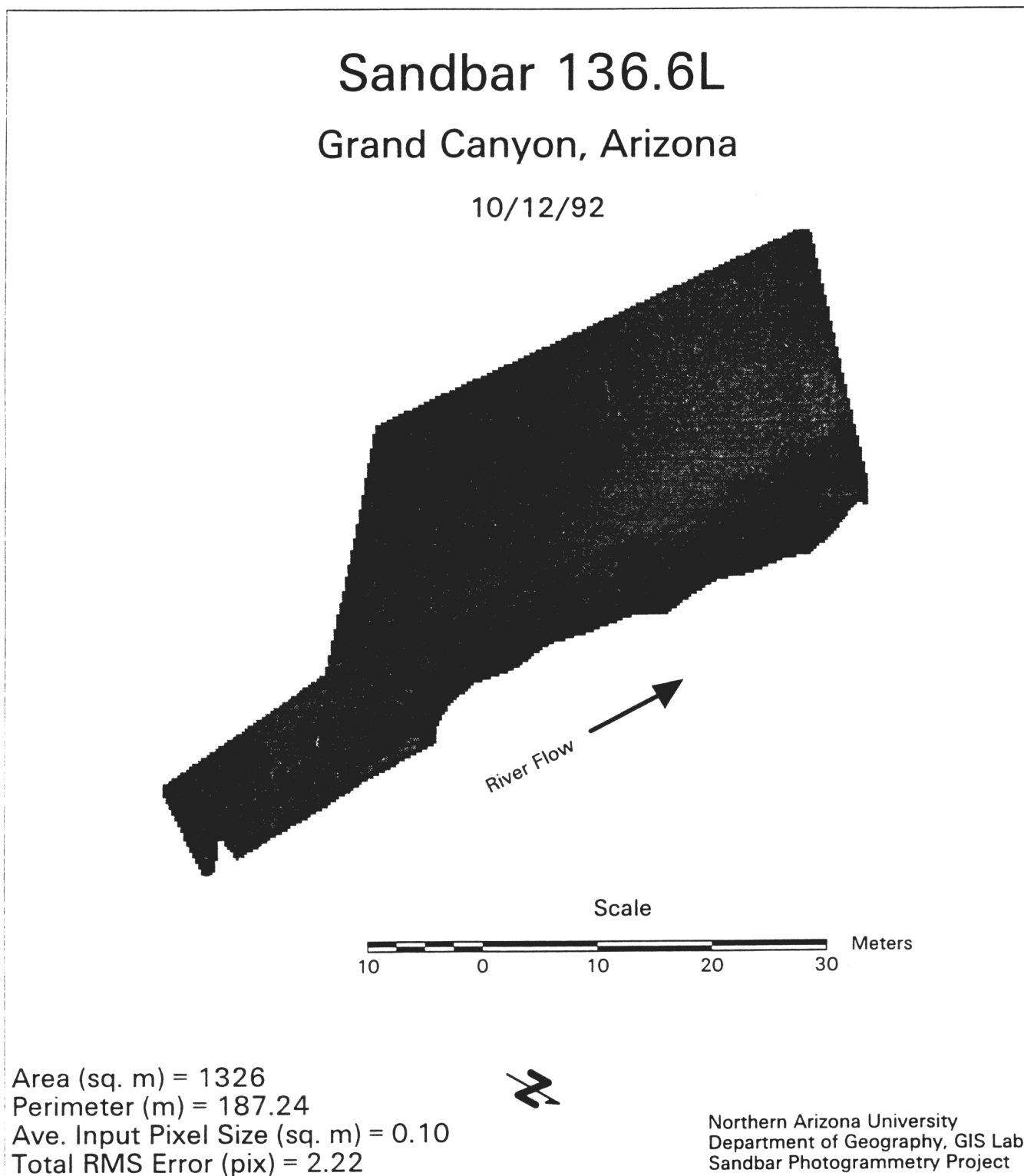
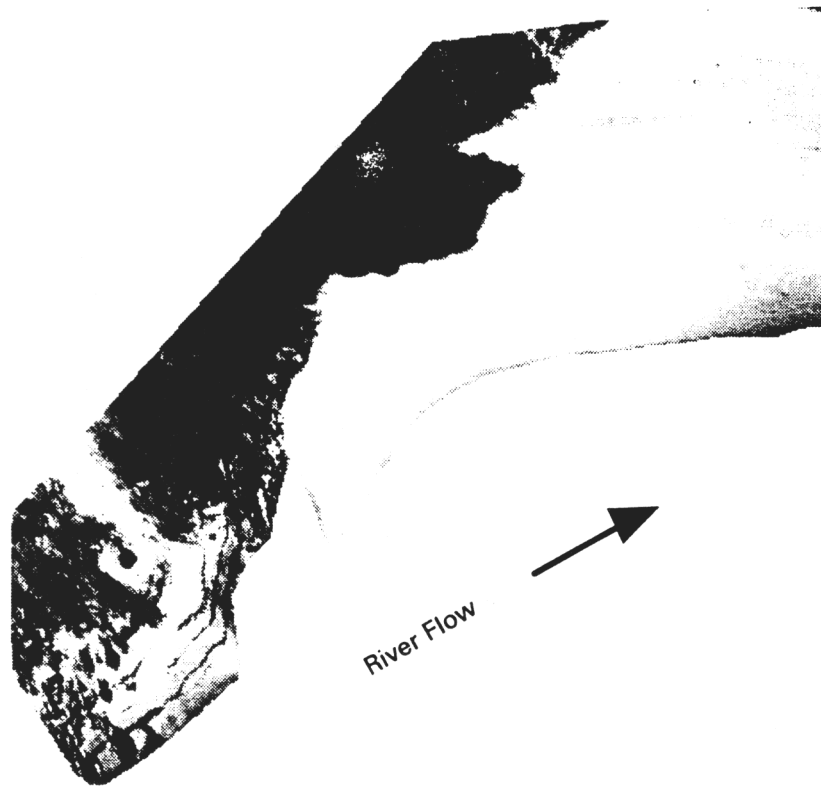


Fig. 38. Rectified image map of sandbar 136.6L, 10/12/92.

Sandbar 136.7L

Grand Canyon, Arizona

10/11/92



Scale



Area (sq. m) = 2921
Perimeter (m) = 284
Ave. Input Pixel Size (sq. m) = 0.15
Total RMS Error (pix) = 6.37



Northern Arizona University
Department of Geography, GIS Lab
Sandbar Photogrammetry Project

Fig. 39. Rectified image map of sandbar 136.7L, 10/11/92.

Sandbar 145.5L

Grand Canyon, Arizona

10/13/92



River Flow →

Scale



Area (sq. m) = 929
Perimeter (m) = 137
Ave. Input Pixel Size (sq. m) = 0.14
Total RMS Error (pix) = 7.11

Northern Arizona University
Department of Geography, GIS Lab
Sandbar Photogrammetry Project

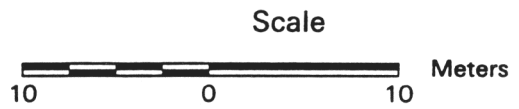
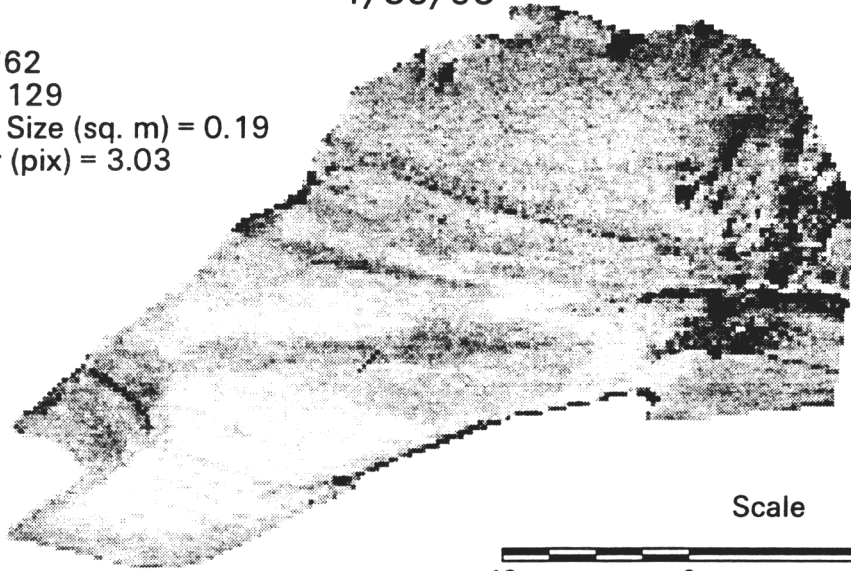
Fig. 40. Rectified image map of sandbar 145.5L, 10/13/92.

Sandbar 145.5L

Grand Canyon, Arizona

1/30/93

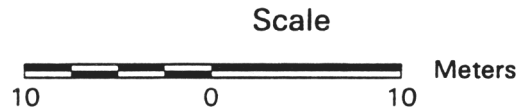
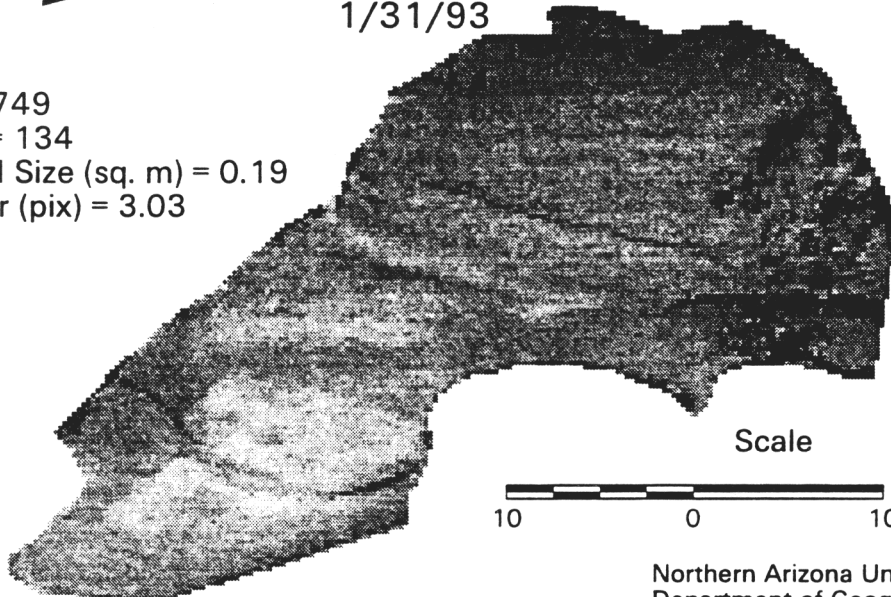
Area (sq. m) = 762
Perimeter (m) = 129
Ave. Input Pixel Size (sq. m) = 0.19
Total RMS Error (pix) = 3.03



River Flow →

1/31/93

Area (sq. m) = 749
Perimeter (m) = 134
Ave. Input Pixel Size (sq. m) = 0.19
Total RMS Error (pix) = 3.03



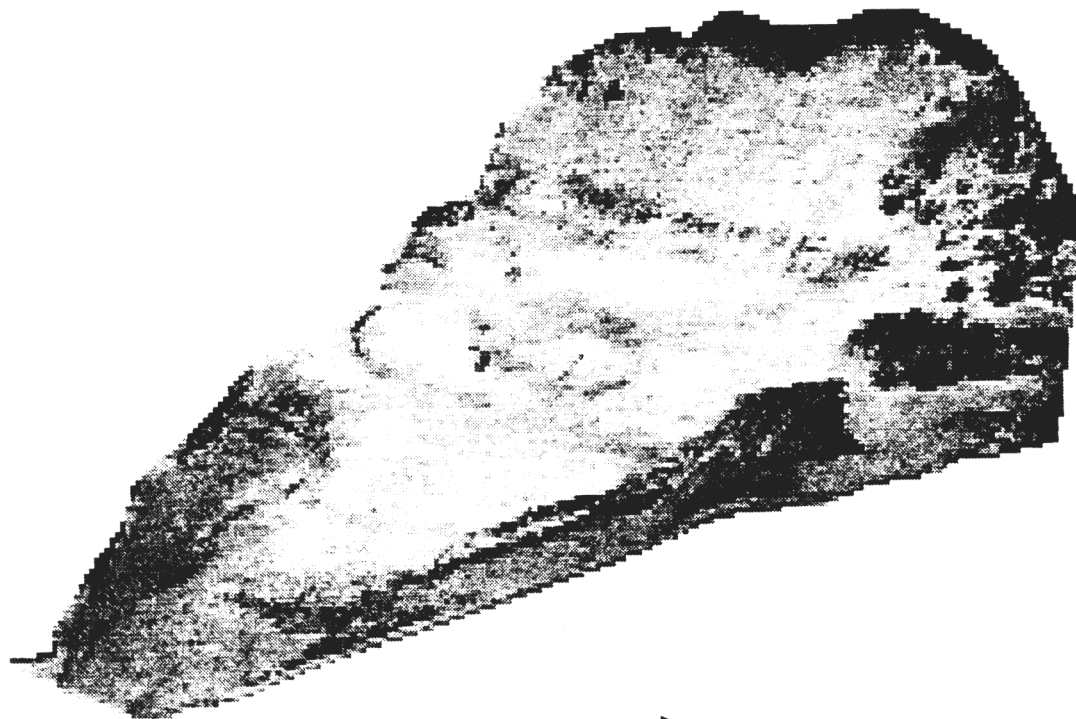
Northern Arizona University
Department of Geography, GIS Lab
Sandbar Photogrammetry Project

Fig. 41 a and b. Rectified image map of sandbar 145.5L, 1/30/93 and 1/31/93.

Sandbar 145.5L

Grand Canyon, Arizona

3/15/93



River Flow 

Scale



Area (sq. m) = 933
 Perimeter (m) = 138
 Ave. Input Pixel Size (sq. m) = 0.14
 Total RMS Error (pix) = 7.11

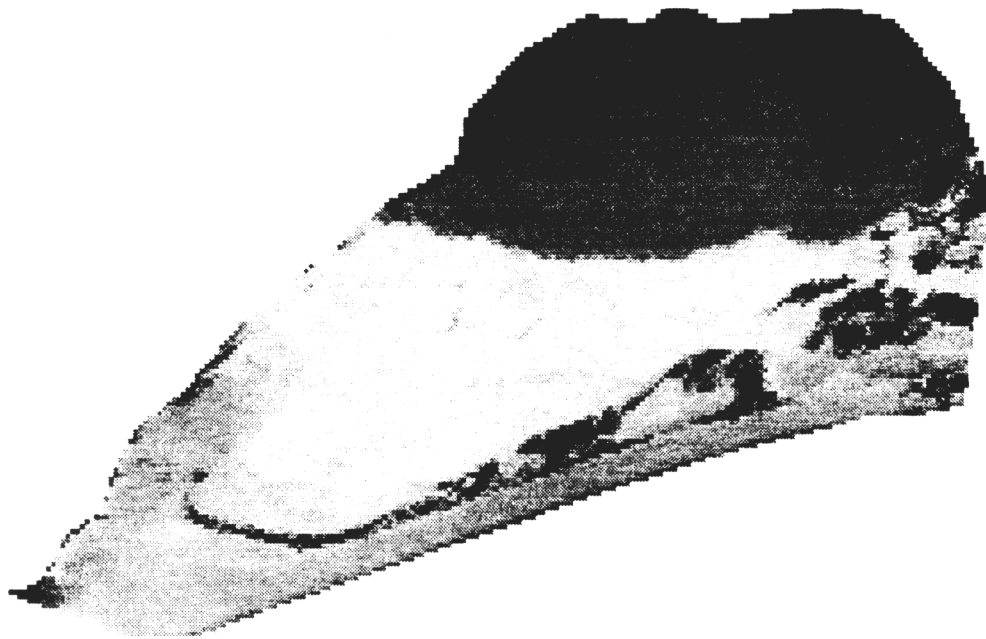
Northern Arizona University
 Department of Geography, GIS Lab
 Sandbar Photogrammetry Project

Fig. 42. Rectified image map of sandbar 145.5L, 3/15/93.

Sandbar 145.5L

Grand Canyon, Arizona

5/31/93



River Flow 

Scale



Area (sq. m) = 931
Perimeter (m) = 139
Ave. Input Pixel Size (sq. m) = 0.14
Total RMS Error (pix) = 7.11

Northern Arizona University
Department of Geography, GIS Lab
Sandbar Photogrammetry Project

Fig. 43. Rectified image map of sandbar 145.5L, 5/31/93.

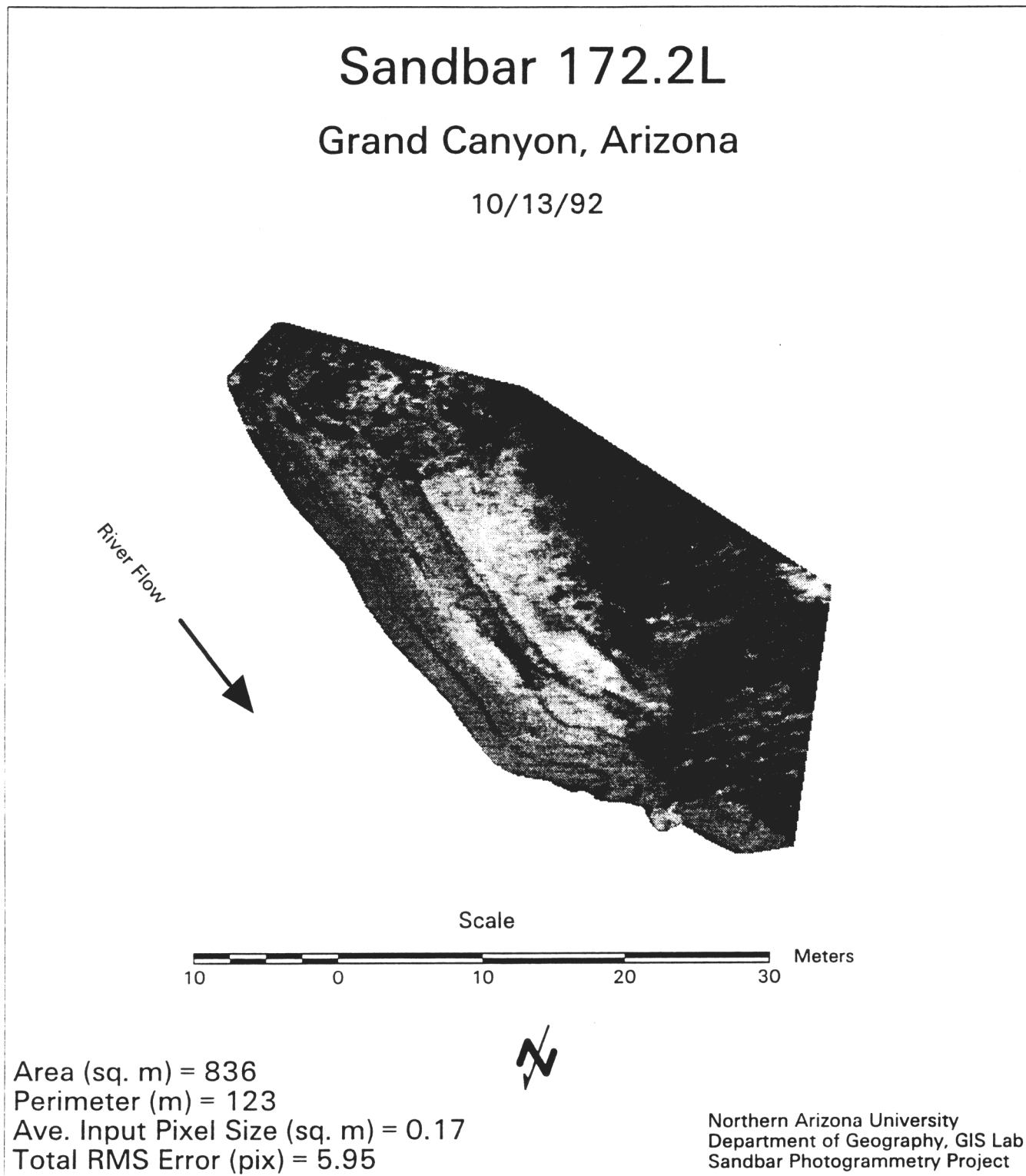
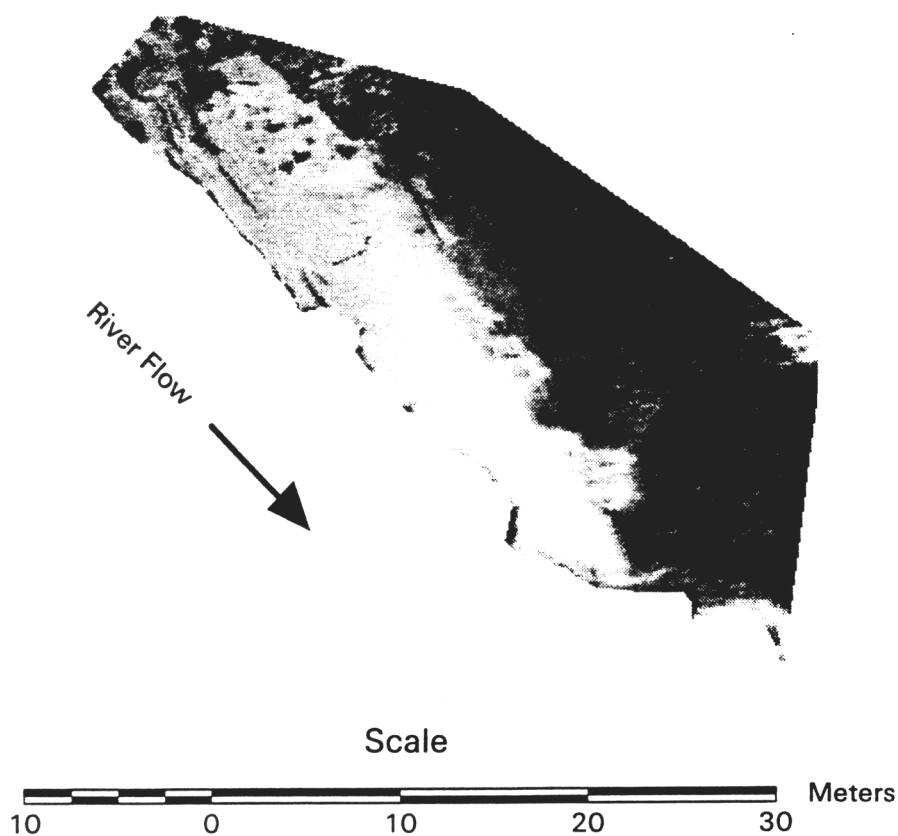


Fig. 44. Rectified image map of sandbar 172.2L, 10/13/92.

Sandbar 172.2L

Grand Canyon, Arizona

5/31/93



Area (sq. m) = 590
Perimeter (m) = 117
Ave. Input Pixel Size (sq. m) = 0.17
Total RMS Error (pix) = 5.95

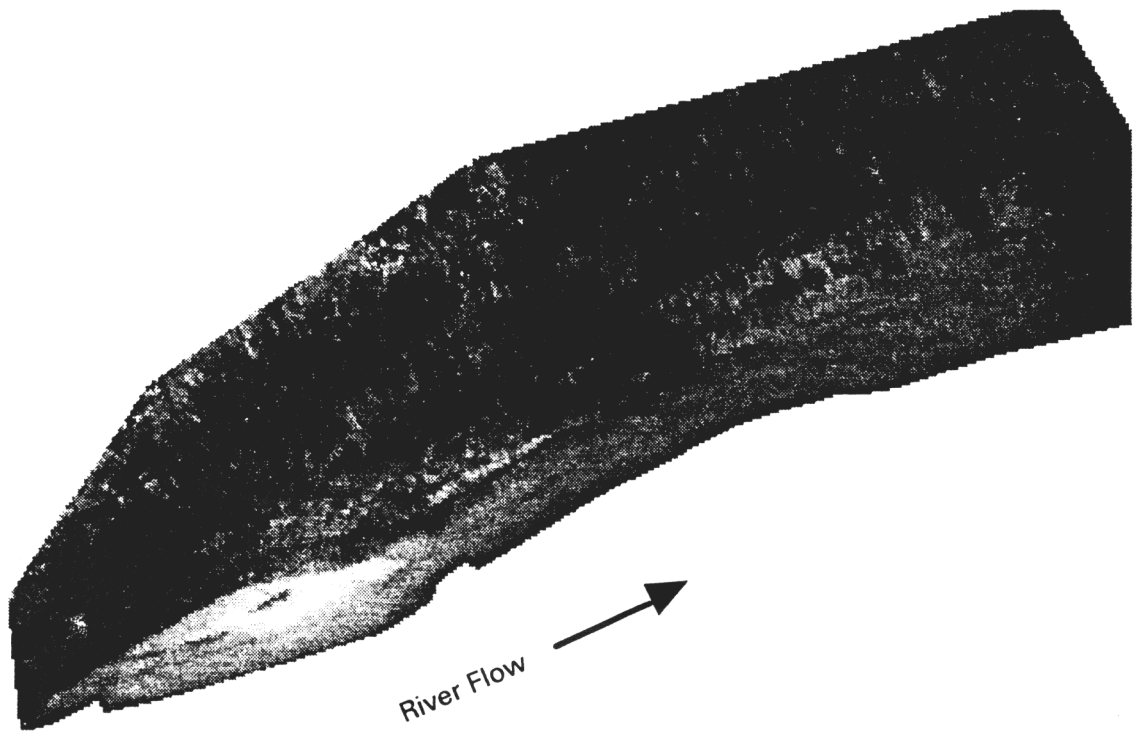
Northern Arizona University
Department of Geography, GIS Lab
Sandbar Photogrammetry Project

Fig. 45. Rectified image map of sandbar 172.2L, 5/31/93.

Sandbar 172.3L

Grand Canyon, Arizona

10/13/92



River Flow 

Scale



Area (sq. m) = 1678
Perimeter (m) = 196
Ave. Input Pixel Size (sq. m) = 0.16
Total RMS Error (pix) = 6.45



Northern Arizona University
Department of Geography, GIS Lab
Sandbar Photogrammetry Project

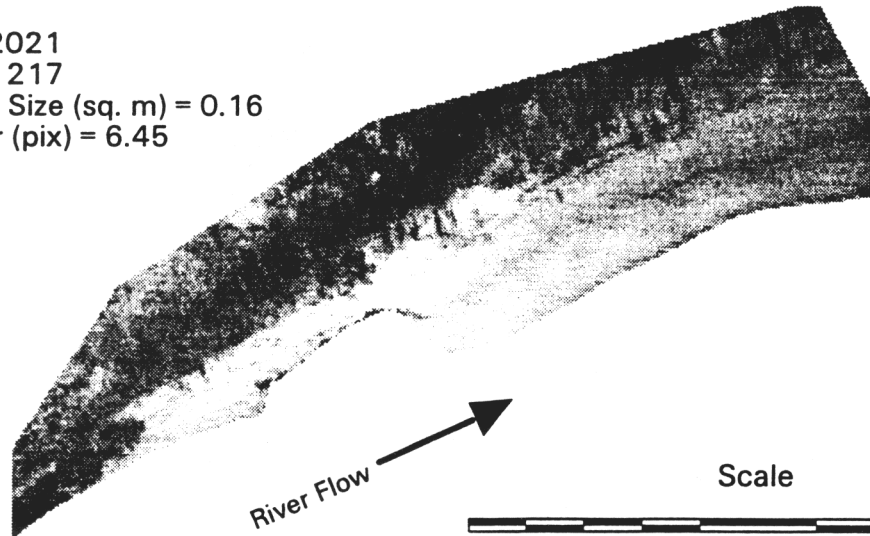
Fig. 46. Rectified image map of sandbar 172.3L, 10/13/92.

Sandbar 172.3L

Grand Canyon, Arizona

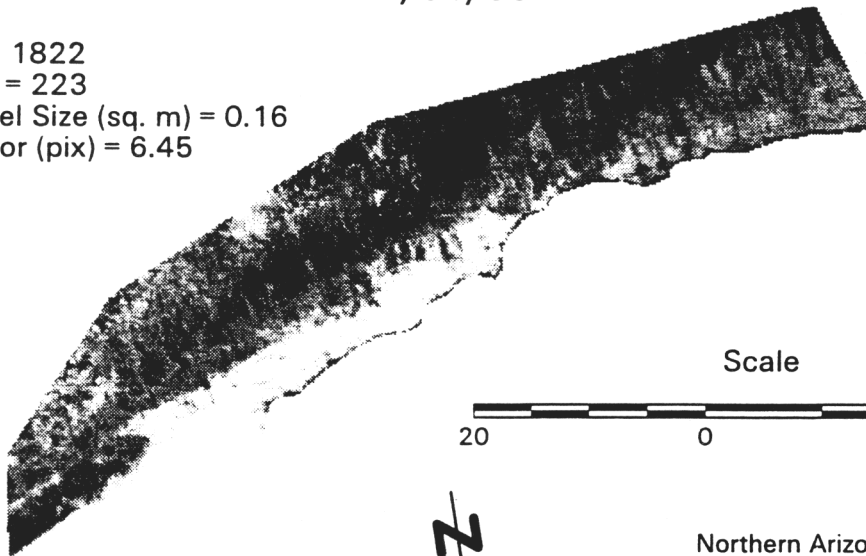
1/30/93

Area (sq. m) = 2021
Perimeter (m) = 217
Ave. Input Pixel Size (sq. m) = 0.16
Total RMS Error (pix) = 6.45



1/31/93

Area (sq. m) = 1822
Perimeter (m) = 223
Ave. Input Pixel Size (sq. m) = 0.16
Total RMS Error (pix) = 6.45



Northern Arizona University
Department of Geography, GIS Lab
Sandbar Photogrammetry Project

Fig. 47 a and b. Rectified image map of sandbar 172.3L, 1/30/93 and 1/31/93.

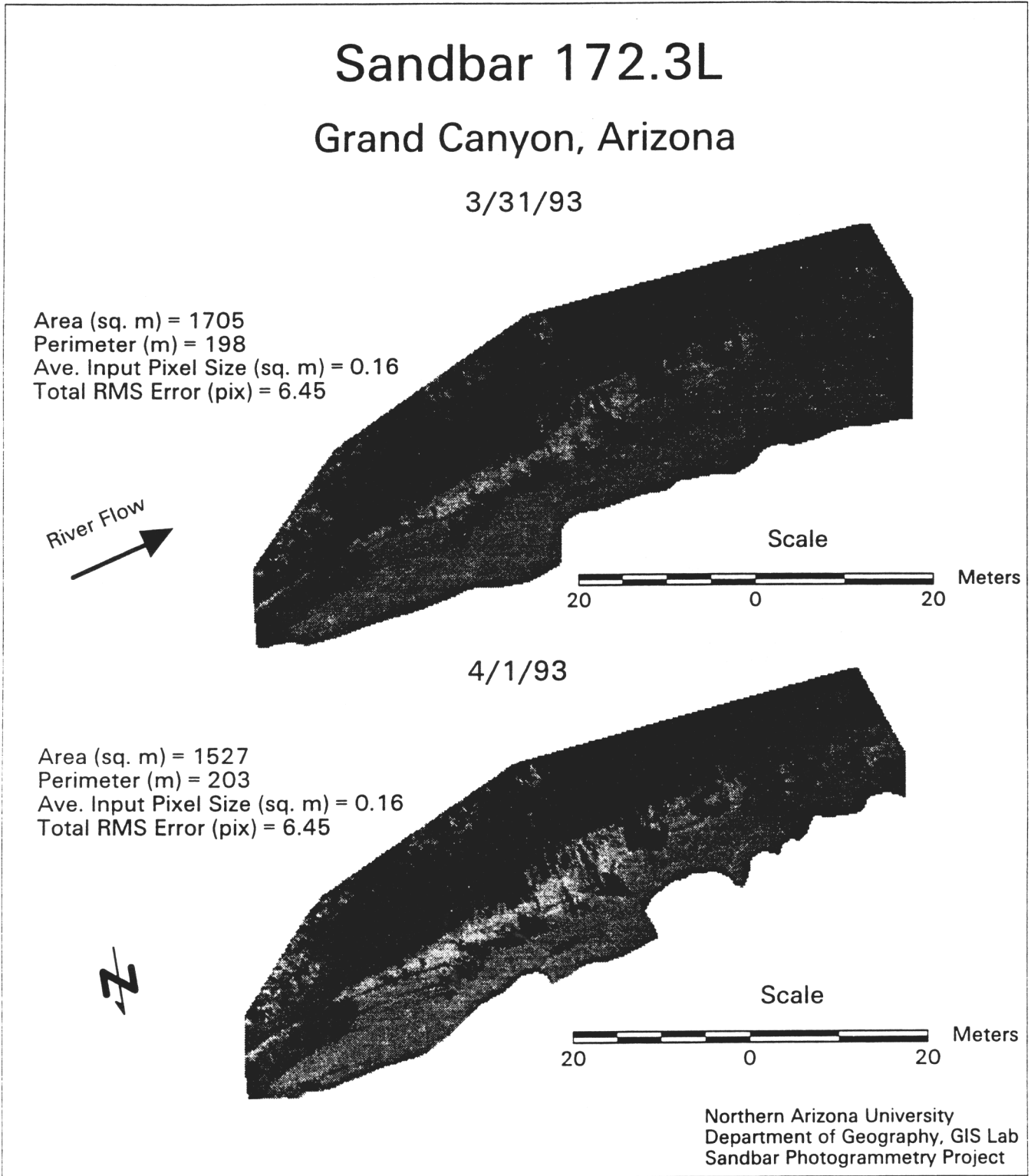
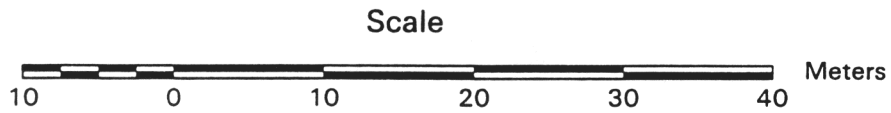
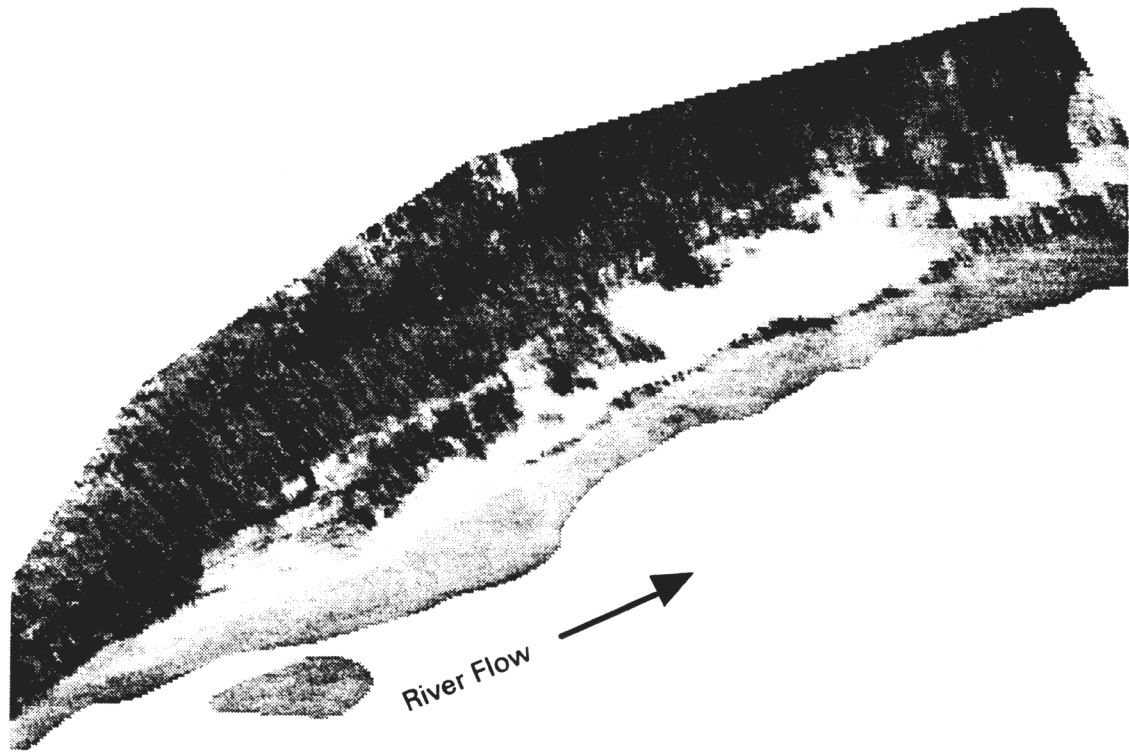


Fig. 48 a and b. Rectified image map of sandbar 172.3L, 3/31/93 and 4/1/93.

Sandbar 172.3L

Grand Canyon, Arizona

5/31/93



Area (sq. m) = 1647
Perimeter (m) = 222
Ave. Input Pixel Size (sq. m) = 0.16
Total RMS Error (pix) = 6.45

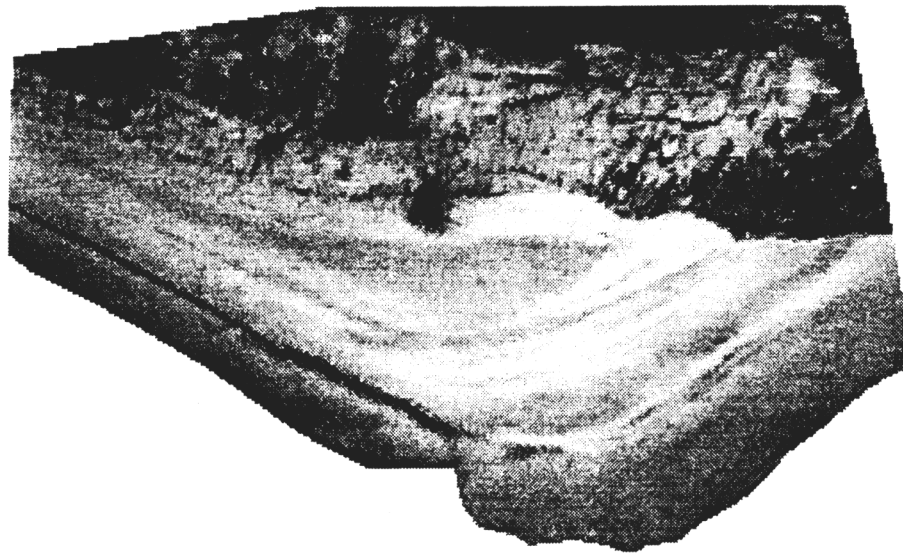
Northern Arizona University
Department of Geography, GIS Lab
Sandbar Photogrammetry Project

Fig. 49. Rectified image map of sandbar 172.3L, 5/31/93.

Sandbar 173.1R

Grand Canyon, Arizona

10/12/92



River Flow



Scale



Area (sq. m) = 1997
Perimeter (m) = 182
Ave. Input Pixel Size (sq. m) = 0.08
Total RMS Error (pix) = 3.34

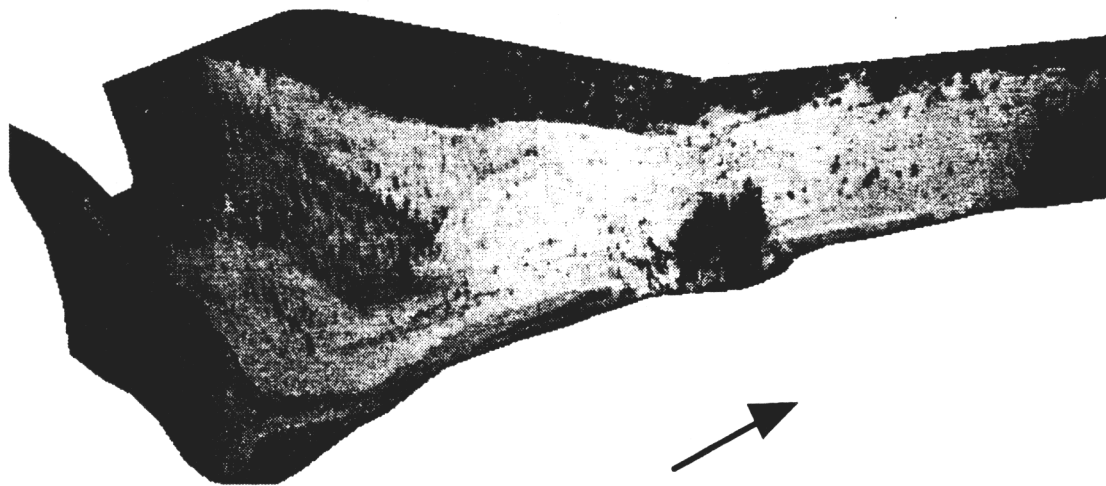
Northern Arizona University
Department of Geography, GIS Lab
Sandbar Photogrammetry Project

Fig. 50. Rectified image map of sandbar 173.1R, 10/12/92.

Sandbar 211.3L

Grand Canyon, Arizona

10/13/92



River Flow



Scale



Area (sq. m) = 4083
Perimeter (m) = 340
Ave. Input Pixel Size (sq. m) = 0.14
Total RMS Error (pix) = 7.99

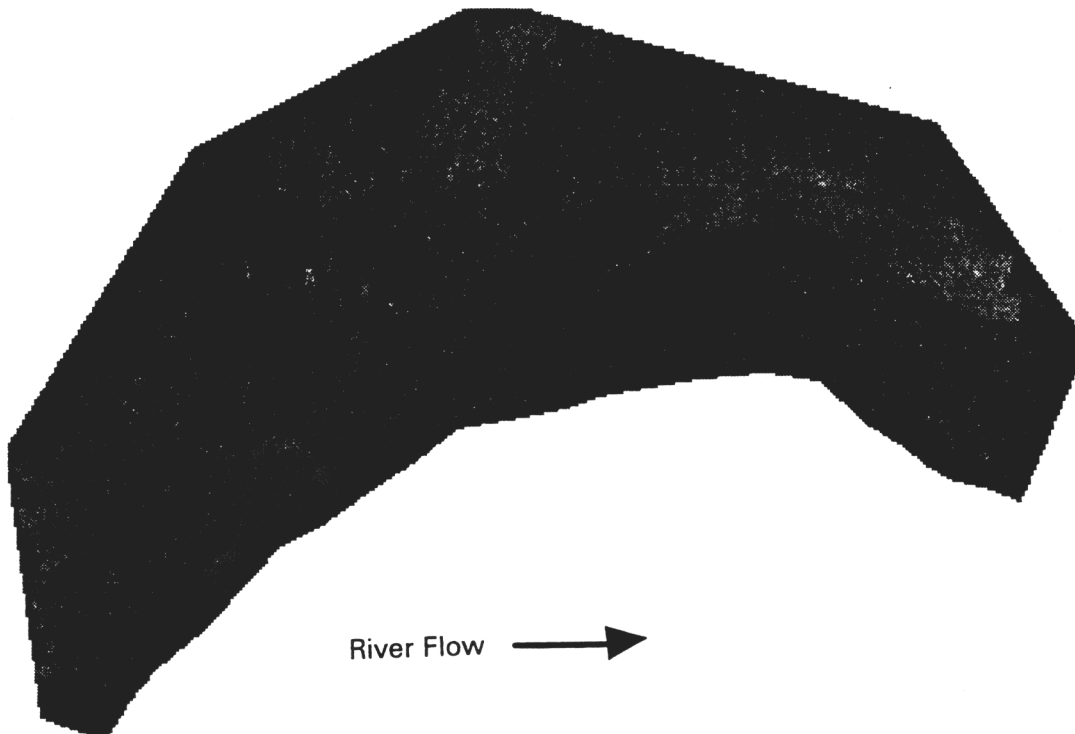
Northern Arizona University
Department of Geography, GIS Lab
Sandbar Photogrammetry Project

Fig. 51. Rectified image map of sandbar 211.3L, 10/13/92.

Sandbar 212.9L

Grand Canyon, Arizona

10/12/92



River Flow →

Scale



Area (sq. m) = 2911
Perimeter (m) = 261
Ave. Input Pixel Size (sq. m) = 0.16
Total RMS Error (pix) = 3.34

Northern Arizona University
Department of Geography, GIS Lab
Sandbar Photogrammetry Project

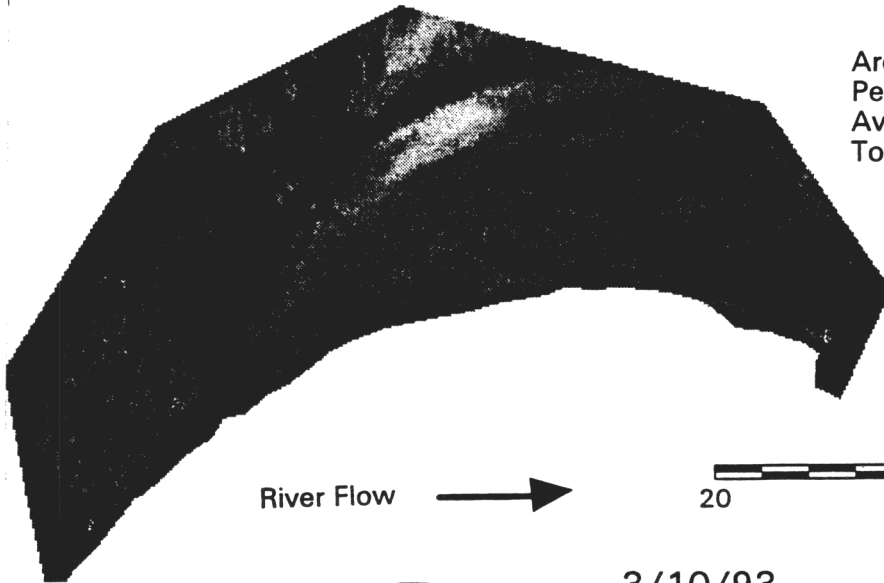
Fig. 52. Rectified image map of sandbar 212.9L, 10/12/92.

Sandbar 212.9L

Grand Canyon, Arizona

3/9/93

Area (sq. m) = 2593
Perimeter (m) = 262
Ave. Input Pixel Size (sq. m) = 0.16
Total RMS Error (pix) = 3.34



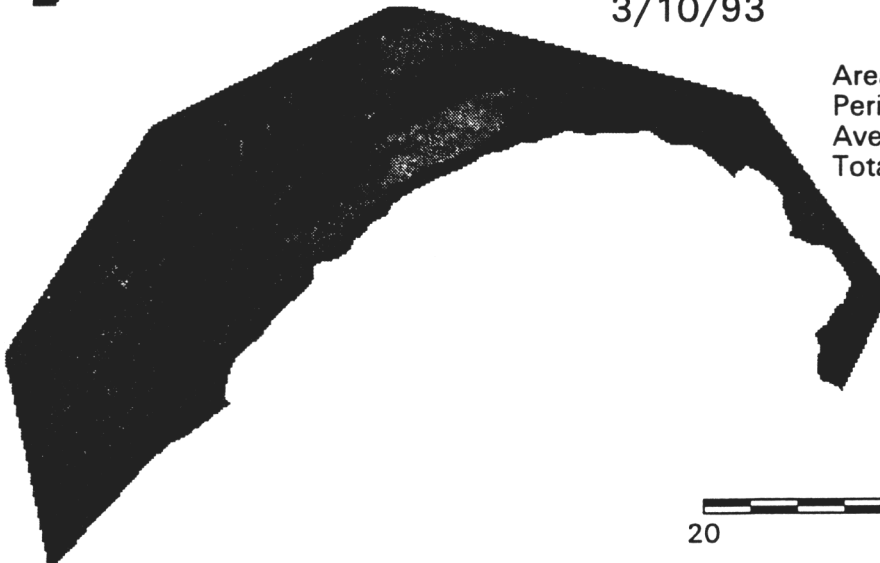
River Flow →

Scale



3/10/93

Area (sq. m) = 1657
Perimeter (m) = 287
Ave. Input Pixel Size (sq. m) = 0.16
Total RMS Error (pix) = 3.34



Scale



Northern Arizona University
Department of Geography, GIS Lab
Sandbar Photogrammetry Project

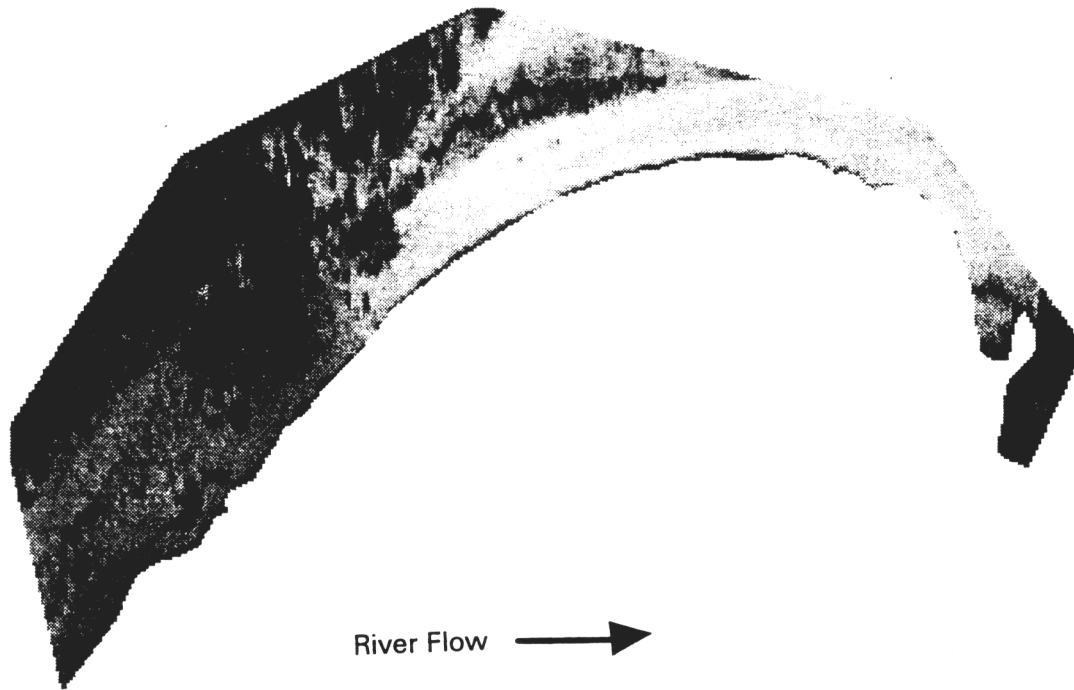


Fig. 53 a and b. Rectified image map of sandbar 212.9L, 3/9/93 and 3/10/93.

Sandbar 212.9L

Grand Canyon, Arizona

4/17/93



River Flow →

Scale



Area (sq. m) = 1581
Perimeter (m) = 290
Ave. Input Pixel Size (sq. m) = 0.16
Total RMS Error (pix) = 3.34

Northern Arizona University
Department of Geography, GIS Lab
Sandbar Photogrammetry Project

Fig. 54. Rectified image map of sandbar 212.9L, 4/17/93.

Table 5. Summary statistics for the twenty sandbars included in this study. Time span covers from March 15, 1992 to December 31, 1993.

MILE	S.I.	BEGIN. AREA (m ²)	END AREA (m ²)	% CHNG.	MAX. AREA (m ²)	MIN. AREA (m ²)	% TOT. DIFF.	MEAN (m ²)	STD. DEV.	C.V.	WI.	NO. EVENT.	MEAN EV. SIZE (m ²)
2.6	1	1529	1045	-31.65	2885	633	78.06	1844	595	0.323	2	2	708
16.4	2	1064	935	-12.12	1565	837	46.52	1140	191	0.168	1	3	63
43.1	3	2946	2605	-11.58	3121	2376	23.87	2726	211	0.077	2	3	57
44.6	3	876	411	-53.08	898	406	54.79	661	148	0.224	3	0	0
44.65	2	5288	4754	-10.10	5733	3303	42.39	4644	707	0.152	3	1	201
60.1	1	809	1551	91.72	2460	620	74.80	1379	567	0.411	2	0	0
61.8	2	3247	4522	39.27	5245	2331	55.56	3805	765	0.201	2	3	45
64.0	1	3277	3406	3.94	5662	2018	64.36	3455	948	0.274	3	2	476
81.2	3	1896	1851	-2.37	1987	1611	18.92	1820	106	0.058	1	0	0
119.0	3	3953	3439	-13.00	4168	2811	32.56	3776	315	0.083	2	3	146
122.3	2	5429	4243	-21.85	5429	3261	39.93	4331	609	0.141	2	1	396
122.7	2	3162	3253	2.88	4149	2297	44.64	3432	446	0.13	3	1	44
136.6	3	1220	1152	-5.57	1347	843	37.42	1192	120	0.101	1	0	0
136.7	2	2861	2025	-29.22	3196	2025	36.64	2664	283	0.106	1	0	0
145.5	3	907	865	-4.63	965	745	22.80	870	70	0.08	1	5	40
172.2	3	770	746	-3.12	851	590	30.67	728	60	0.082	2	7	32
172.3	2	1549	1560	0.71	2136	1024	52.06	1627	267	0.164	2	8	293
173.1	2	1433	1363	-4.88	1977	1254	36.57	1585	214	0.135	2	0	0
211.3	2	3938	3191	-18.97	4839	3115	35.63	3675	393	0.107	2	2	245
212.9	2	2249	2070	-7.96	2911	1442	50.46	2145	442	0.206	2	1	936
MEAN		2420	2249	-5	3076	1677	44	2375	373	0.161	2	2.1	184.1
ST. DV.		1460	1340	29	1664	973	16	1274	255	0.091	1	2.315	262.01

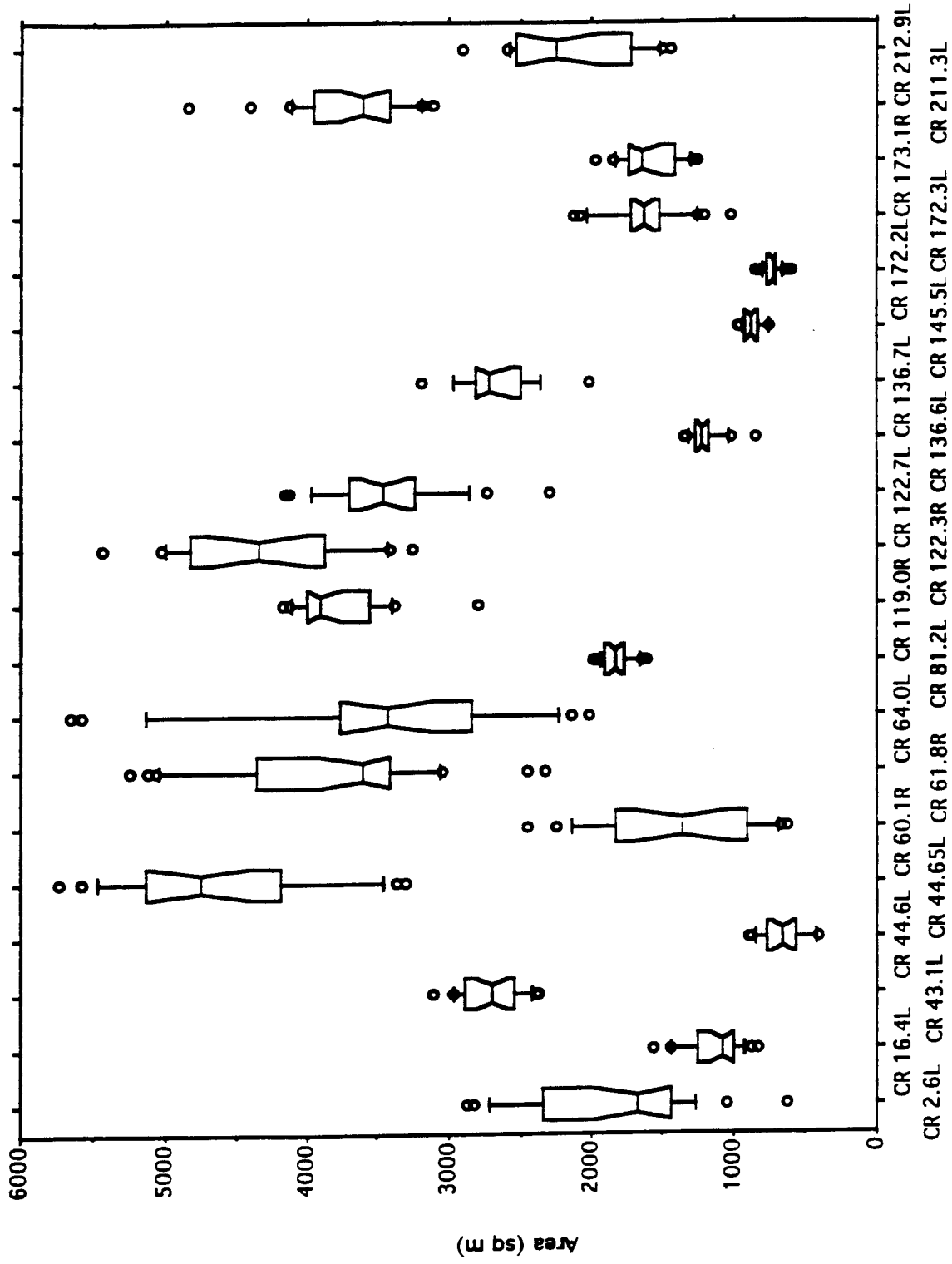


Fig. 55. Box and whisker plots of sandbar area value distribution. The line at the waist of the box is the median, the top of the box is the 75th percentile, the bottom of the box is the 25th percentile, the top whisker is the 90th percentile and the bottom whisker is the 10th percentile. Dots represent individual extreme values. True horizontal axis scale is not implied.

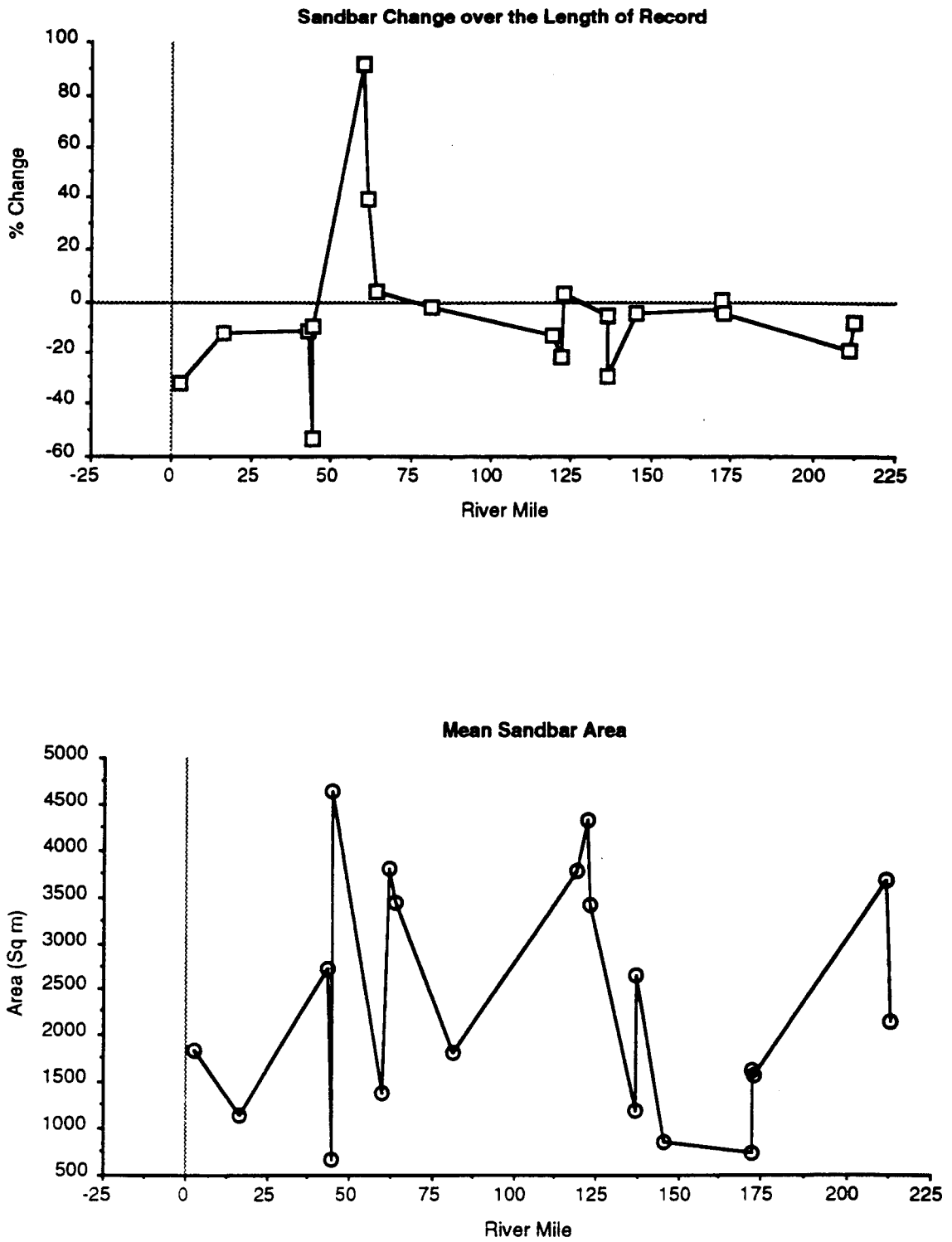


Fig. 56. Relationship between river mile and percent change in area (top) and river mile and mean sandbar area (bottom).

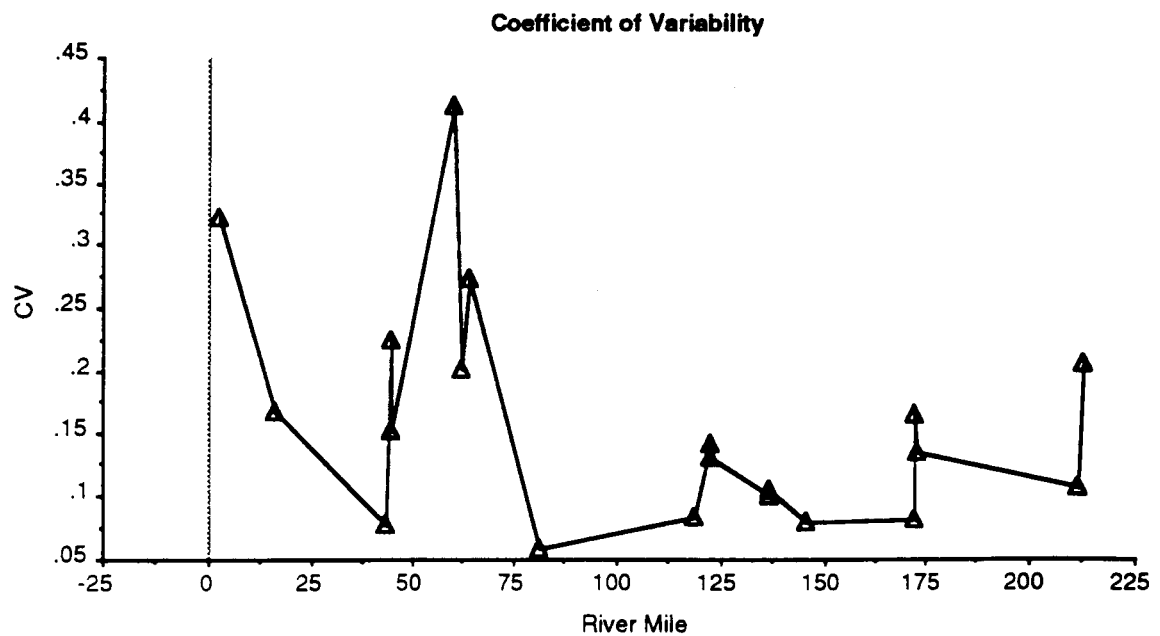
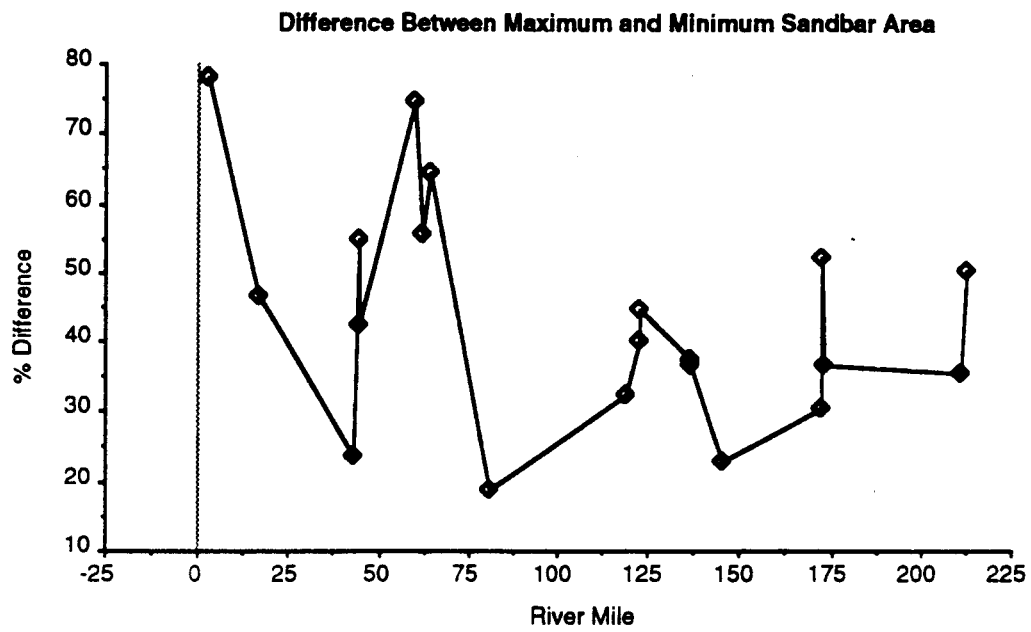


Fig. 57. Relationship between river mile and difference in area (top) and river mile and coefficient of variability (bottom).

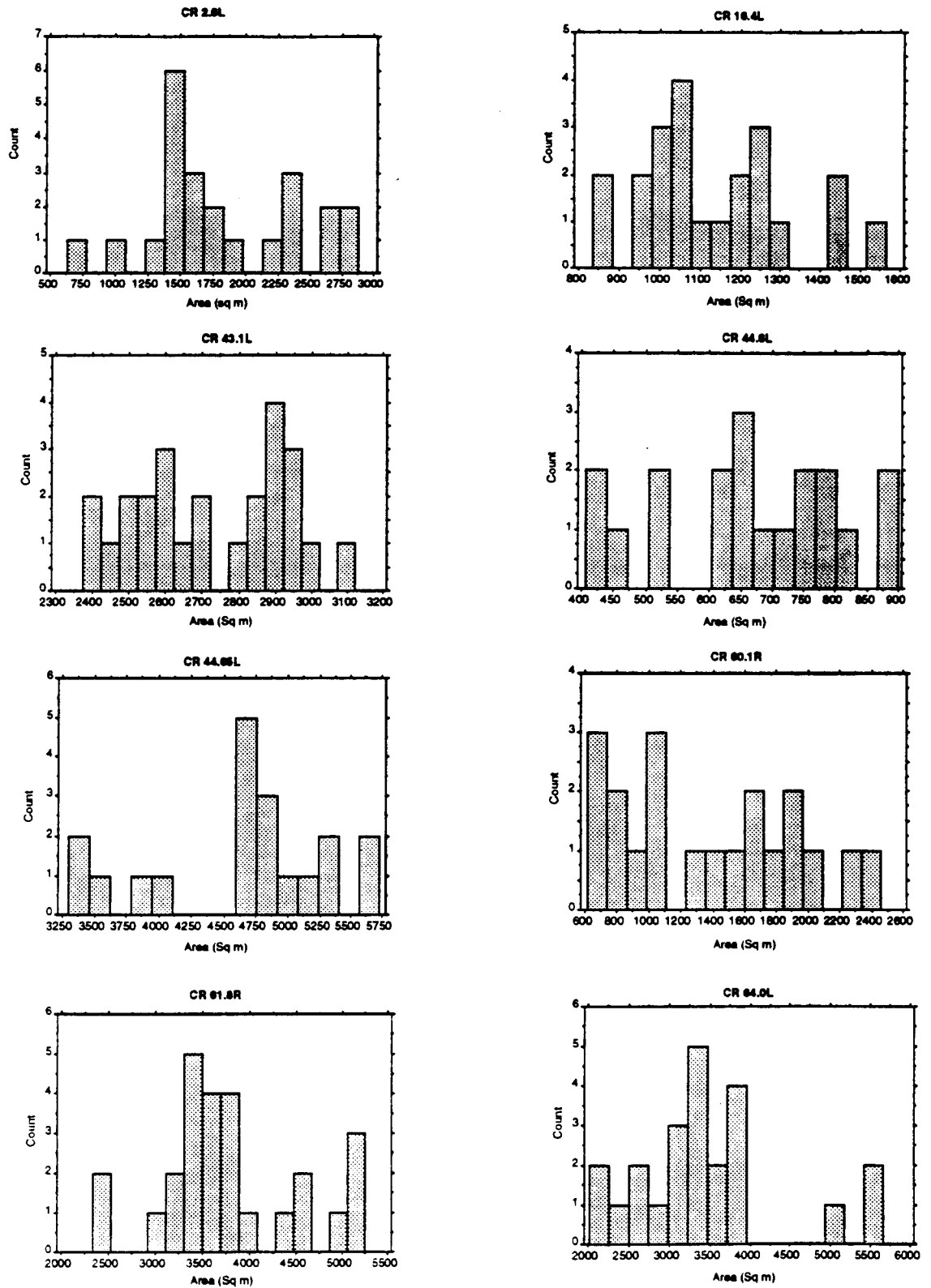


Fig. 58. Composite figure of frequency distributions for the twenty rectified sandbars, March 15, 1992 through December 31, 1993.

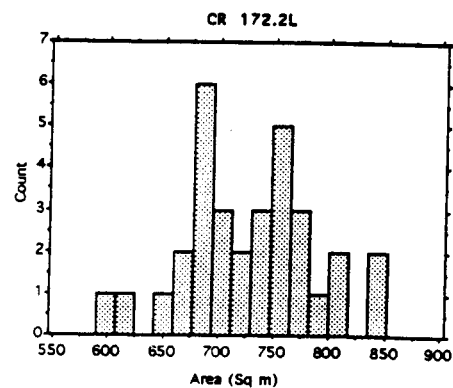
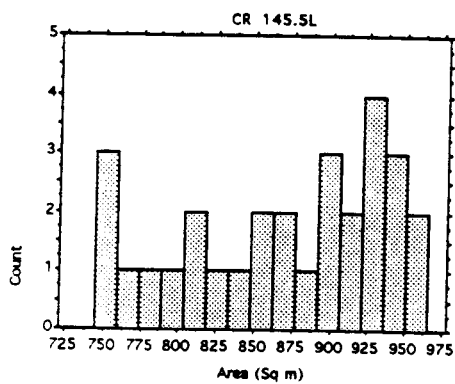
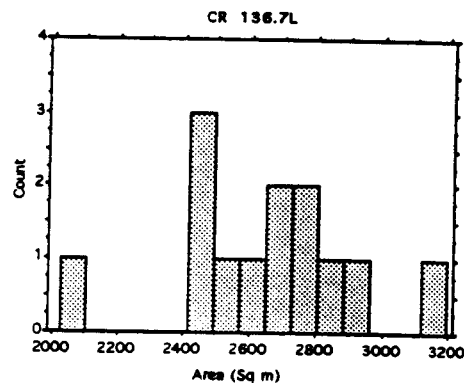
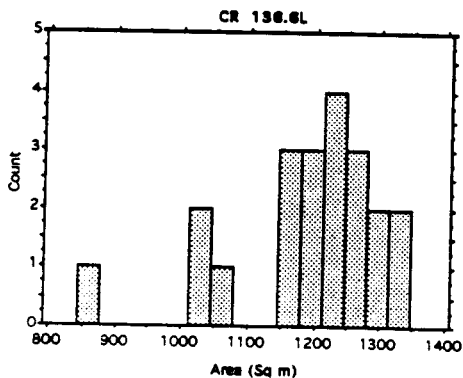
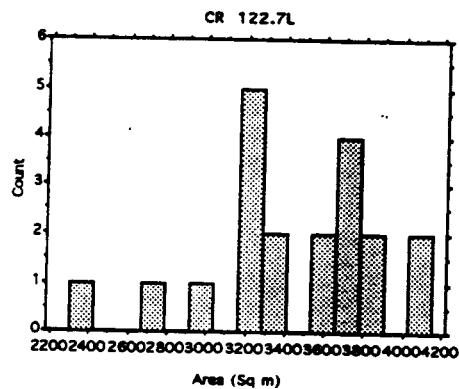
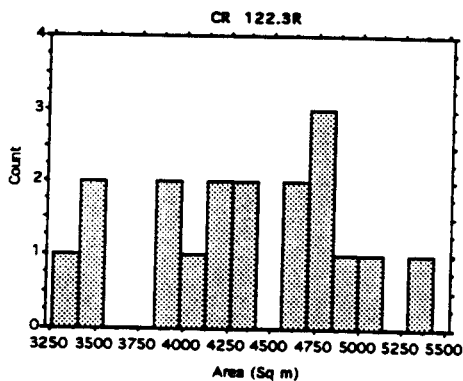
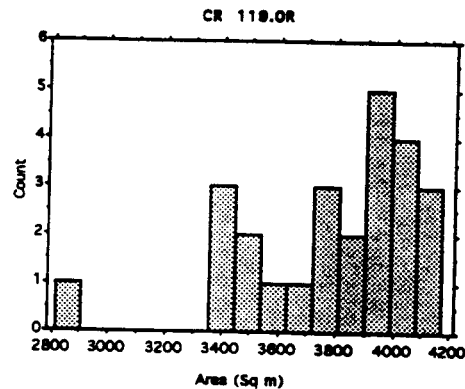
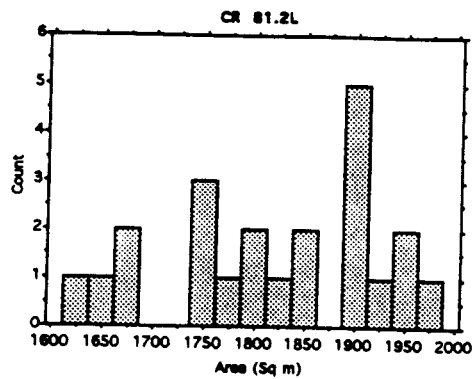


Fig. 58 (Continued). Composite figure of frequency distributions for the twenty rectified sandbars, March 15, 1992 through December 31, 1993.

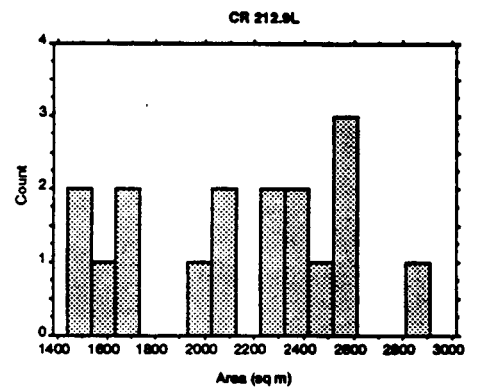
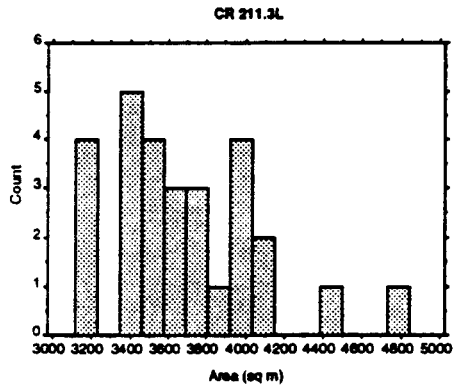
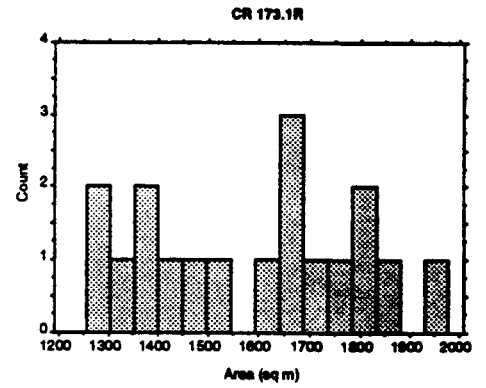
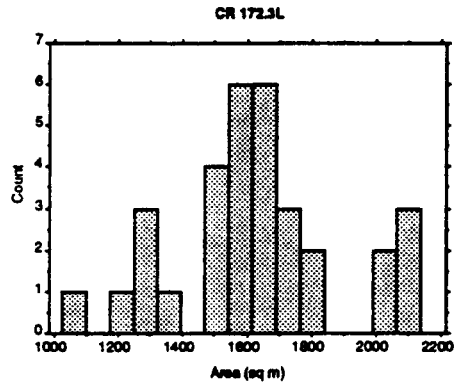


Fig. 58 (Continued). Composite figure of frequency distributions for the twenty rectified sandbars, March 15, 1992 through December 31, 1993.

Table 6. A summary of frequency distribution characteristics of the sandbars included in this study compared to a synthetically generated normally distributed simulated sandbar. Eighteen out of twenty sandbars are strongly bimodal or tail heavy.

SAND BAR	LOWER TAIL	MEAN 3 CLASSES	UPPER TAIL	KURTOSIS	SKEWNESS	MODE TYPE
NORM.	10 29%	15 43%	10 29%	0.083	-0.035	UNIMODAL
2.6L	12 57%	3 14%	6 29%	-0.71	0.17	BIMODAL
16.4L	11 58%	1 5%	7 37%	-0.46	0.51	BIMODAL
43.1L	11 44%	3 12%	11 44%	-1.2	-0.06	BIMODAL
44.6L	5 26%	6 32%	8 42%	-0.88	-0.25	UNIMODAL
44.65L	5 26%	8 42%	6 32%	-0.6	-0.57	BIMODAL
60.1R	9 45%	3 15%	8 40%	-1.13	0.29	BIMODAL
61.8R	10 38%	9 35%	7 27%	-0.39	0.3	BIMODAL
64.0L	6 26%	10 43%	7 30%	0.55	0.87	BIMODAL ?
81.2L	7 32%	4 18%	11 50%	-0.89	-0.36	BIMODAL
119.0R	7 28%	6 24%	12 48%	1.47	-1.2	BIMODAL
122.3R	6 33%	4 22%	8 44%	-0.87	-0.18	UNIMODAL
122.7L	8 40%	4 20%	8 40%	0.47	-0.64	BIMODAL
136.6L	4 19%	10 48%	7 33%	1.54	-1.28	UNIMODAL
136.7L	4 31%	4 31%	5 38%	0.63	-0.4	BIMODAL
145.5L	10 34%	5 17%	14 48%	-1.08	-0.46	BIMODAL
172.2L	11 34%	8 25%	13 41%	-0.22	-0.05	BIMODAL
172.3L	10 31%	15 47%	7 22%	-0.06	0.08	UNIMODAL
173.1R	7 39%	2 11%	9 50%	-1.1	0.01	BIMODAL
211.3L	13 46%	7 25%	8 29%	1.05	0.99	BIMODAL
212.9L	6 35%	4 24%	7 41%	-1.11	-0.15	BIMODAL ?

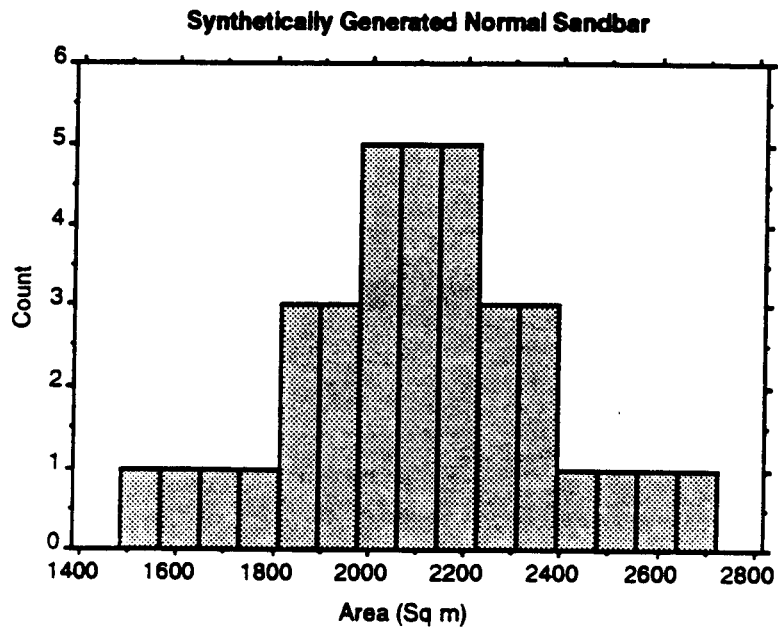


Fig. 59. Frequency distribution of a synthetic sandbar. This normal distribution was generated to produce area values and a sample size similar to that acquired for actual sandbars.

Table 7. Summary statistics for the synthetic normal sandbar distribution.

Mean:	Std. Dev.:	Std. Error:	Variance:	Coef. Var.:	Count:
2104.514	267.611	45.235	71615.904	12.716	35
Minimum:	Maximum:	Range:	Sum:	Sum of Sqr.:	# Missing:
1480	2717	1237	73658	157449254	0
# < 10th %:	10th %:	25th %:	50th %:	75th %:	90th %:
3	1793	1943.25	2100	2289.25	2415
# > 90th %:	Mode:	Geo. Mean:	Har. Mean:	Kurtosis:	Skewness:
3	•	2087.583	2070.149	.083	-.035

Table 8. Seasonal trends in sandbar area. Data in this table were derived by comparing seasonally averaged sandbar areas with the overall mean area for each sandbar. A class was assigned as 1 = smaller than average area, 2 = average area and 3 = larger than average area.

SEASON	SPRING 1992	SUMMER 1992	FALL 1992	WINTER 1993	SPRING 1993	SUMMER 1993	FALL 1993
MILE							
2.6L	1	1	3	3	3	1	1
16.4L	3	3	3	2	1		2
43.1L	3	2	2	1	2		2
44.6L	3	1	3	2	3	2	2
44.65L	2	1	3	1	2		2
60.1R	1	1	2	1	3	3	3
61.8R	1	1	2	2	2		3
64.0L	2	1	1	2	1	3	2
81.2L	3	3	2	1	1	2	3
119.0R	3	3	3	3	3	1	3
122.3R	3		3	2	3	1	2
122.7L	3	2	3	2	3	1	3
136.6L	2	2	3	1	2	1	3
136.7L	2		2	1	3		3
145.5L	3	2	2	1	3	2	3
172.2L	3	2	3	2	1	2	3
172.3L	1	3	3	3	2	1	2
173.1R	1	2	3	3	3	3	2
211.3L	3	1	2	2	3	2	3
212.9L	3	1	3	2	1	2	3
SUM	46	32	51	37	45	27	50
MEAN	2.30	1.78	2.55	1.85	2.25	1.80	2.50
ST. DV.	0.86	0.81	0.60	0.75	0.85	0.77	0.61

Table 9. Distribution characteristics within seasonal subsets of sandbar area data. Data represent numbers of individual frequency distributions from seasonally averaged area values showing each of the following diagnostic distributional characteristics.

Season	Insufficient Data	Bimodal	Unimodal/ Skewed	Unimodal/ No Skew	Total
Spring 92	0	13	2	5	20
Summer 92	5	8	4	3	20
Fall 92	0	12	4	4	20
Winter 93	0	12	5	3	20
Spring 93	2	13	3	2	20
Summer 93	10	8	2	0	20
Fall 93	1	10	3	6	20
Total	18	76	23	23	140
Percent	13	54	16	16	100

2.6L

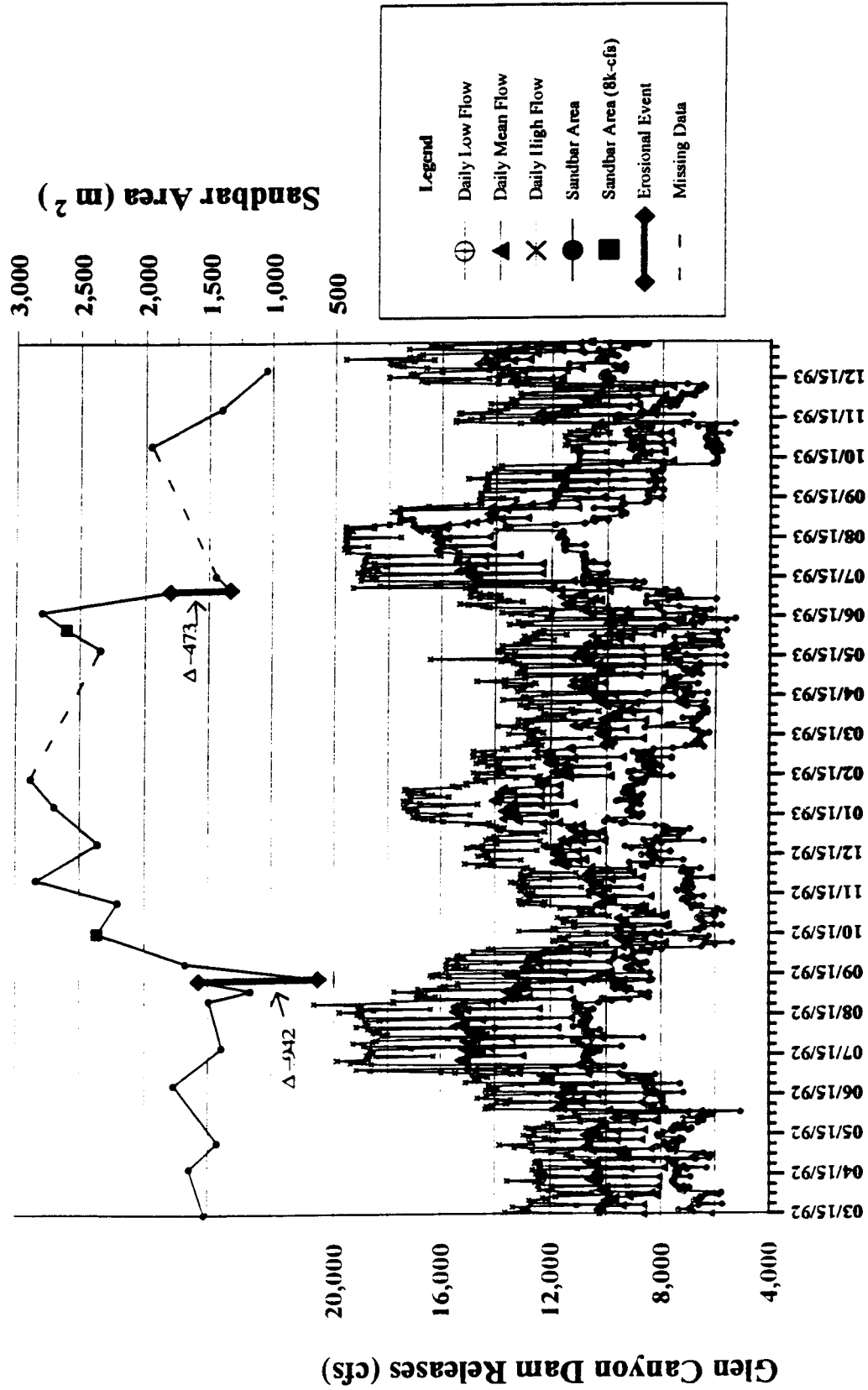


Fig. 60. Time-series plot showing area and discharge for sandbar 2.6L.

16.4L

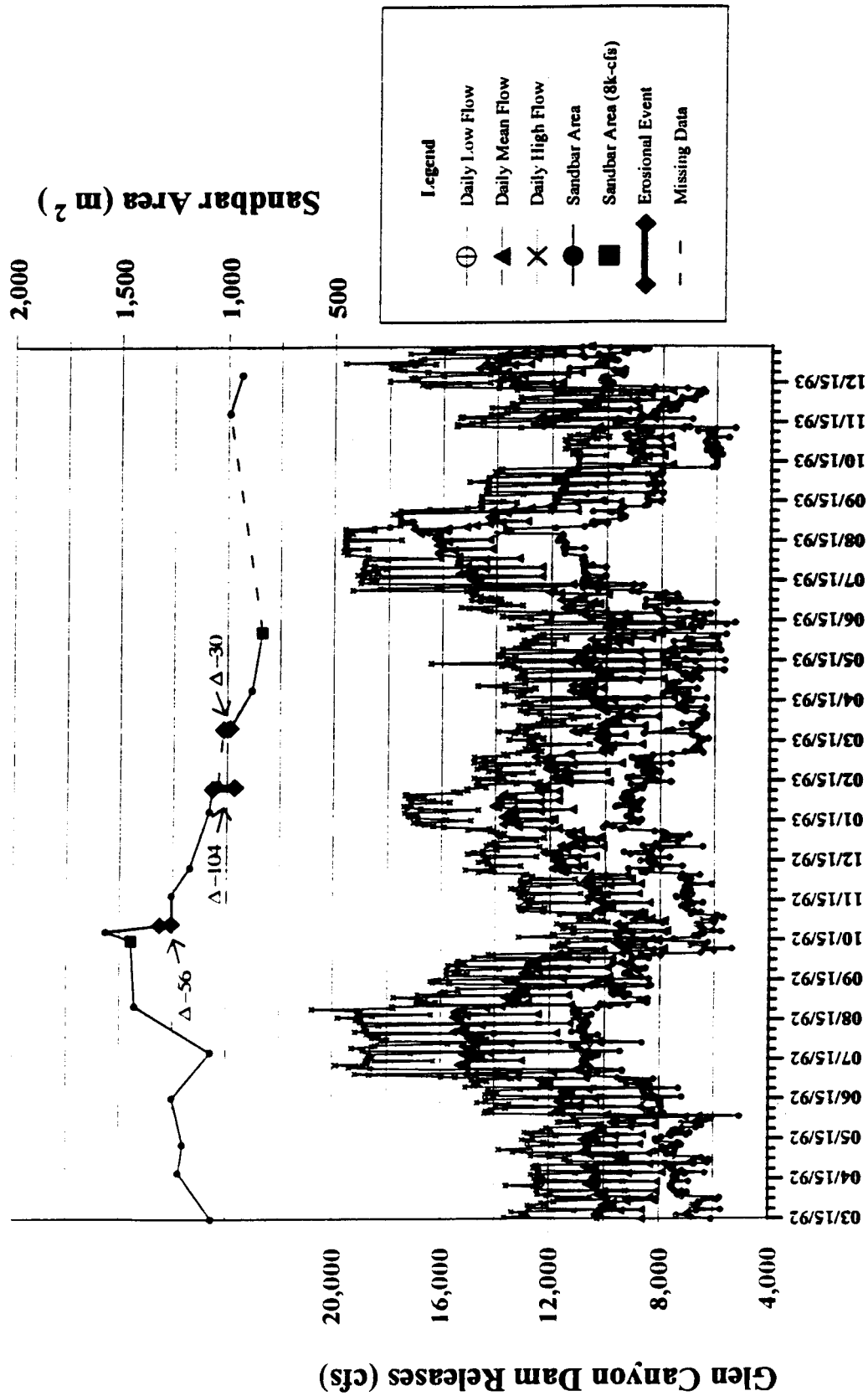


Fig. 61. Time-series plot showing area and discharge for sandbar 16.4L.

43.1L

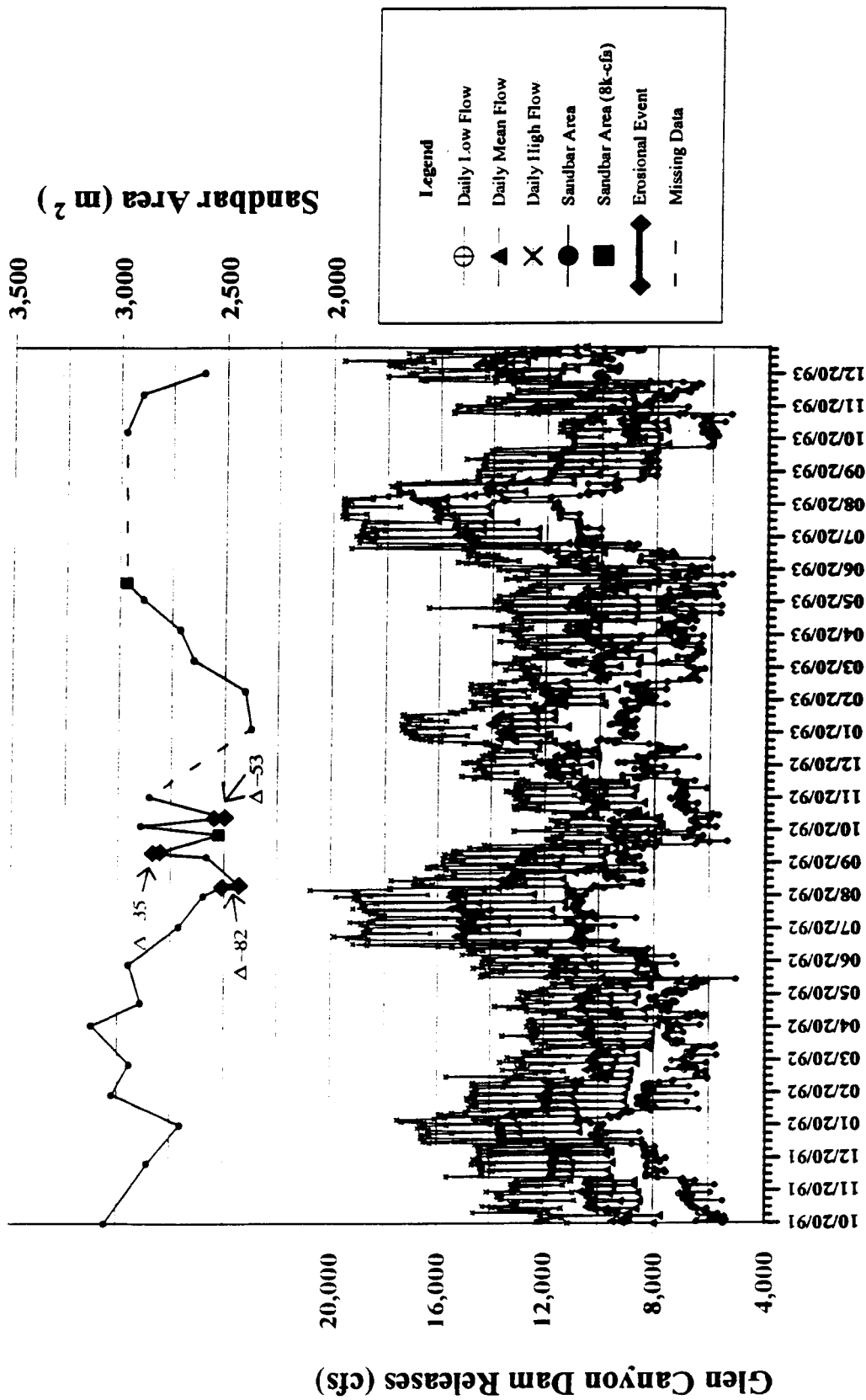


Fig. 62. Time-series plot showing area and discharge for sandbar 43.1L.

44.6L

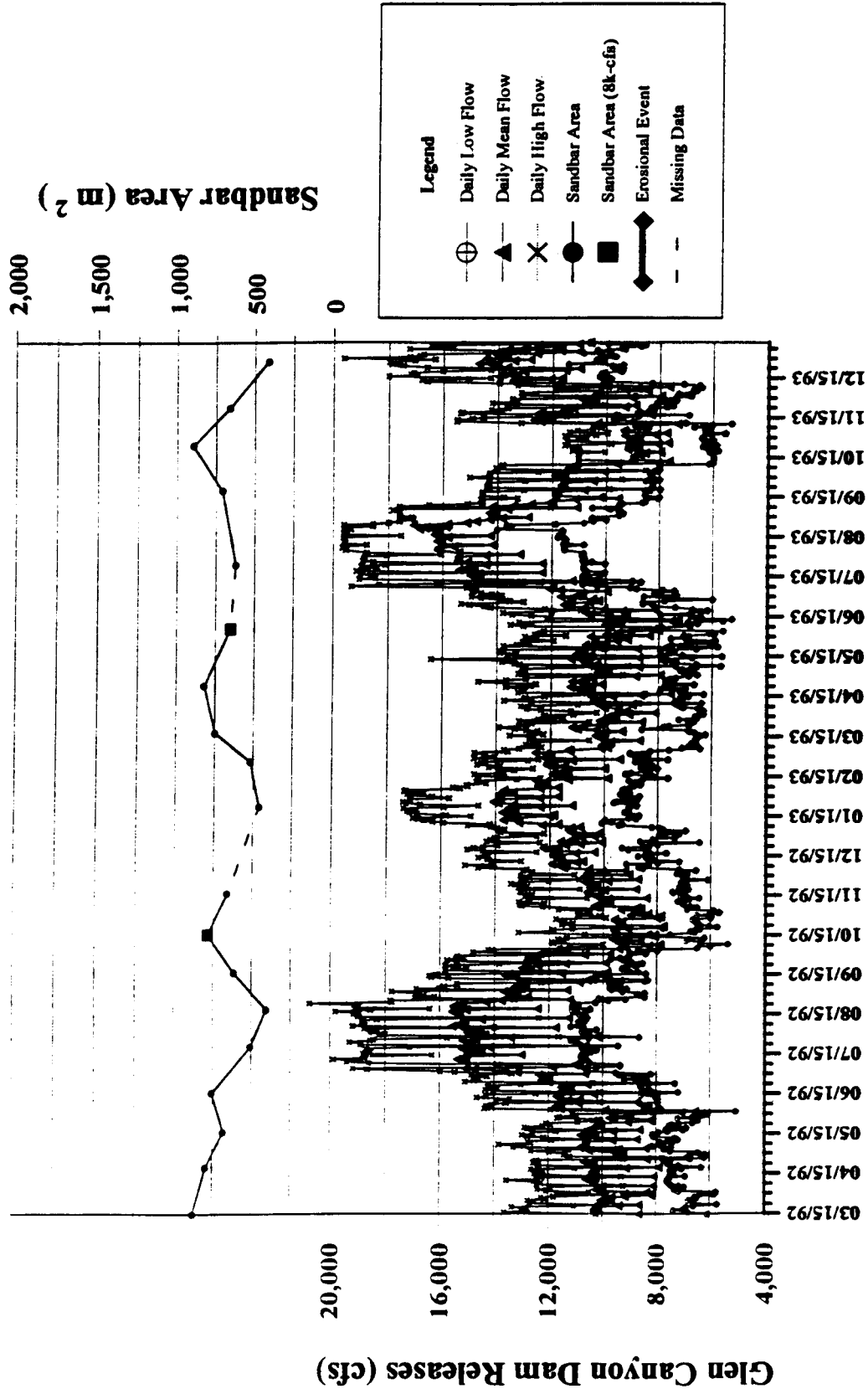


Fig. 63. Time-series plot showing area and discharge for sandbar 44.6L.

44.65L

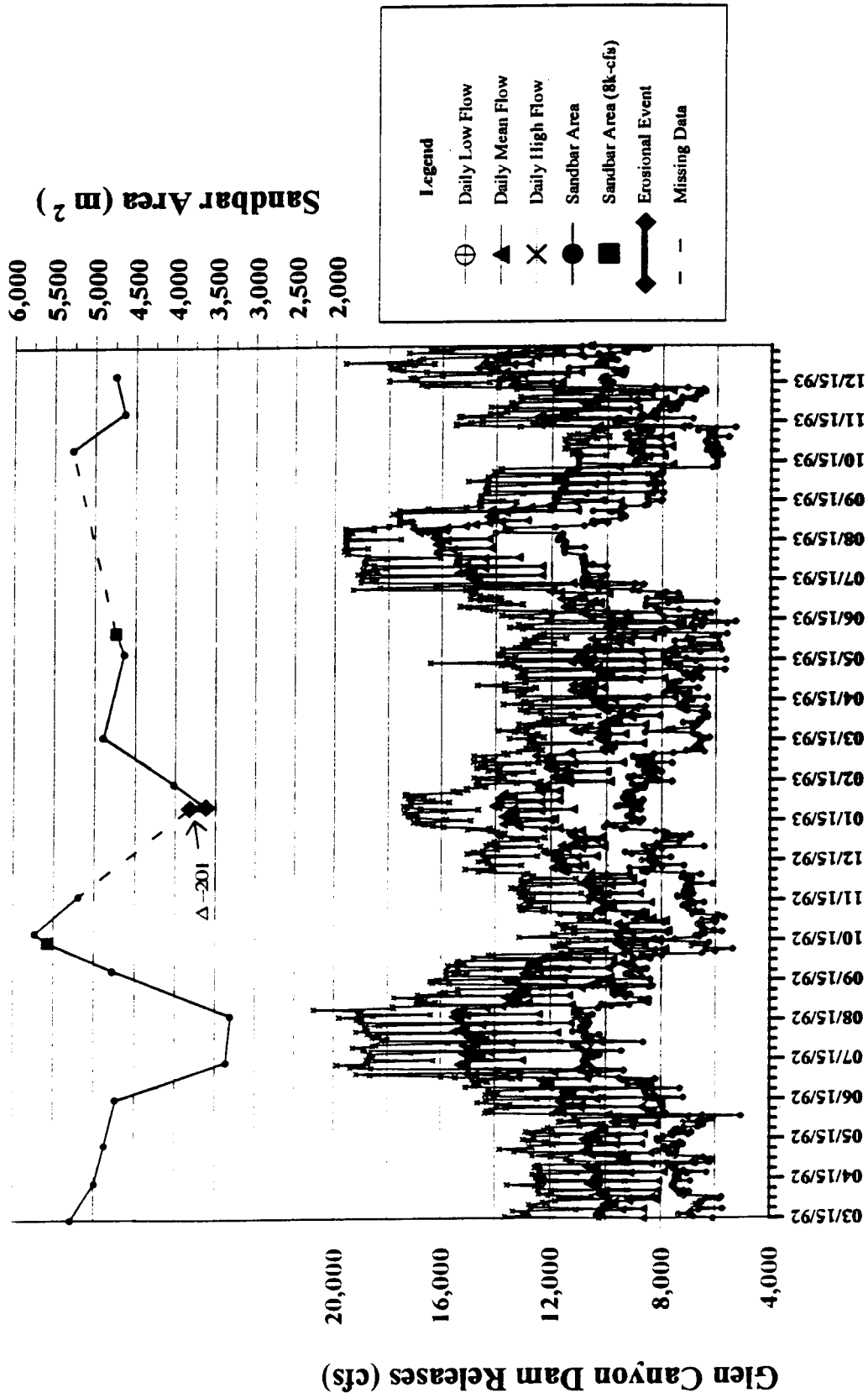


Fig. 64. Time-series plot showing area and discharge for sandbar 44.65L.

60.1R

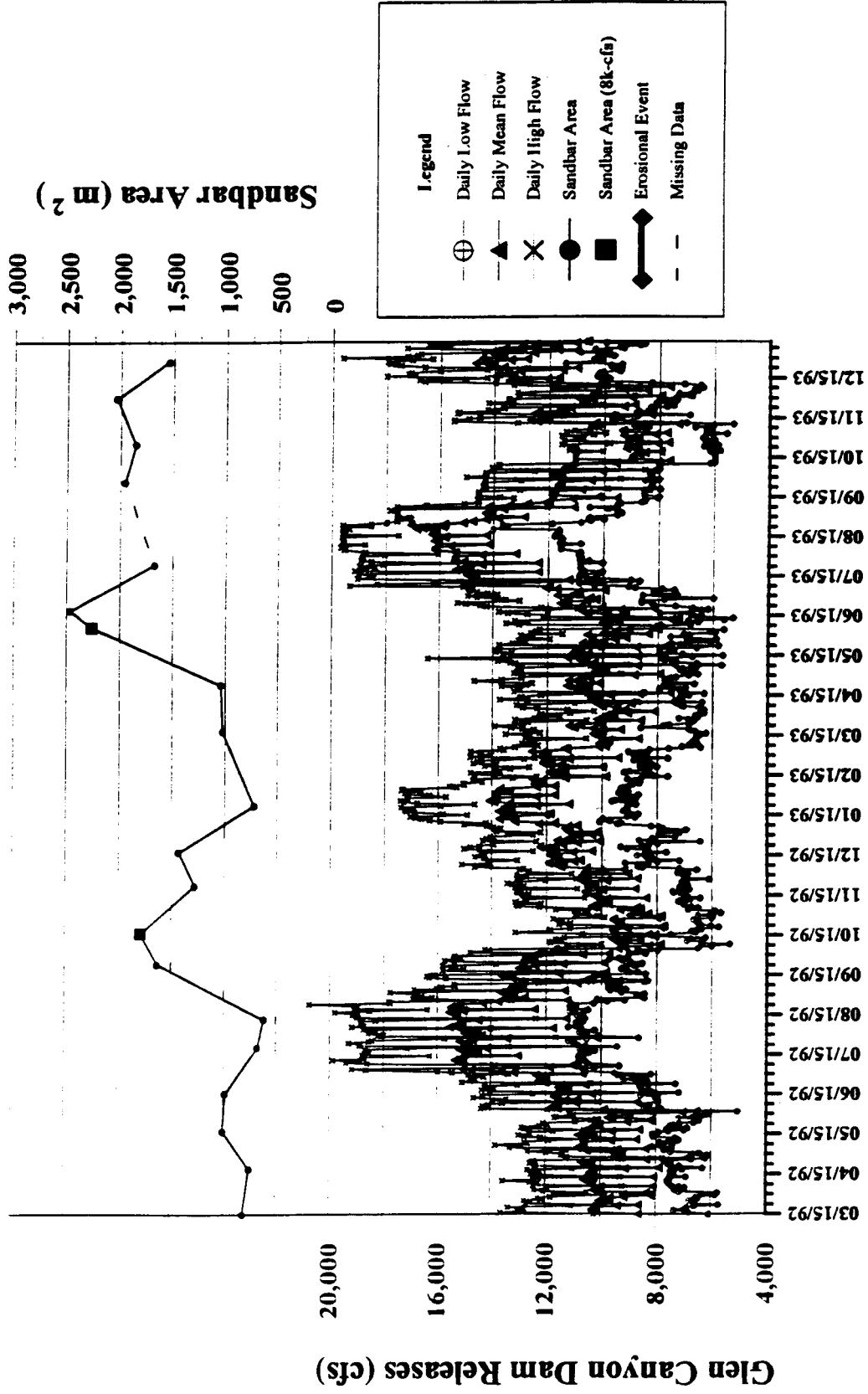


Fig. 65. Time-series plot showing area and discharge for sandbar 60.1L.

61.8R

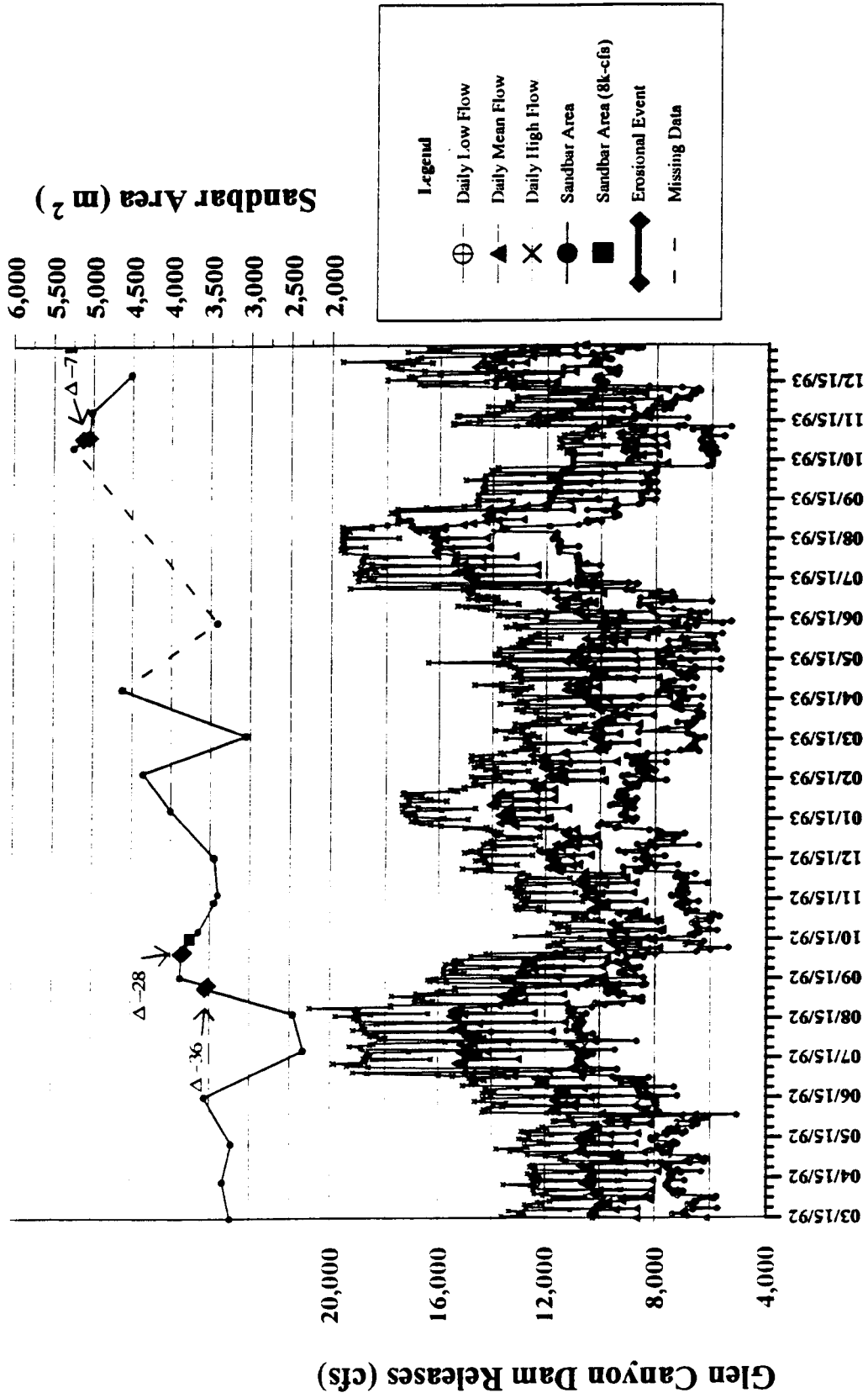


Fig. 66. Time-series plot showing area and discharge for sandbar 61.8R.

64.0L

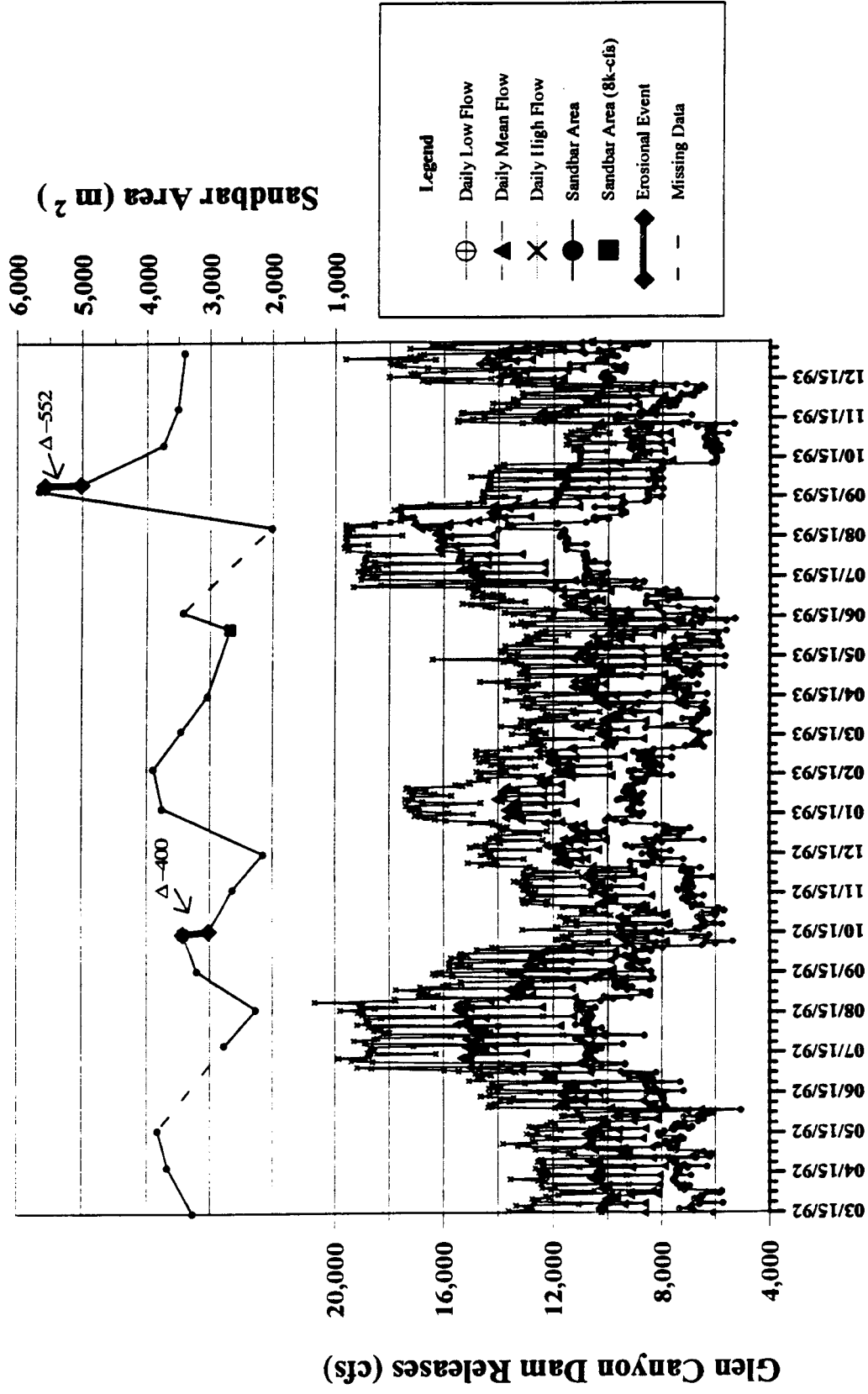


Fig. 67. Time-series plot showing area and discharge for sandbar 64.0L.

81.2L

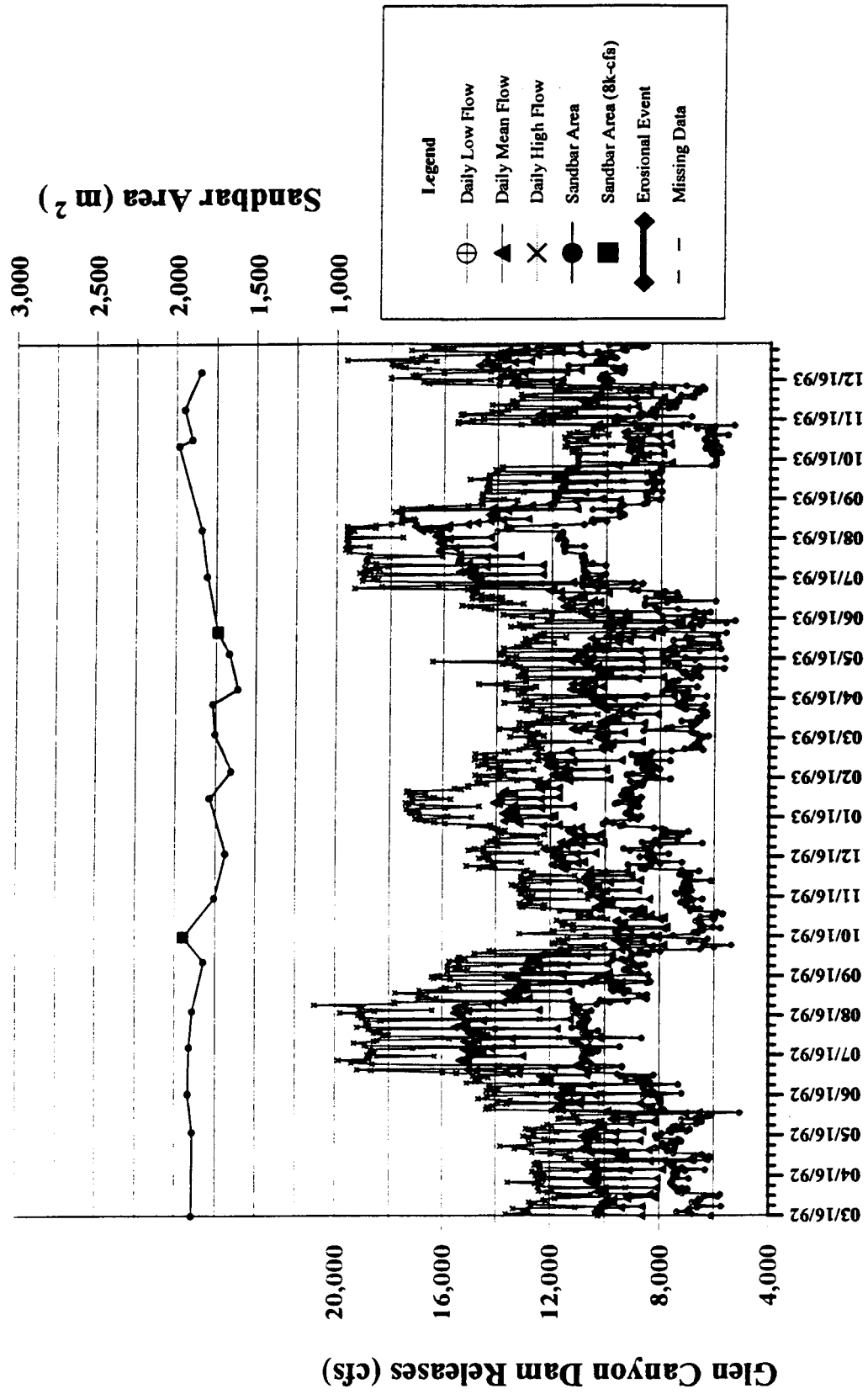


Fig. 68. Time-series plot showing area and discharge for sandbar 81.2L.

119.0R

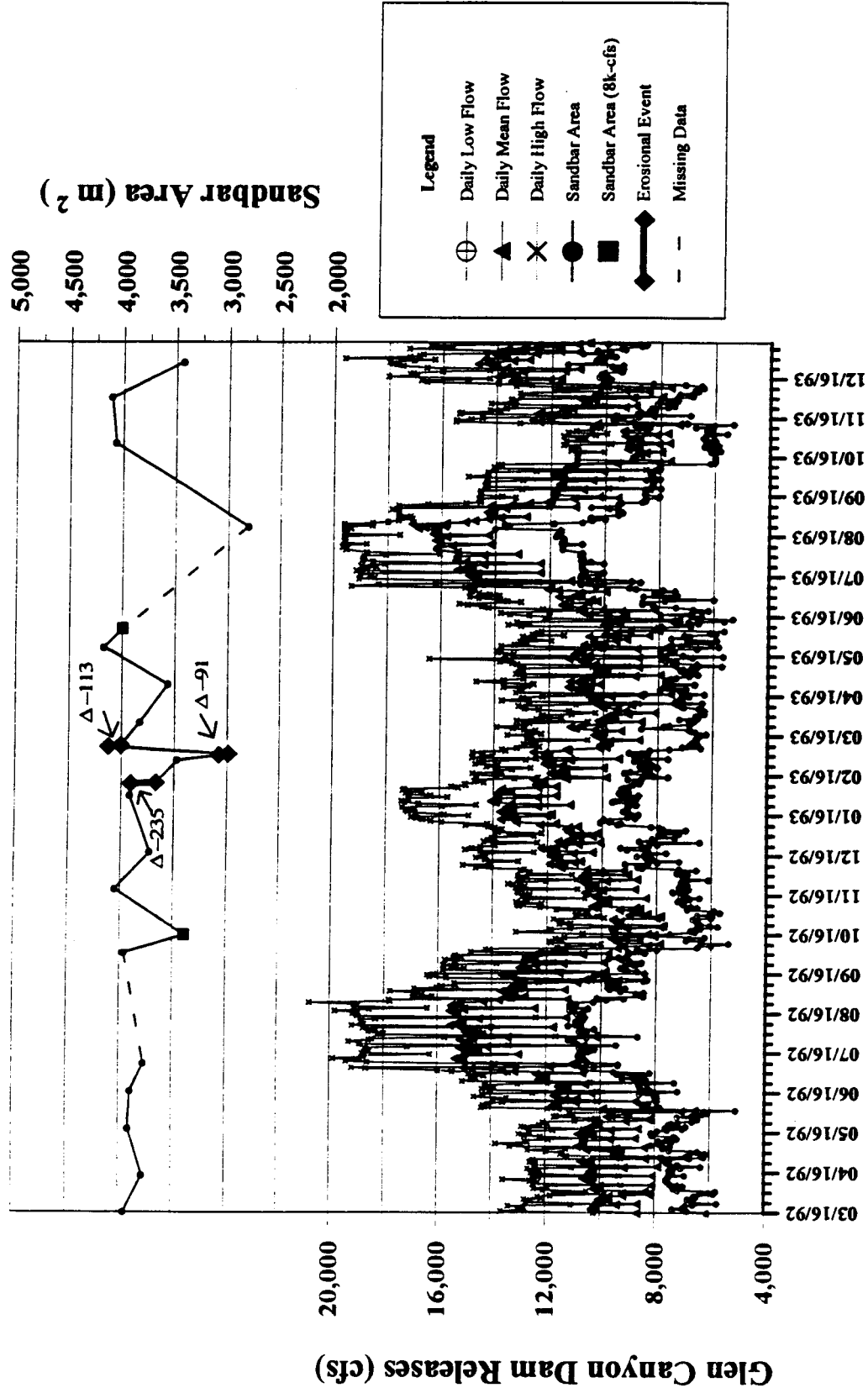


Fig. 69. Time-series plot showing area and discharge for sandbar 119.0R.

122.3R

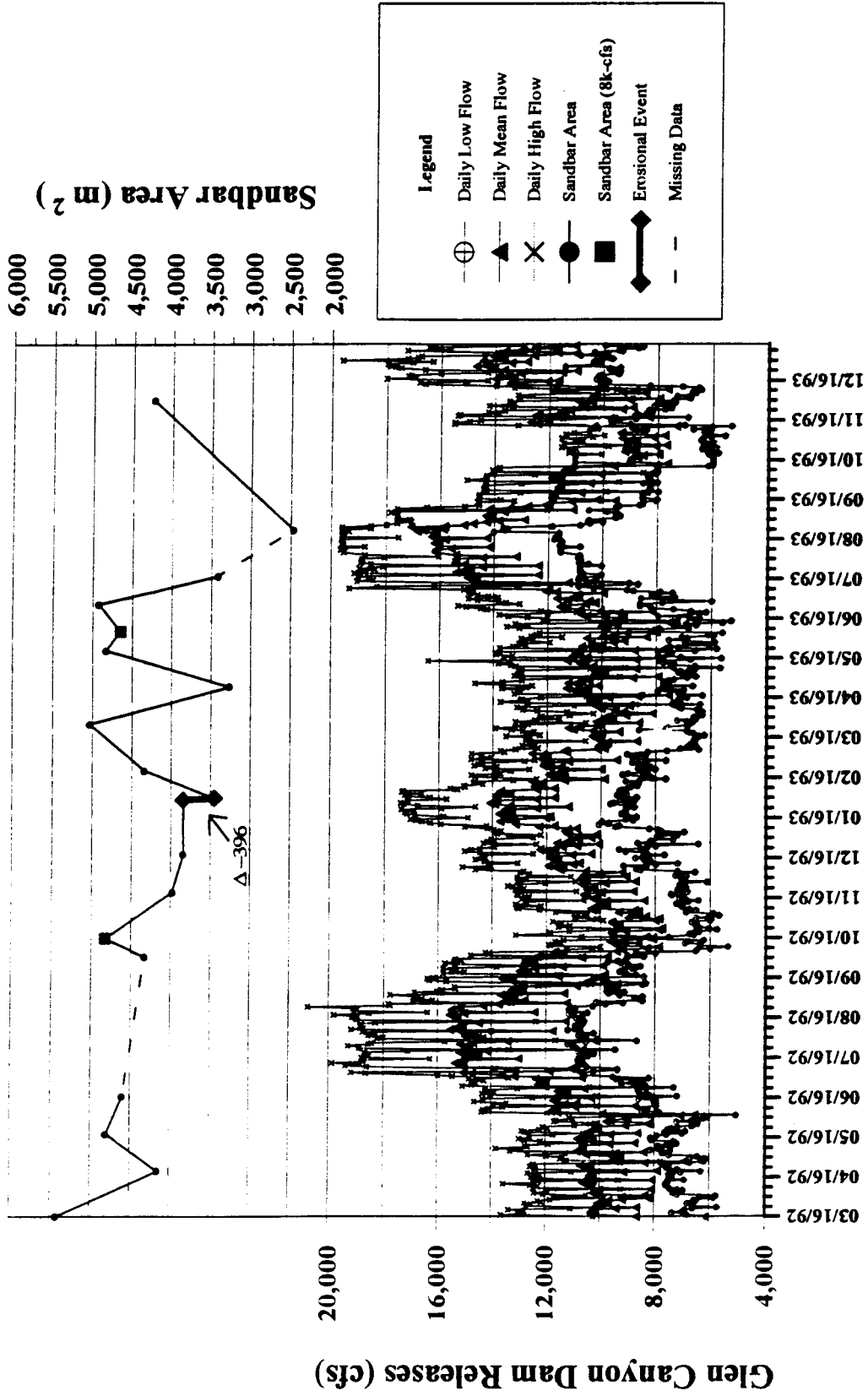


Fig. 70. Time-series plot showing area and discharge for sandbar 122.3R

122.7L

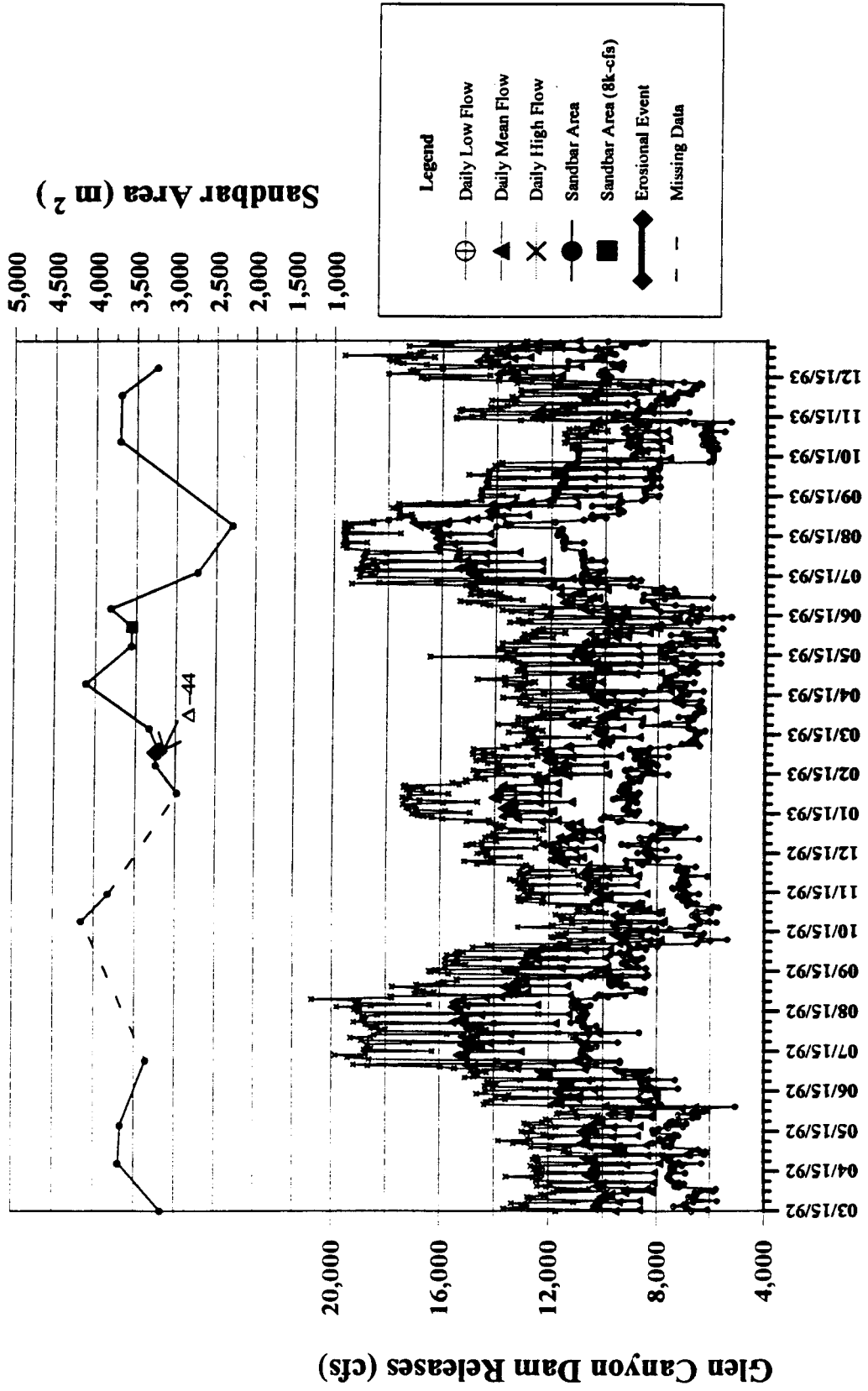


Fig. 71. Time-series plot showing area and discharge for sandbar 122.7L.

136.6L

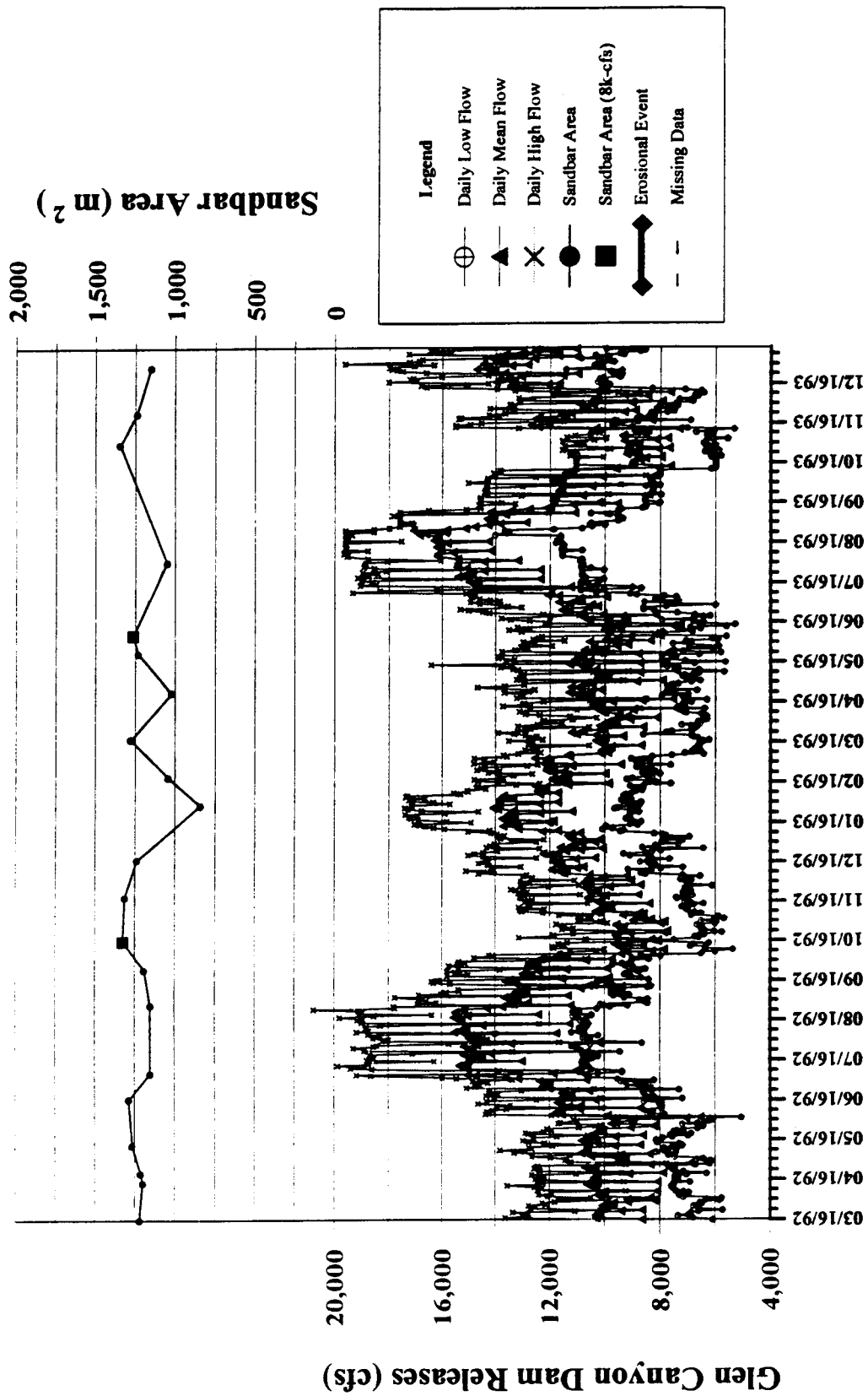


Fig. 72. Time-series plot showing area and discharge for sandbar 136.6L.

136.7L

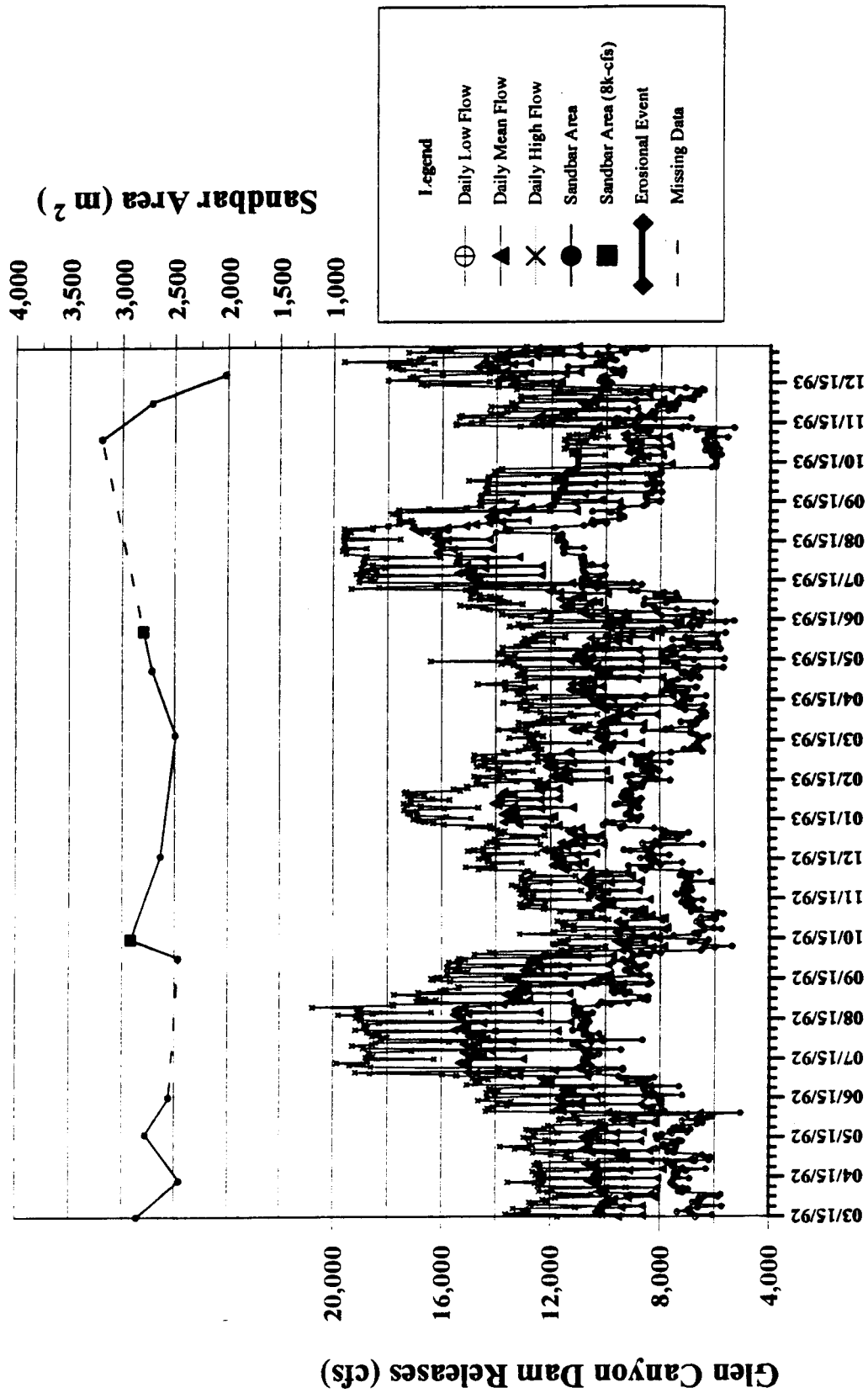


Fig. 73. Time-series plot showing area and discharge for sandbar 136.7L.

145.5L

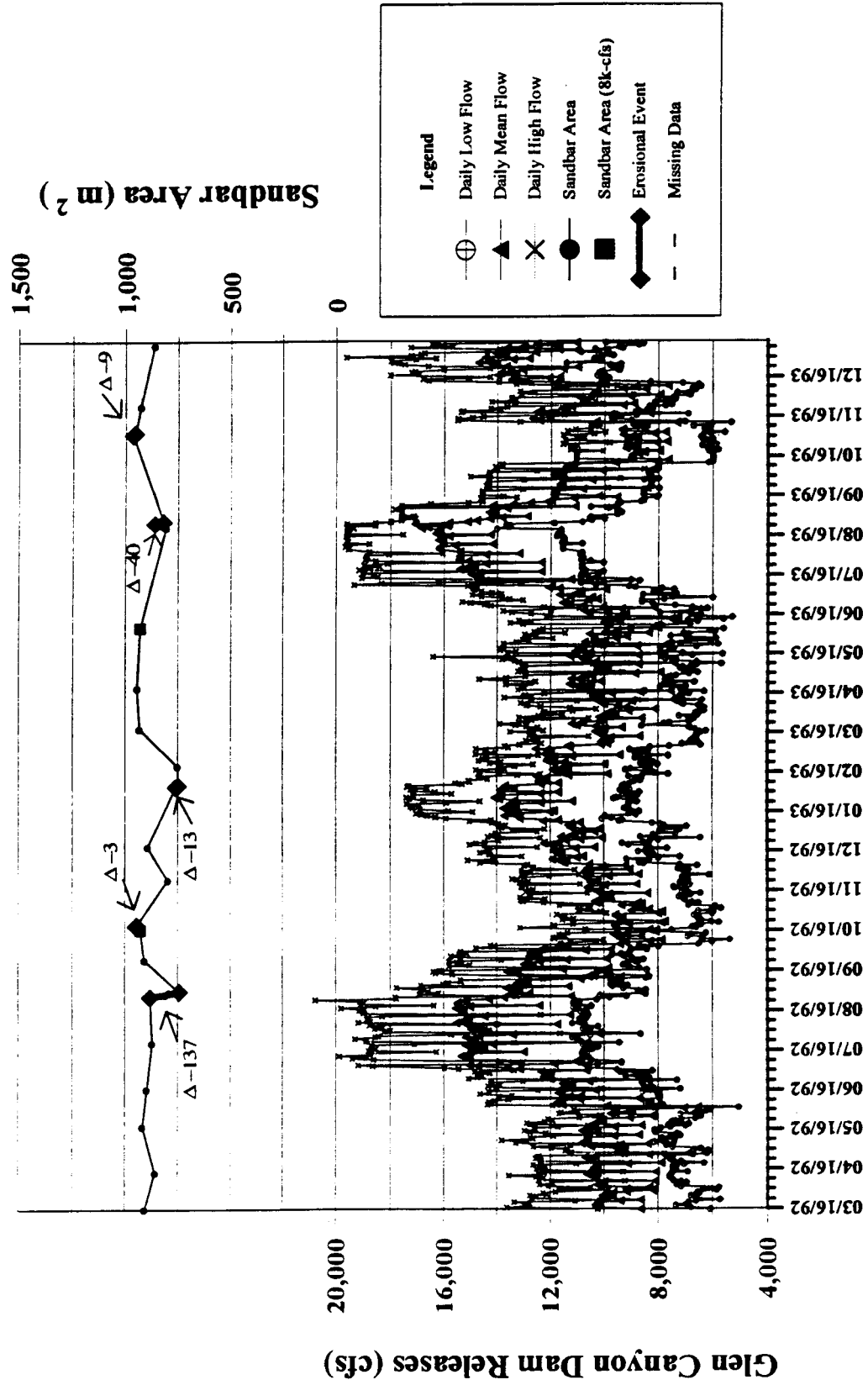


Fig. 74. Time-series plot showing area and discharge for sandbar 145.5L.

172.2L

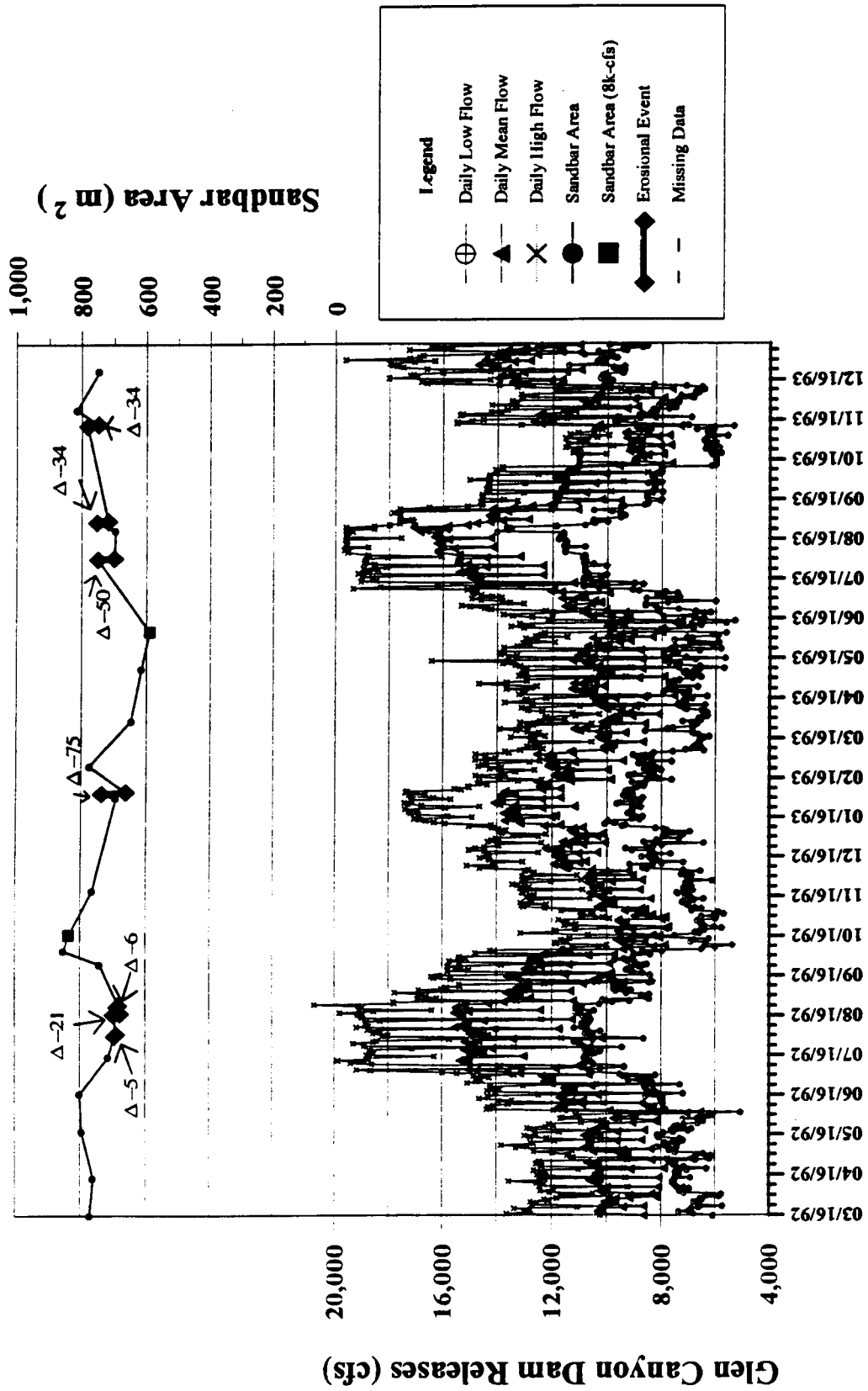


Fig. 75. Time-series plot showing area and discharge for sandbar 172.2L.

172.3L

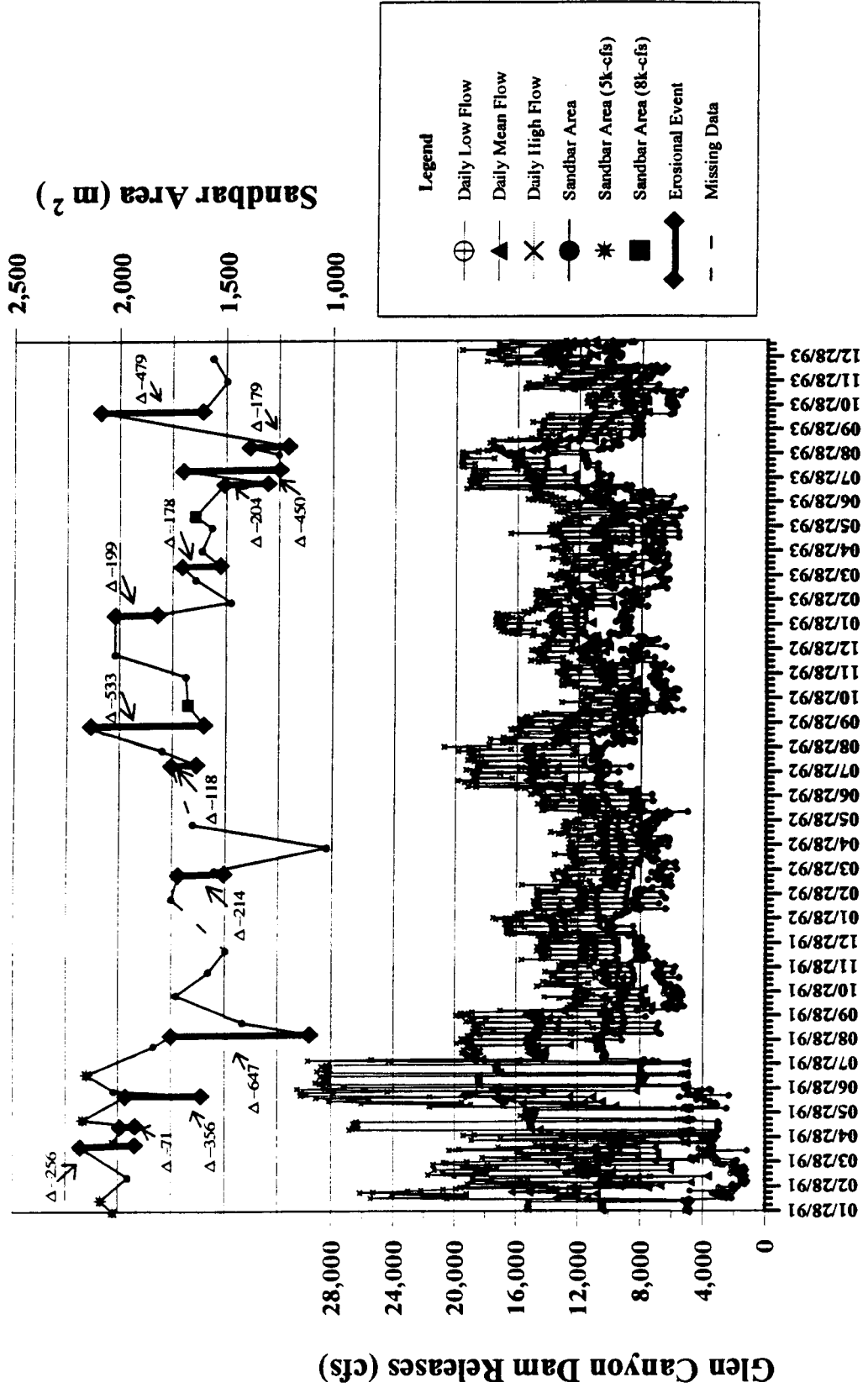


Fig. 76. Time-series plot showing area and discharge for sandbar 172.3L. This plot includes a longer record than the other time-series plots. Test flows end and interim flows begin in July 1991.

173.1R

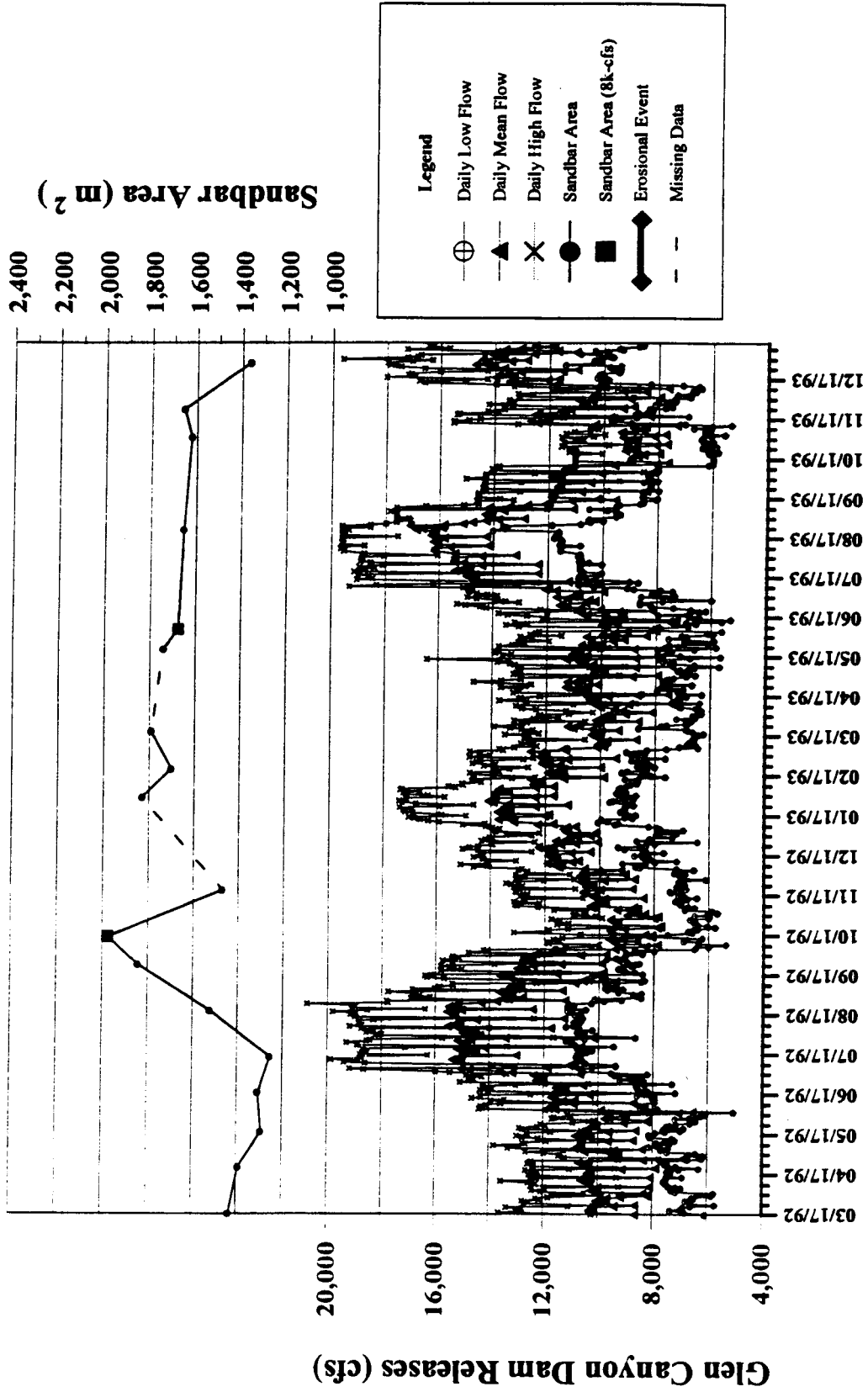


Fig. 77. Time-series plot showing area and discharge for sandbar 173.1R

211.3L

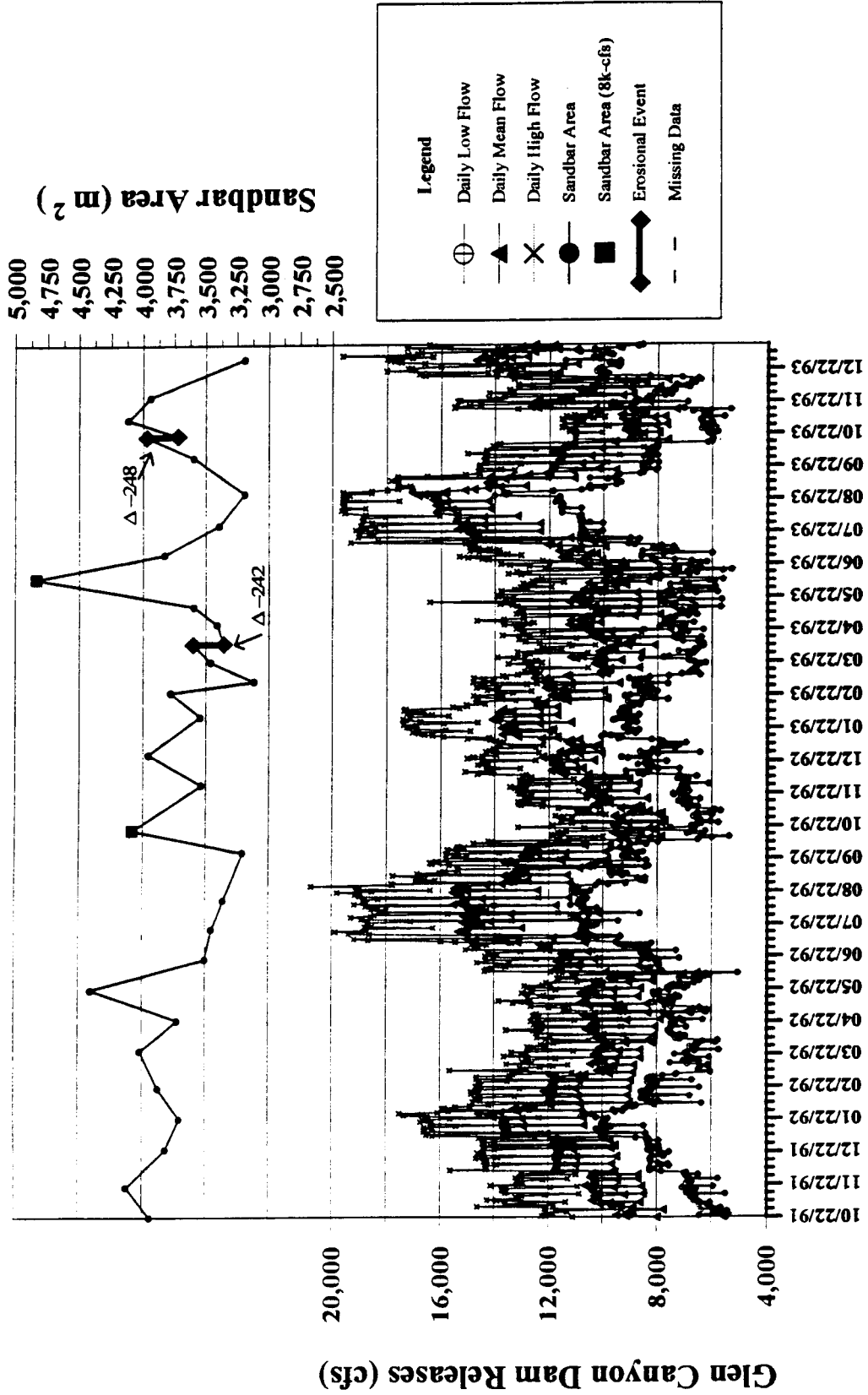


Fig. 78. Time-series plot showing area and discharge for sandbar 211.3L.

212.9L

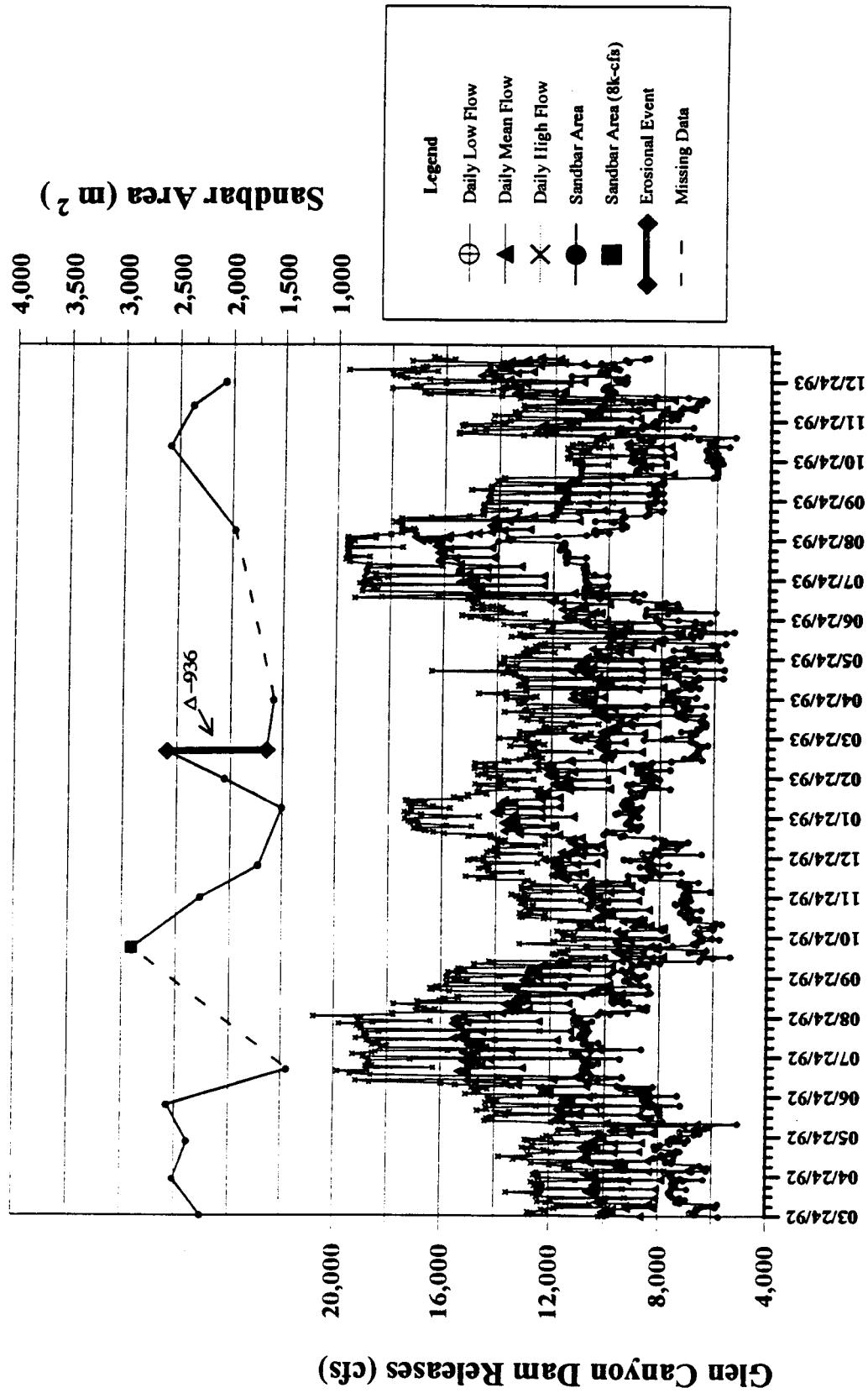


Fig. 79. Time-series plot showing area and discharge for sandbar 212.9L.

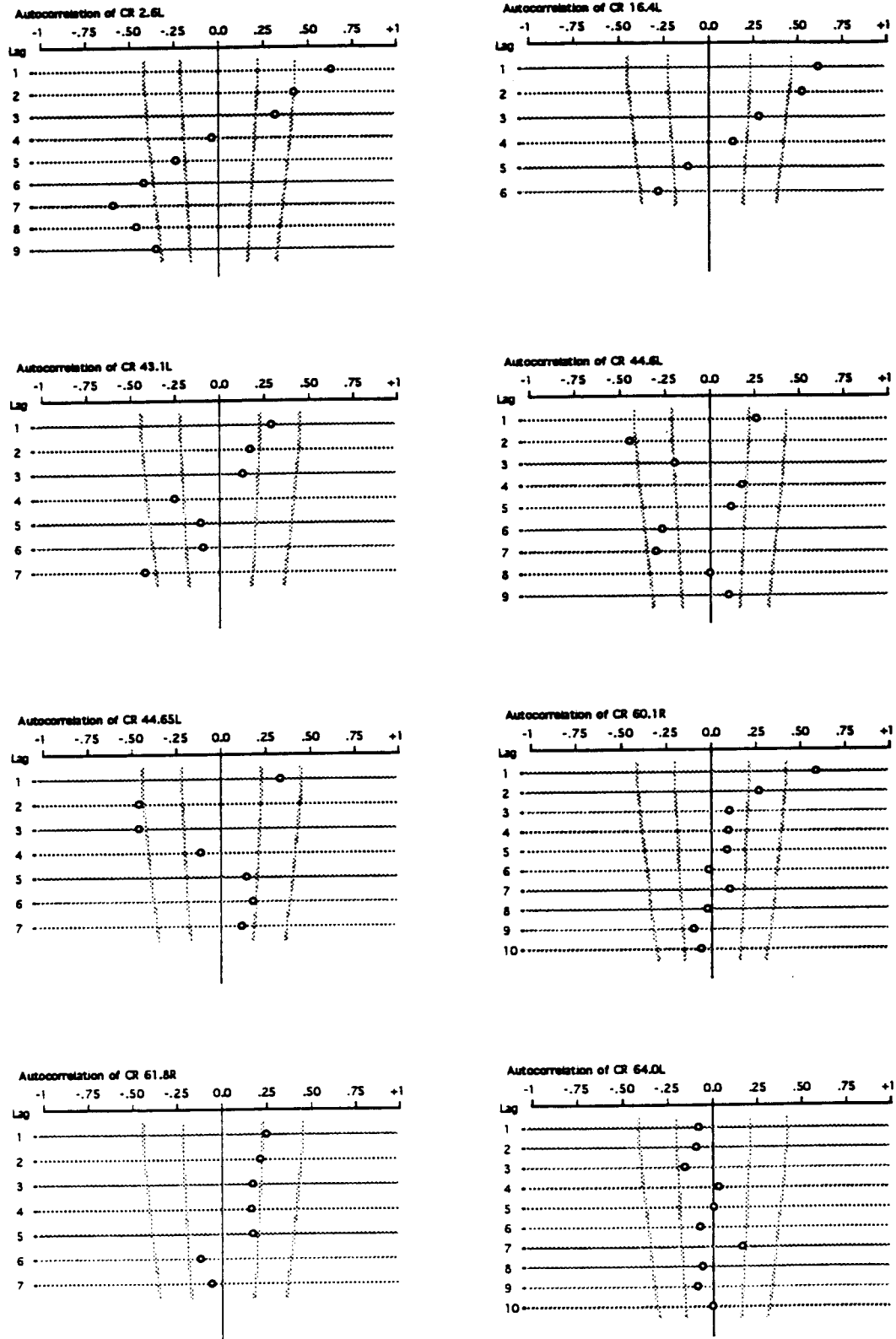


Fig. 80. Composite figure of time-series correlograms for the twenty rectified sandbars, March 15, 1992 through December 31, 1993.

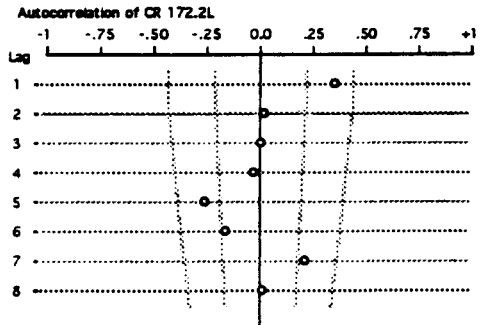
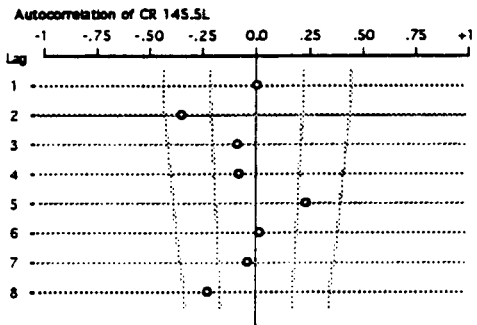
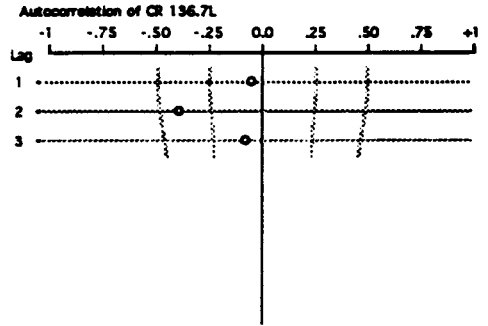
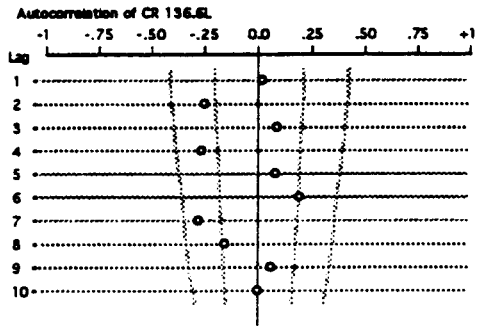
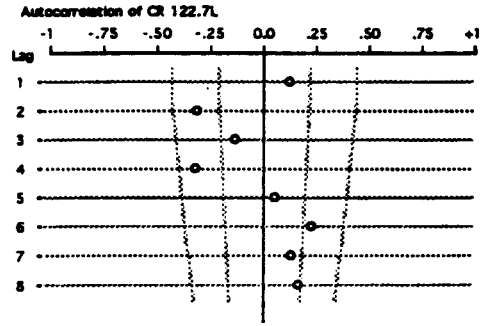
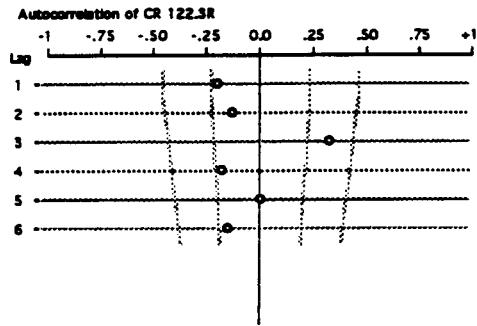
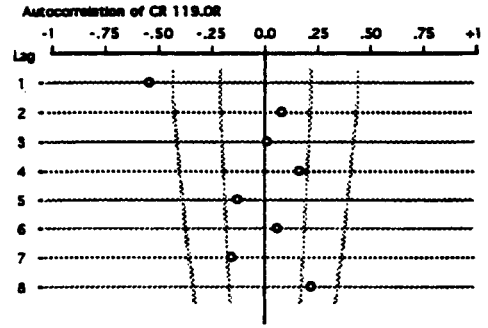
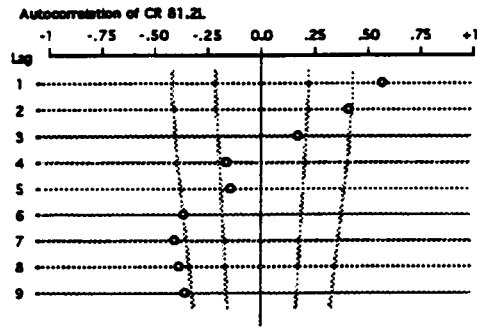


Fig. 80 (Continued). Composite figure of time-series correlograms for the twenty rectified sandbars, March 15, 1992 through December 31, 1993.

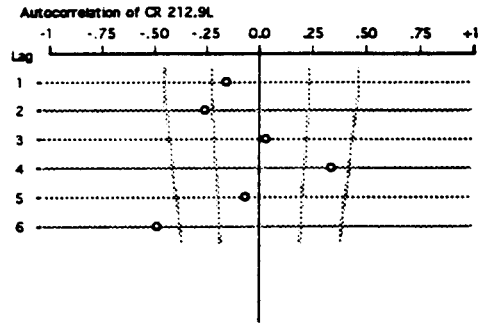
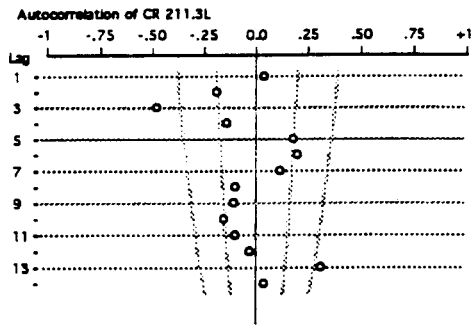
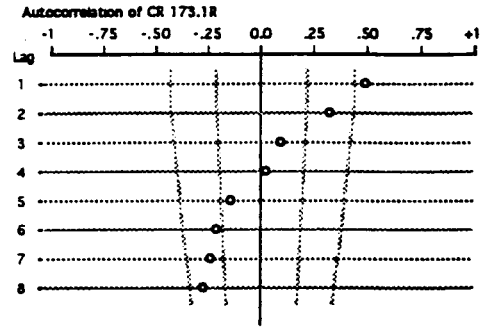
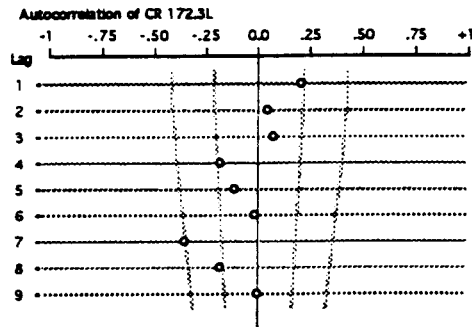


Fig. 80 (Continued). Composite figure of time-series correlograms for the twenty rectified sandbars, March 15, 1992 through December 31, 1993.

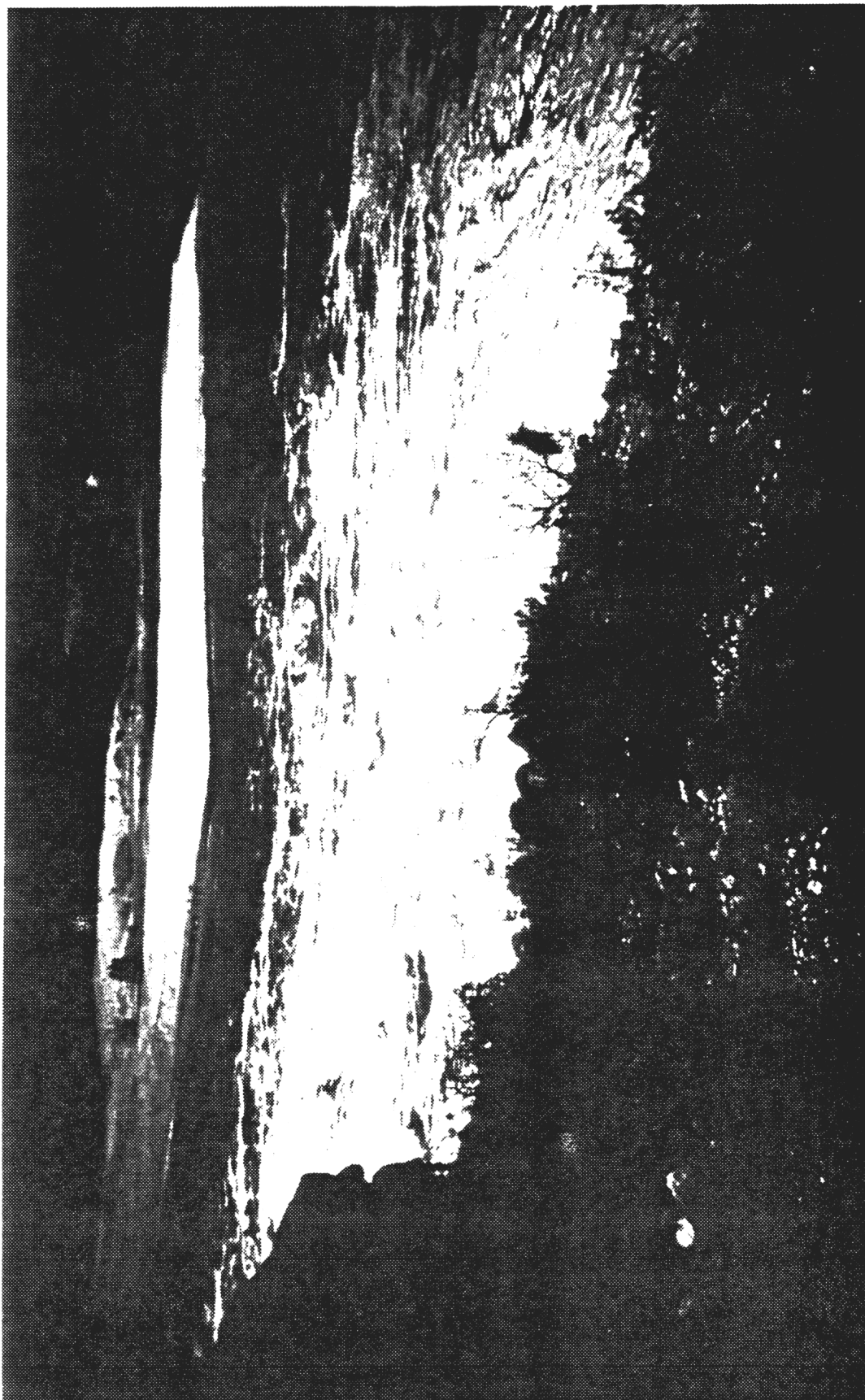


Fig. 81. Sandbar at 215.7R on 13 March 1993, pre-failure.

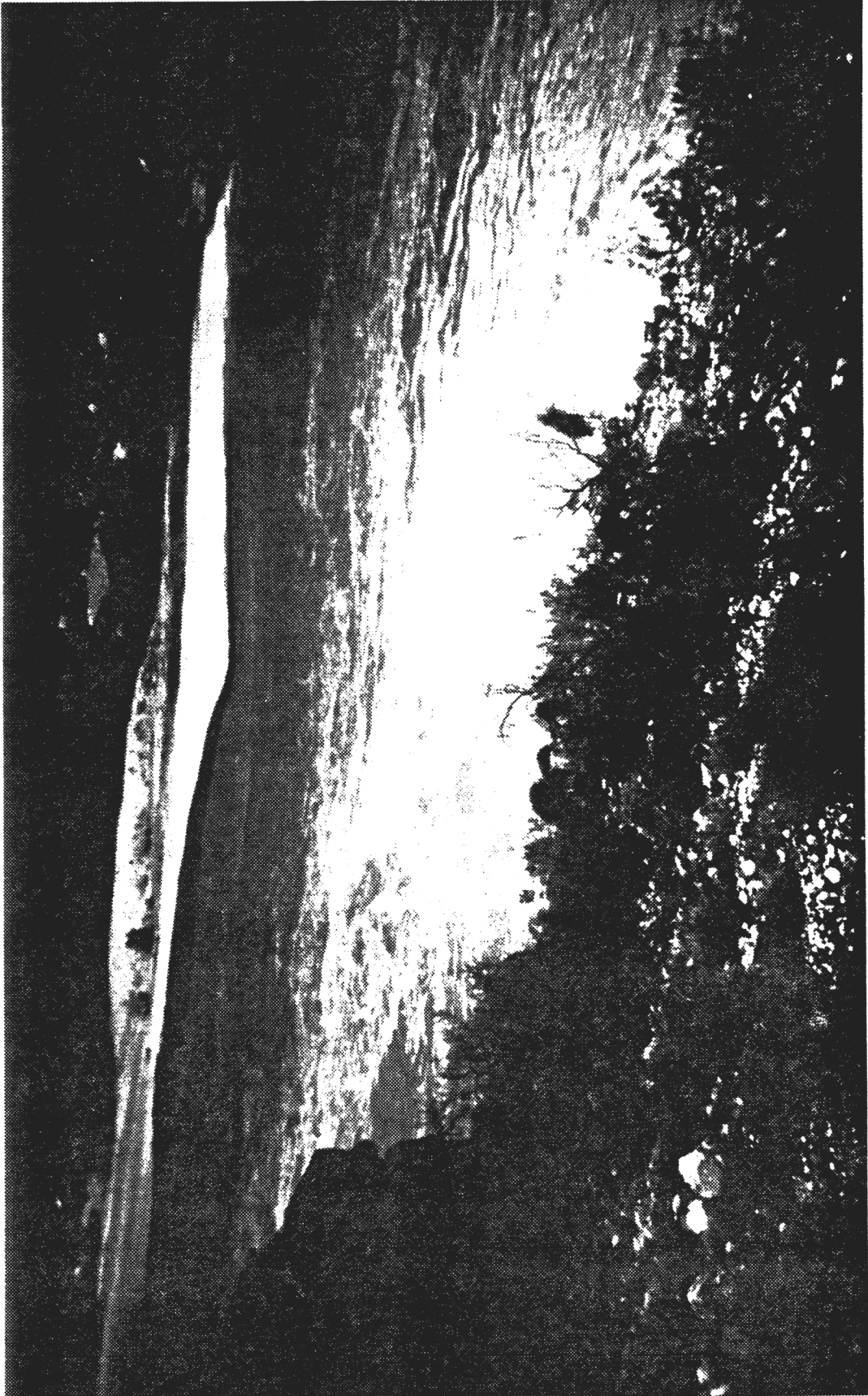


Fig. 82. Sandbar at 215.7R on 14 March 1993, post-failure.

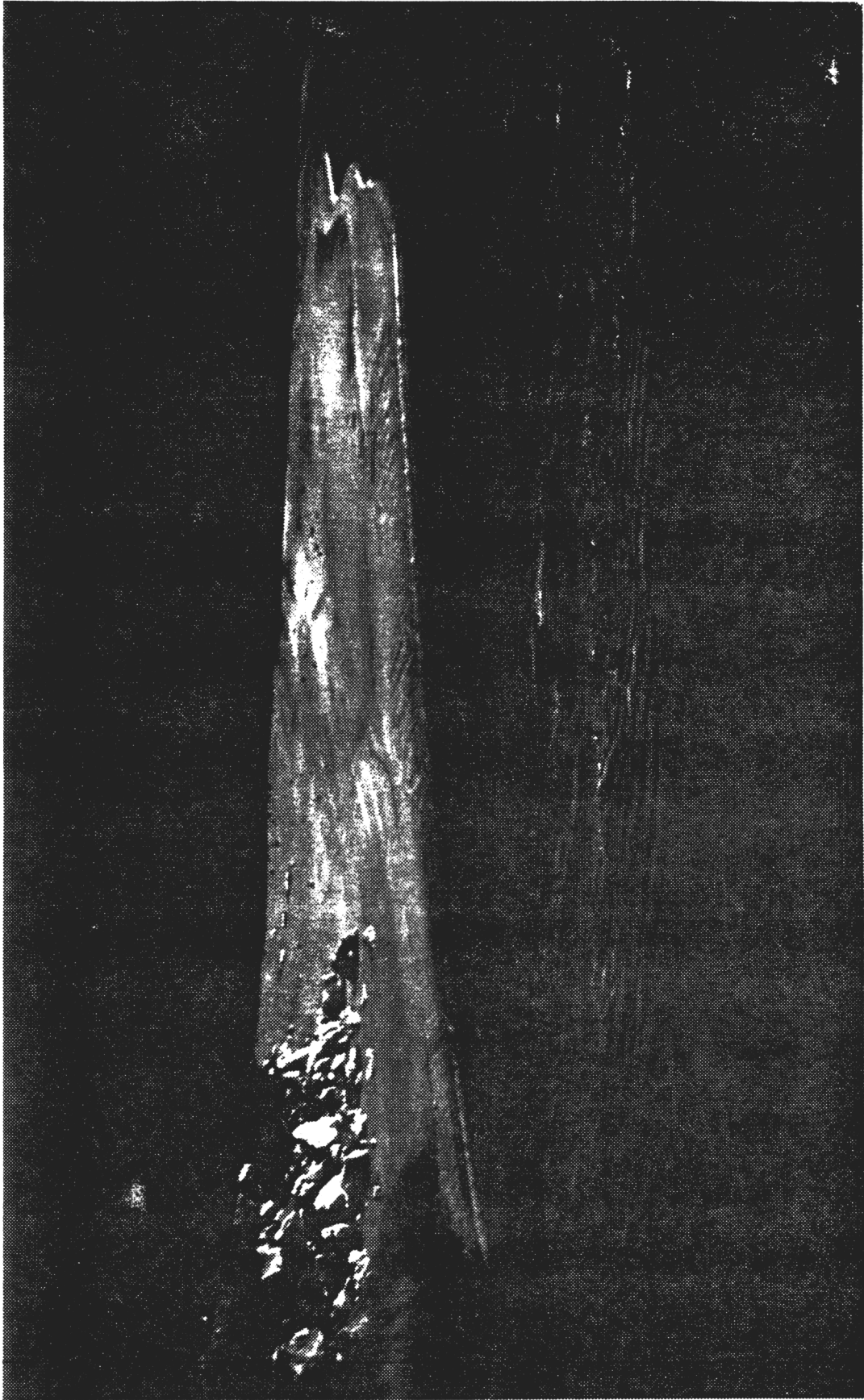


Fig. 83. Sandbar at 16.4L. on 22 October 1992, pre-failure.

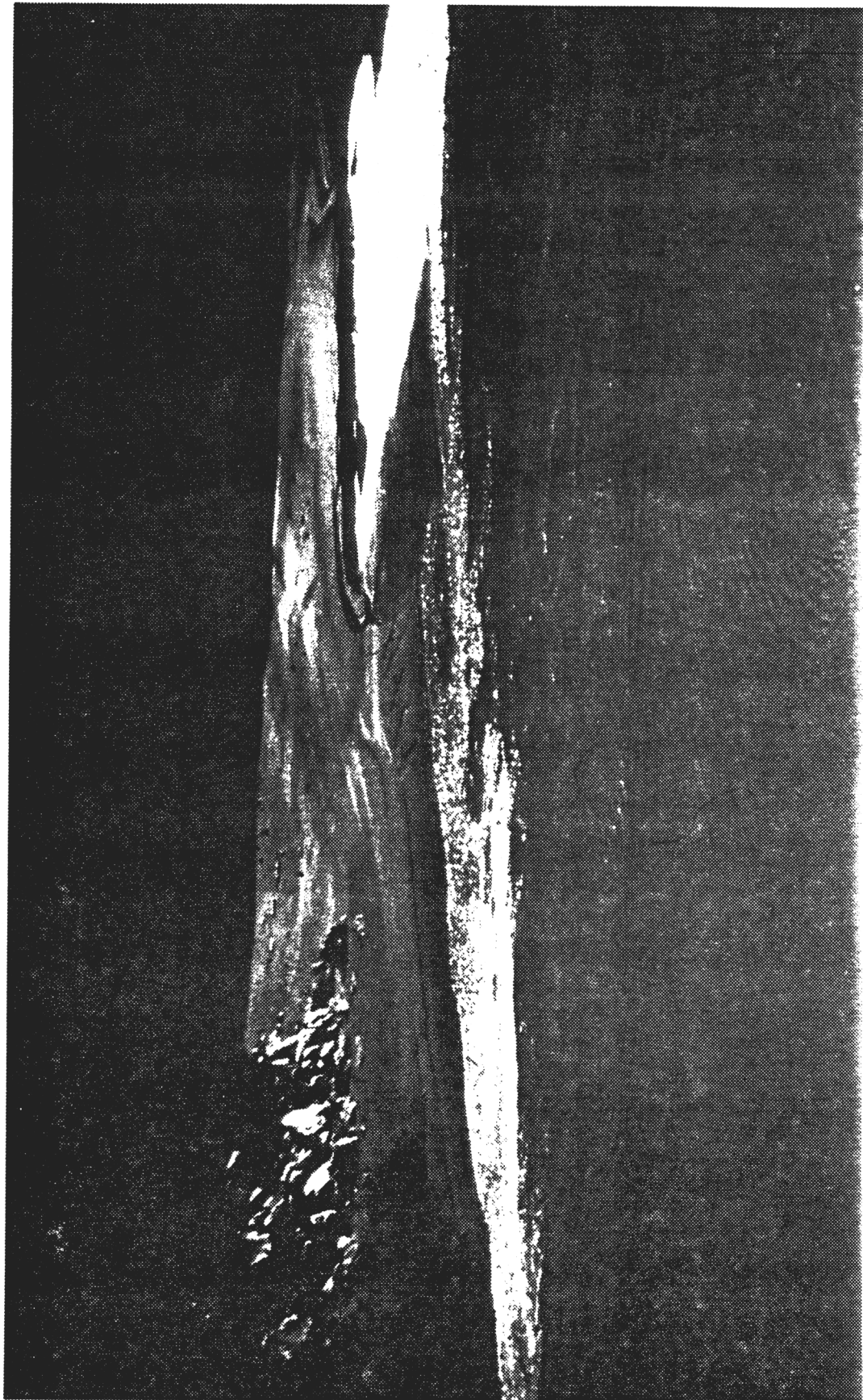


Fig. 84. Sandbar at 16.41, on 23 October 1992, during failure.

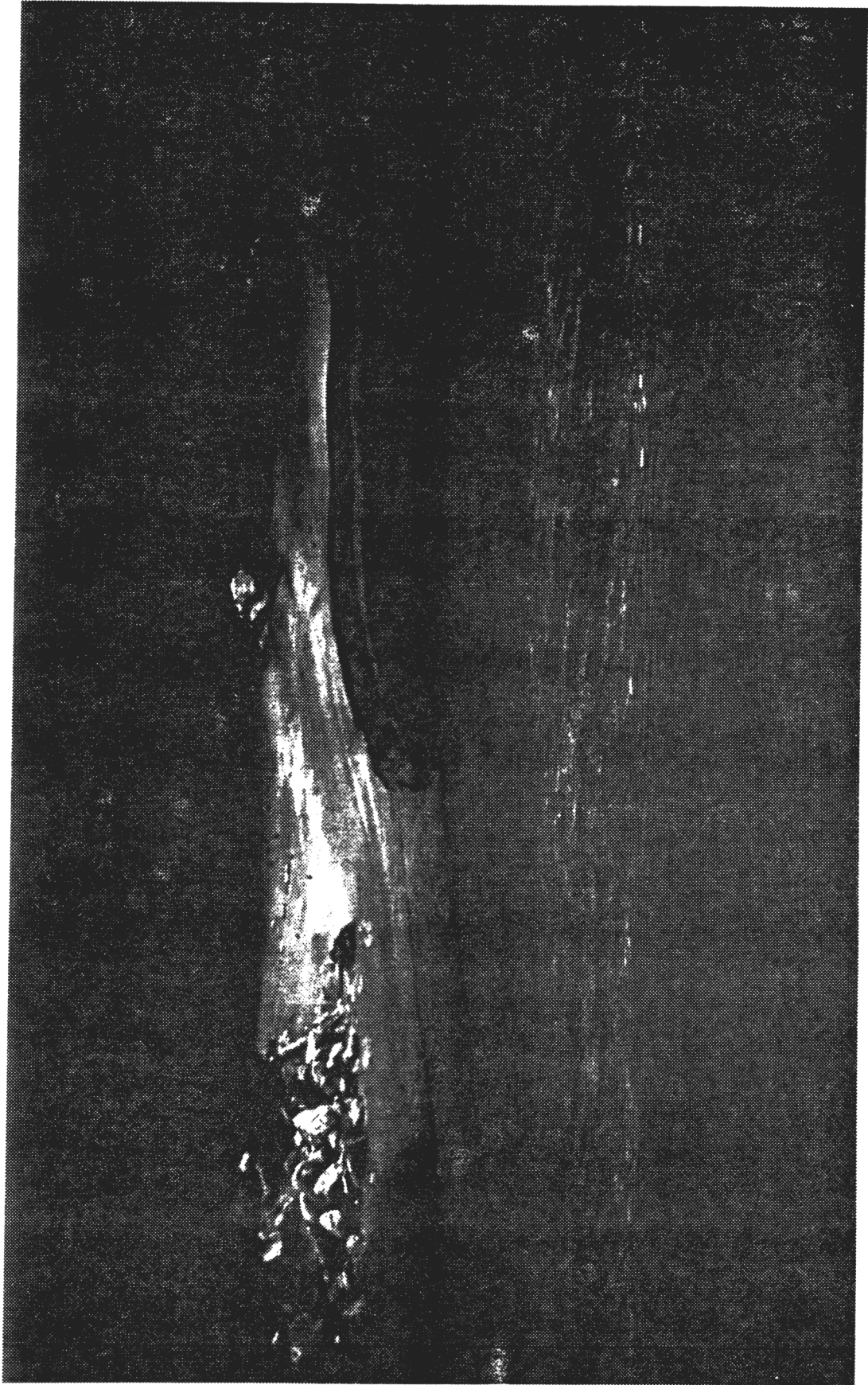


Fig. 85. Sandbar at 16.4L. on 24 October 1992, post-failure.

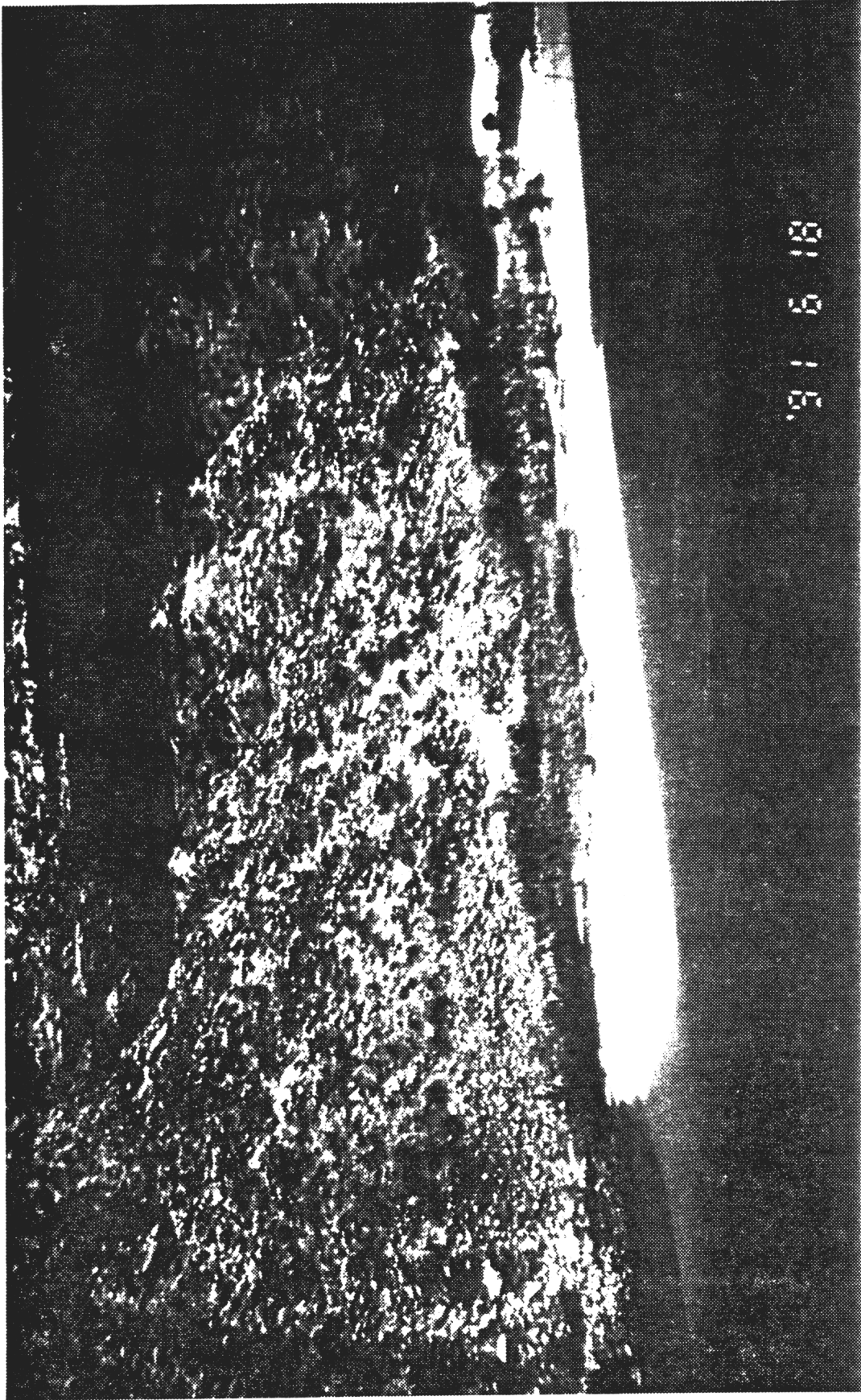


Fig. 86. Sandbar at 172.31, on 18 June 1991 pre-failure.

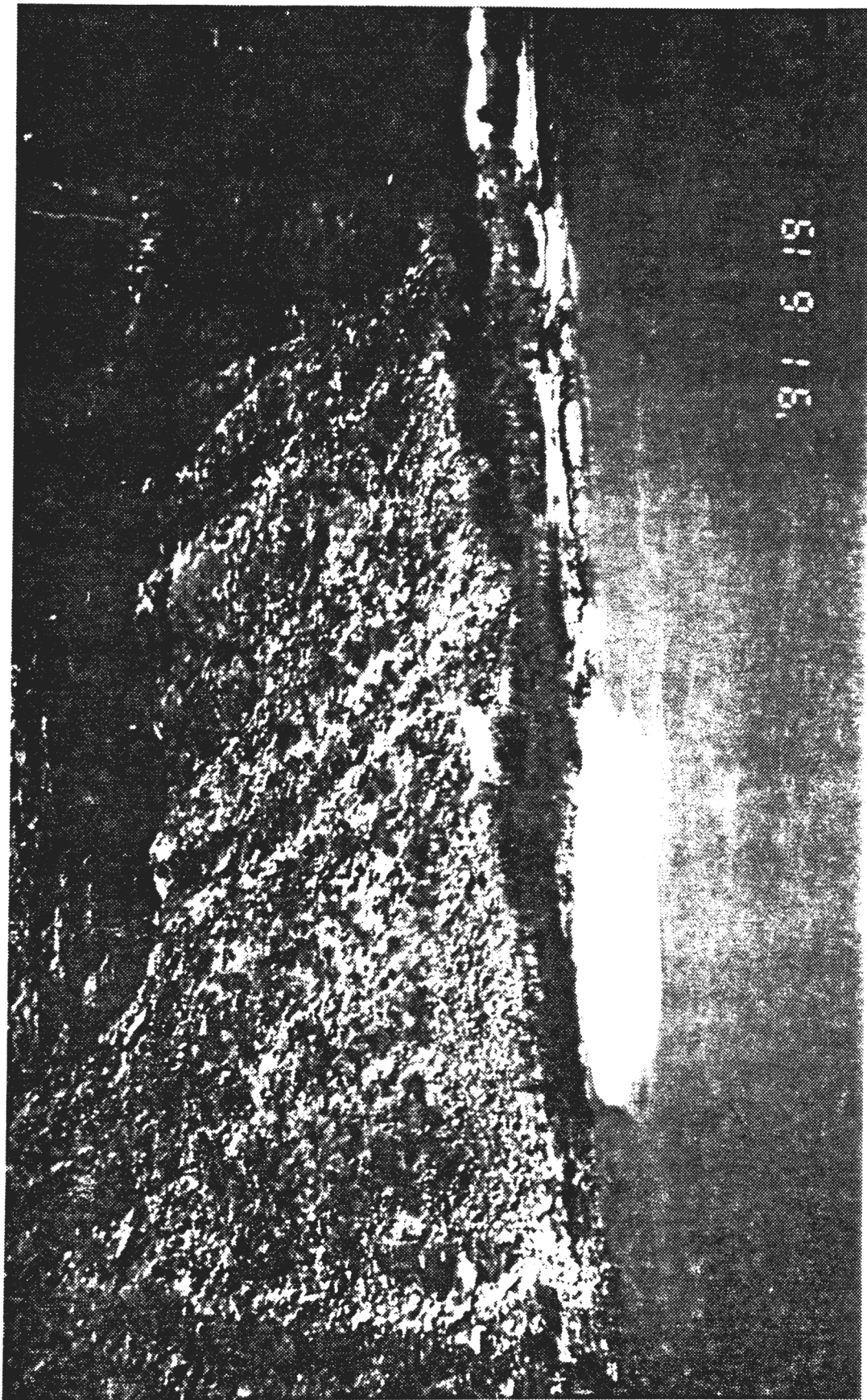


Fig. 87. Sandbar at 172.31, on 19 June 1991 post-failure.

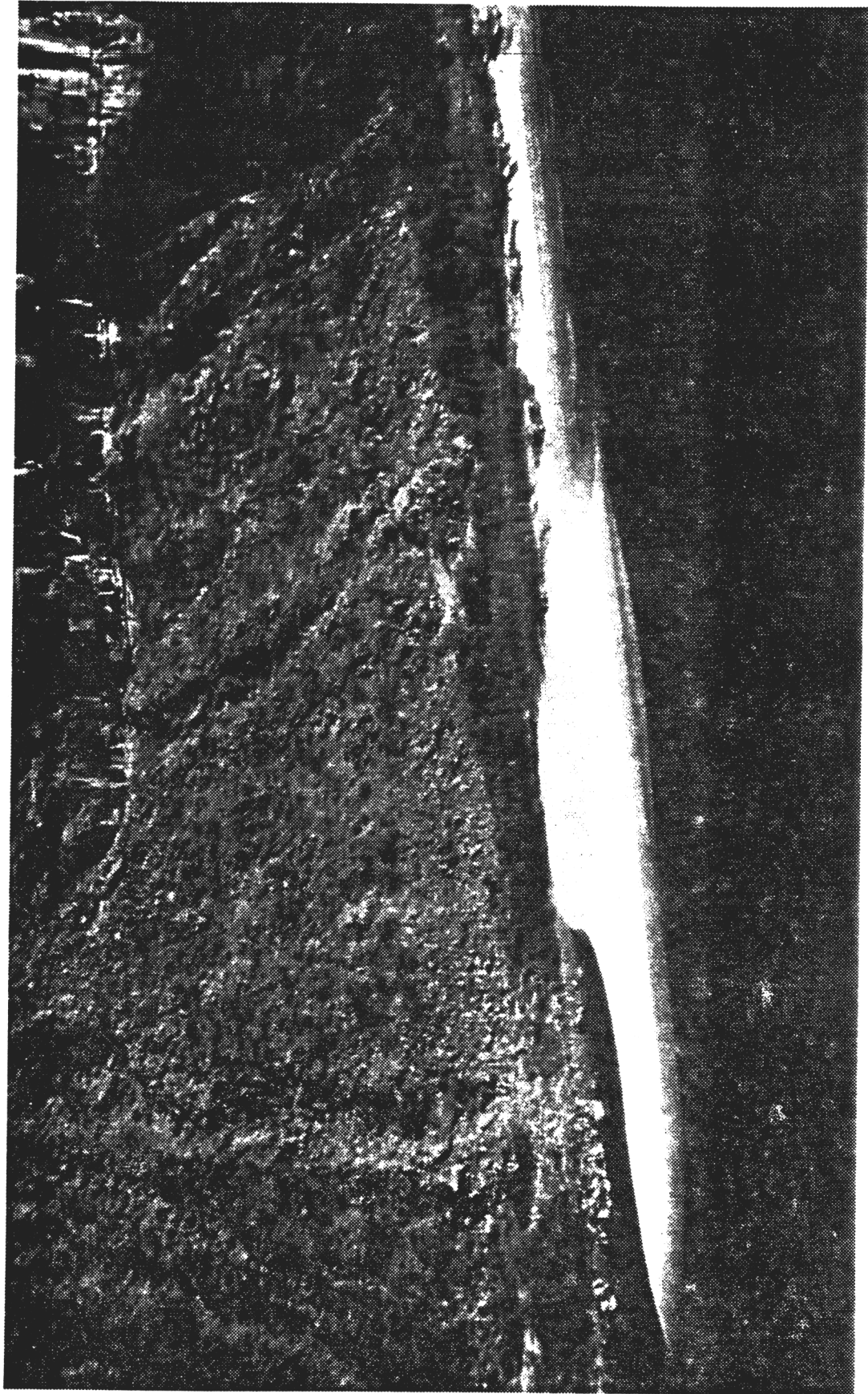


Fig. 88. Sandbar at 172.31 on 1 July 1991 approximately two weeks after failure and following rebuilding.

Table 10. Summary statistics for rapid erosional events.

Site	2.6L	16.4L	43.1L	44.6L	44.65L	60.1R	61.8R	64.0L	81.2L	119.0R	122.3R	122.7L	136.6L	136.7L	145.5L	172.2L	172.3L	173.1R	211.3L	212.9L
Mean Area	1844	1140	2752	661	4644	1379	3805	3455	1820	3776	3805	3432	1192	2664	870	728	1708	1585	3707	2145
Area Loss During Events	942	56	82		201		36	400		235	396	44			137	5			242	936
	473	104	35				28	552		91						21			248	
		30	53				71			113						6				
																75				
																50				
																34				
																34				
																199				
																178				
																204				
																450				
																179				
																479				
Num. Events	2	3	3	0	1	0	3	2	0	3	1	1	0	0	5	7	10	0	2	1
Sum	1415	190	170	0	201	0	135	952	0	439	396	44	0	0	202	225	3201	0	490	936
Mean	707.5	63.3	56.7		201.0		45.0	476.0		146.3	396.0	44.0			40.4	32.1	320.1		245.0	936.0
Std. Dev.	331.6	37.5	23.7				22.9	107.5		77.6					55.8	24.9	187.0		4.2	
% Dev.	18	3.3	0.9				0.6	3.1		2.1					6.4	3.4	10.9		0.1	
Site Return Periods	2.6L	16.4L	43.1L	44.6L	44.65L	60.1R	61.8R	64.0L	81.2L	119.0R	122.3R	122.7L	136.6L	136.7L	145.5L	172.2L	172.3L	173.1R	211.3L	212.9L
	295	101	31				25	339		22					51	16	133		222	
		47	32				388			9					106	6	48			
															234	160	134			
															66	178	61			
																28	72			
																73	17			
																29	29			
																43	43			
Num. Periods	1	2	2	0	0	0	2	1	0	2	0	0	0	0	4	6	8	0	1	0
Sum	295	148	63	0	0	0	413	339	0	31	0	0	0	0	457	461	537	0	222	0
Mean	295.0	74.0	31.5				206.5	339.0		15.5					114.3	76.8	67.1		222.0	
Std. Dev.		38.2	0.7				256.7			9.2					83.1	75.2	44.4			
Site Days From Trough of a Weekend or Other Low Flow	2.6L	16.4L	43.1L	44.6L	44.65L	60.1R	61.8R	64.0L	81.2L	119.0R	122.3R	122.7L	136.6L	136.7L	145.5L	172.2L	172.3L	173.1R	211.3L	212.9L
	6	1	1		6		0	0	0	0	0	3			0	0	1		3	1
	1	0	5				0	5		3					0	4	3		6	
			1				0			0					0	1	2			
							0			0					2	0	0			
							0			0					0	0	1			
							0			0					0	1	6			

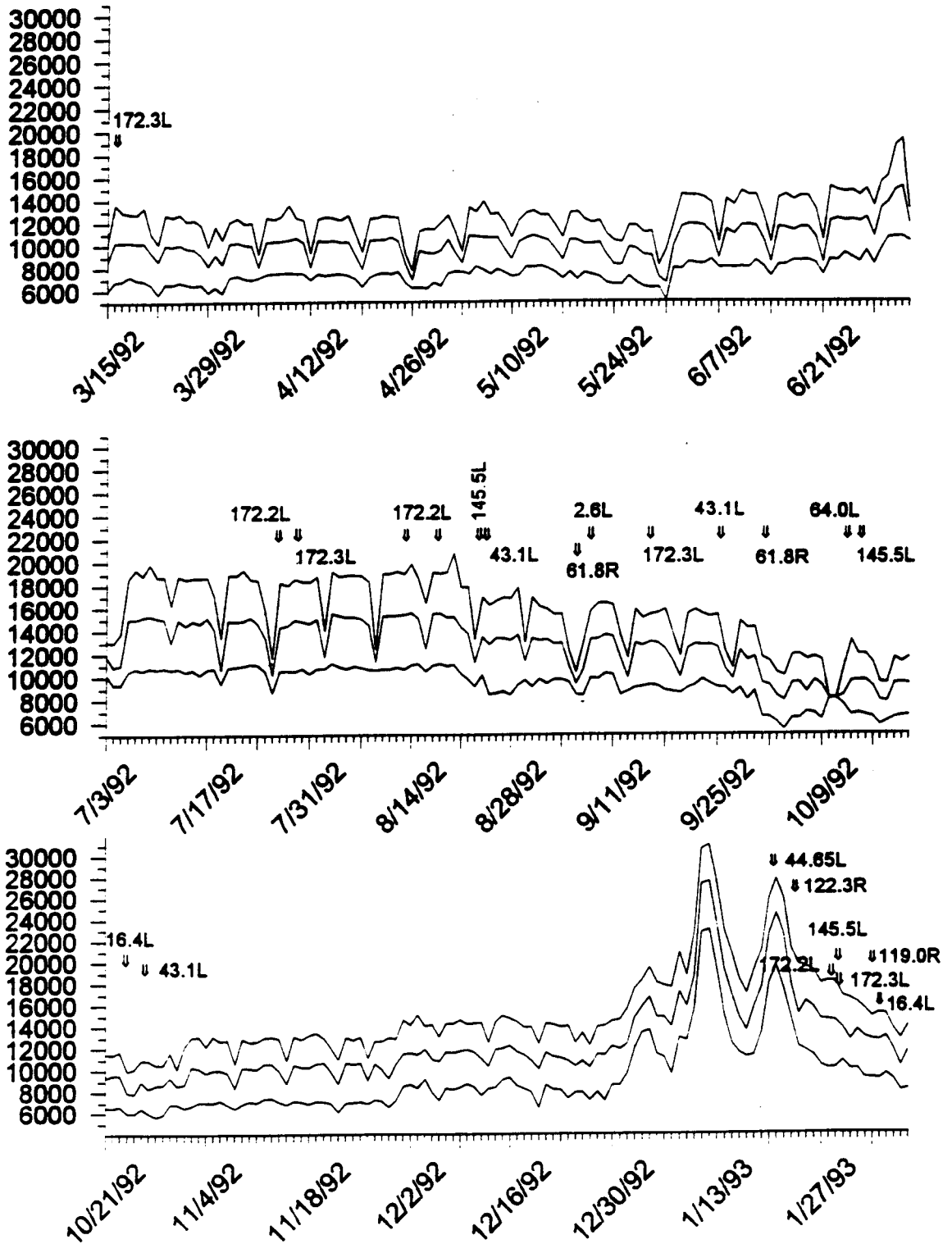


Fig. 90. Erosional event-discharge graphs illustrating the timing and river mile location of erosional events with respect to mainstem discharge (maximum, mean and minimum). Over 70% of the erosional events occurred during or within two days of a weekend low discharge.

Discussion & Conclusions

Magnitude of Erosional Events

Events which were considered mass motion failures (seepage induced slumping) or rapid erosional events are highlighted on the time series plots (Figures 60 through 79) along with the measured change in area. Table 5 shows the mean event removed 184 m² of sandbar area (s.d. 262 m²) with the largest event removing 936 m² of sandbar area.

The erosional event that occurred on July 30, 1993 at sandbar 172.3L shown on the time series plot (Figures 76) was also quantified by bathymetric field surveys a few hours before and eight hours after the event. Roughly 12,000 m³ of sediment were removed from eddy bar storage in that event which reduced the exposed area about 450 m². Events with similar area magnitudes were documented 14 times between April 1991 and October 1993. If one assumes that surface area change corresponds roughly to the volume of material eroded, the 14 events documented at 172.3L represent approximately 100,000 m³ of sediment interchanging between the channel and channel margin storage in 30 months. The monthly average is approximately 3,300 m³ at a minimum. Some events documented were not measured and an unqualified number of events probably occurred during breaks in the record. This corresponds to a minimum of 53,000 metric tons on an annual basis from one sandbar.

Frequency Distributions of Sandbar Areas

Daily, Weekly and Monthly Time Scales

Erosional events reoccurred with a variety of magnitudes and return periods and were documented at 14 of 20 (70%) sample sites during the study period (Table 10). While most of the comparative statistics presented in this report are restricted to the time period between March 1992 and December 31, 1993 (except where noted), we have extended records of oblique photographs from as early as August 1990 at seven pilot sites.

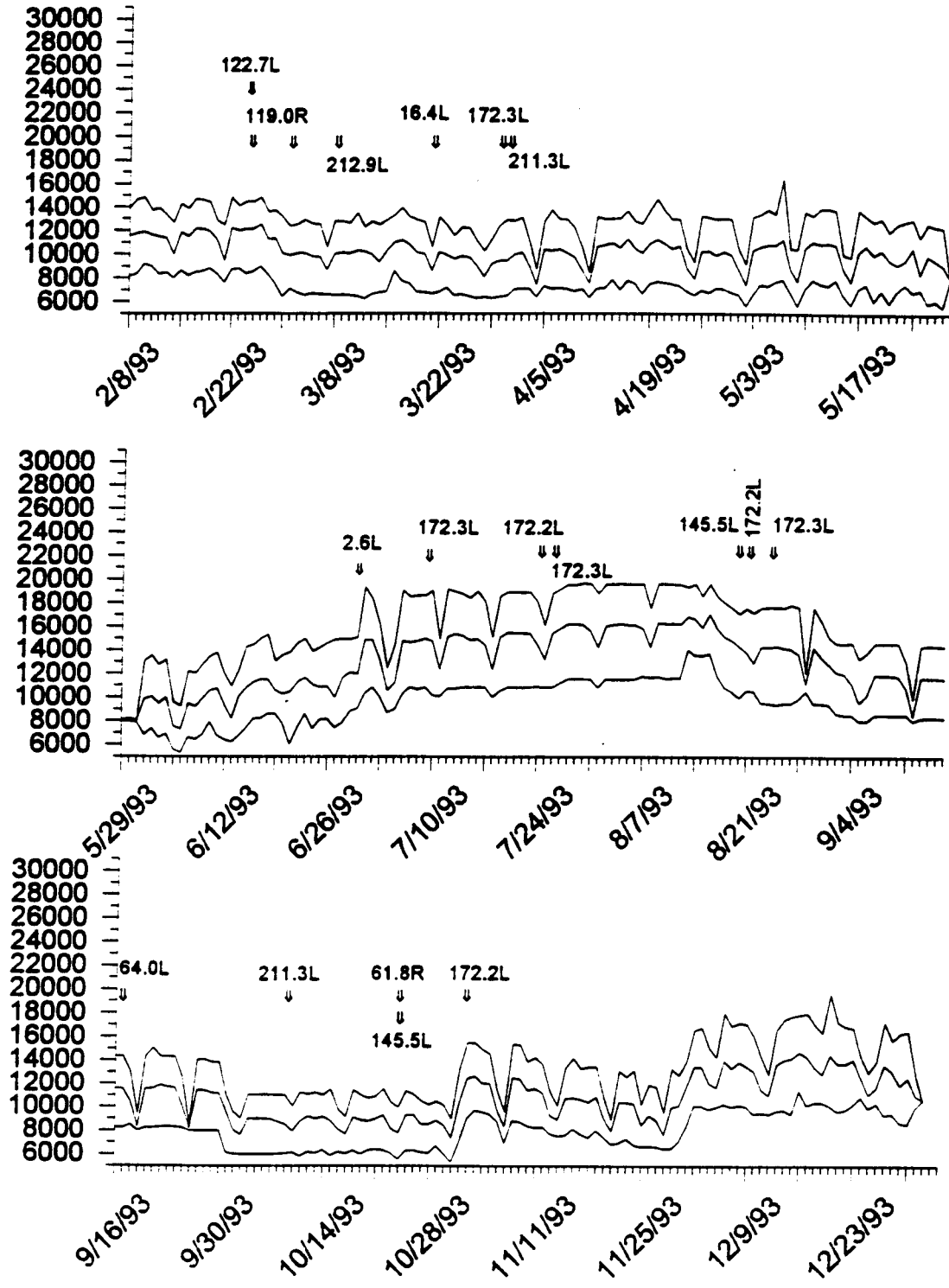


Fig. 90 (continued). Erosional event-discharge graphs illustrating the timing and river mile location of erosional events with respect to mainstem discharge (maximum, mean and minimum). Over 70% of the erosional events occurred during or within two days of a weekend low discharge.

Analysis of the extended record documents rapid erosional events at 100% of these seven sites with return intervals of 110 days. When compared with the shorter record from March 1992 to December 1993, the fraction of sites displaying erosional events increases as record length increases. These results indicate that erosional events are not restricted to a portion of the population but occur at all locations with different return periods. The return periods and number of events reported are likely to be minimum values because erosional events may have occurred during the missing periods of record. Table 9 shows that a very strong bimodal area pattern persists even at the subseasonal time scale.

Frequencies at Seasonal Time Scales

Analysis of seasonally averaged sandbar areas (Table 8) show that, in most cases, individual sandbars are largest in the spring and fall, are smaller in the winter, and are smallest in the summer. This general time-area pattern is strongly correlated to mean discharge levels and is probably less of a direct erosion-deposition effect.

Low discharge levels expose more sandbar area to subareal conditions while high discharge levels submerge more of the sandbar area. Discharge is smallest in the spring and fall as a result of lower overall power demand. Discharge is largest in the summer as a result of high power demands mainly for refrigeration use. Discharge shows a second modest peak in the winter as a result of increased power demands mainly for heating use.

While this particular seasonal area-time relation does not reflect overall erosion losses or deposition gains, the relationship still has significance in erosional processes. Larger exposed sand areas provide more opportunity for subaerially driven erosion during the lower discharge seasons when the smaller winter fluctuating flow peak occurs. Beus and Avery's (1992) volumetric studies indicate that winter is indeed a high erosion season.

Annual Time Scales

Under the current management scheme of the Colorado River, the sandbars we have studied do not appear to follow a normal distribution (i.e. a stable mean area configuration with a few excursions to small or large areas). Rather, as documented in Table 6 and 9, over 80 percent of the sandbars we have studied are decidedly bimodal and display negative kurtosis (i.e. they have two pronounced stable configurations with a decided lack of mean area configurations).

While it may be tempting to relate the bimodal area distributions strictly to sudden changes between high and low seasonal discharge regimes, this does not appear to be the case for two reasons. First, Table 9 shows that a very strong bimodal area pattern persists even at the sub-seasonal time scale. Second, Figures 8 and 9 show that discharge frequencies have a much more central distribution than do the sandbar area frequencies. We feel the bimodal area characteristic is evident at several different temporal scales and we have integrated this bimodal characteristic into a general erosional-depositional cycle model discussed later.

Temporal Tends of Erosion

Punctuated Events

A wide range of aggradation and degradation rates were measured during the course of this investigation, even at individual sites. Aggradation occurred at rates such that sandbar areas often increased 1,500 m² in one month. The greatest aggradation rates on an individual site basis followed erosional events. It was not uncommon for large areas degraded during an event to be aggraded to original size within two weeks. The rates appear to depend upon location and site specific variables such as channel width, sediment supply, and subsequent hydrologic inputs. Aggradation also occurred at lower rates most commonly when areas were near maximum size.

Thus, in general, aggradation was greatest immediately following erosional events or upon reversal of degradation periods. The aggradation rates decreased as areas increased, reaching minimum rates as area approached maximum values.

During periods of degradation, rates similar to aggradation were measured in many instances. However, the major difference between aggradation and degradation rates is that many periods of erosion were actually very short periods of time typically less than 24 h - thus the usage 'events' in this report (see Figures 81 through 88 for examples). Degradation was typically a punctuated event while aggradation was prolonged. This characteristic has been incorporated in an overall sandbar cycle model presented later (Figure 96).

Rapid erosional events were discovered in 1990 during the course of the pilot study leading to this investigation. They are important at many different levels and very little is known about the causal processes. Documentation that erosional events occur at every site given sufficient sampling period is significant because it suggests that erosional events are ubiquitous. They occurred in the past but were not detected by investigations designed to measure at time intervals longer than the response cycle. Results presented here show that through erosional events and redeposition, individual sandbars cycle through large volumes of sand in between periods of time traditionally chosen for measurement intervals. Every time sand cycles from the sandbar into the channel, another opportunity for further downstream sediment transport is presented.

The photography and photogrammetry used in this study reveals a much more active sediment recycling system than one would conclude from the long term studies results only. Data for a number of Grand Canyon sandbar studies (Table 11) show lateral erosional and deposition rates. As the sampling interval shortens, the maximum instantaneous erosional rates climb in a near logarithmic increase (Figure 91). Consequently, this suggests that some reinterpretation of results from prior investigations using annual time steps is needed.

Table 11. Summary of measured lateral erosion and deposition rates versus sample frequency.

Reference	Interval	Erosion(m/yr)	Deposition(m/yr)
Beus et. al. 1992	10 Years	0.8	1.7
Howard & Dolan 1979	8 Years	1.15	0.7
Howard & Dolan 1979	1 Year	2.45	0.7
Schmidt & Graf 1990	4.5 Months	34.7	26.7
Beus et. al. 1992	2 Weeks	520	390
Cluer Pres. Comm.	2 Weeks	780	520
This study	Daily	36,500	2,550

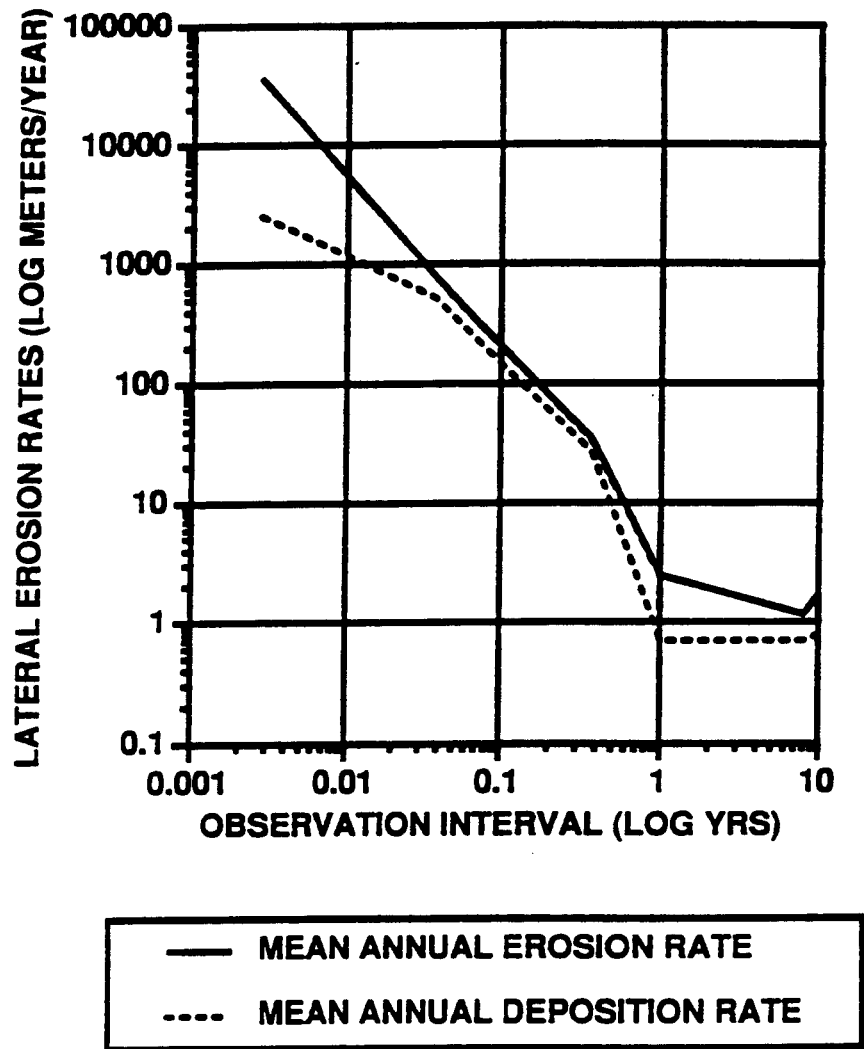


Fig. 91. Log scaled plot of measured lateral erosion rates versus sample frequency.

Temporal Connection to Discharge Patterns

In addition to the daily discharge fluctuation for hydropower optimization, there is a very strong weekly cycle to dam discharge (Figure 11). The weekly pattern results from discharge being reduced during weekends as electrical demand decreases. The minimum discharge is not reduced by the same magnitude as the mean and maximum discharges. Downstream of the dam this operation results in two days of low flow with occasional but greatly reduced midday peaks. The two day low flow travels downstream resulting in lower than normal stages as seen in the photography. This investigation took advantage of the regularly occurring low flow periods to make measurements of sandbar area. These weekend low flow periods coincide temporally with a large percentage of erosional events (Figure 90).

A count of erosional events temporally coincident with weekend low flow periods shows that out of 41 events recorded, 17 occurred during a weekend low flow. Ten additional events occurred within one day after a weekend low flow and three events occurred within two days after a low flow. Thus, 73% of the events documented occurred during, or within two days of weekend discharges. Similar results were found during the test flow period when 11 of 23 documented erosional events occurred during, or within two days following a low flow period. This indicates that whatever the processes are that drive erosional events, the processes are triggered by either the low discharge itself or the increased range in discharge resulting from weekend operations.

Response to a Natural Flood

The LCR flooded in January 1993 with discharges exceeding 13,000 cfs for two days (Figure 92). Discharges exceeded 5,000 cfs for five days, January 10-14, and again for four days January 20-23. When combined with dam releases, discharges downstream of the LCR peaked at approximately 31,000 cfs on January 11-12. A second peak of approximately 28,000 cfs occurred on January 21-22, following a five day period of lower discharge after the first peak.

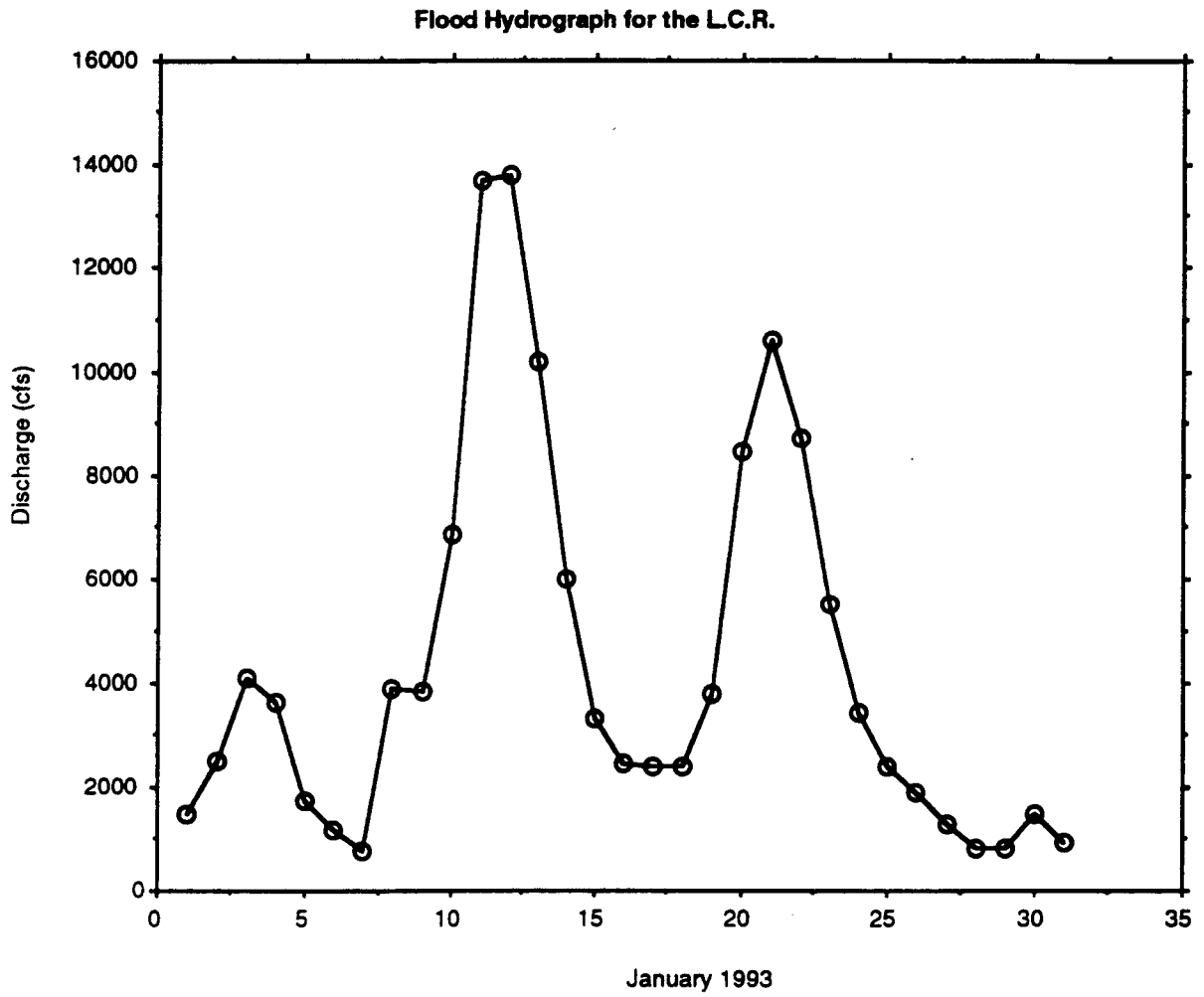


Fig. 92. Flood hydrograph for the Little Colorado River as gauged at Cameron, Arizona, January 1993.

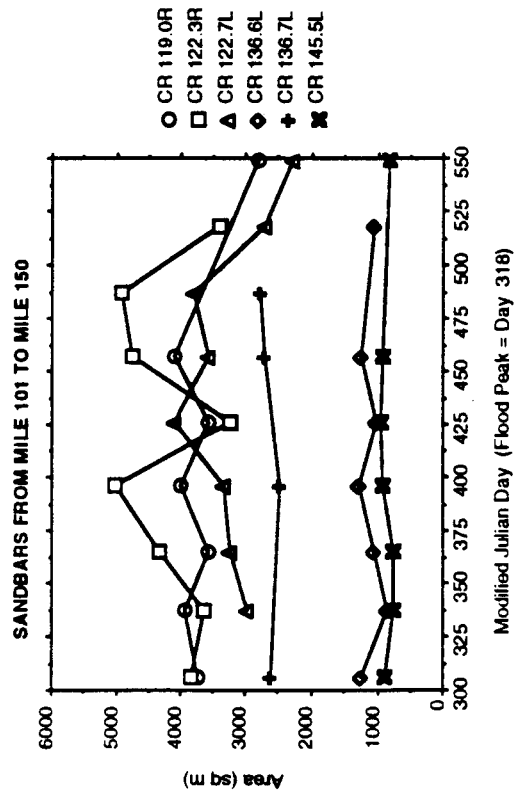
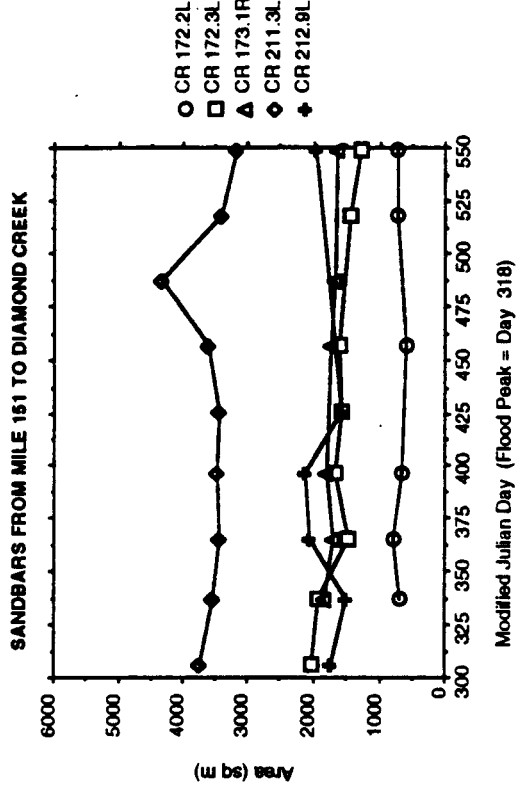
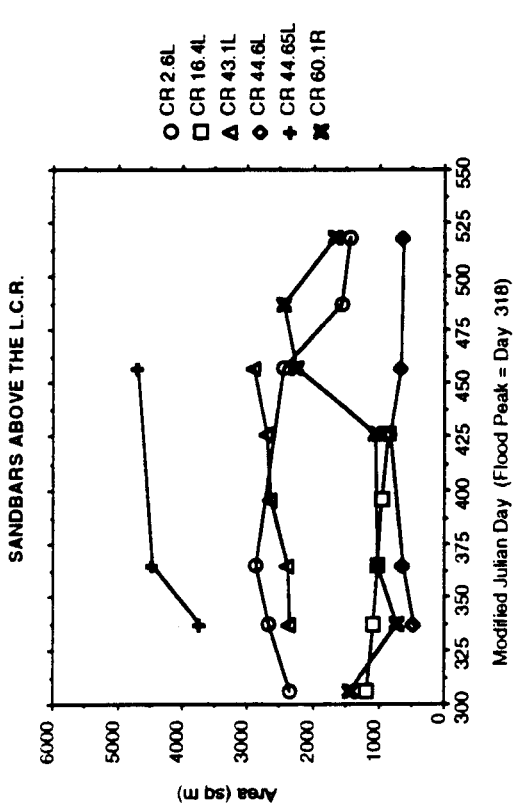
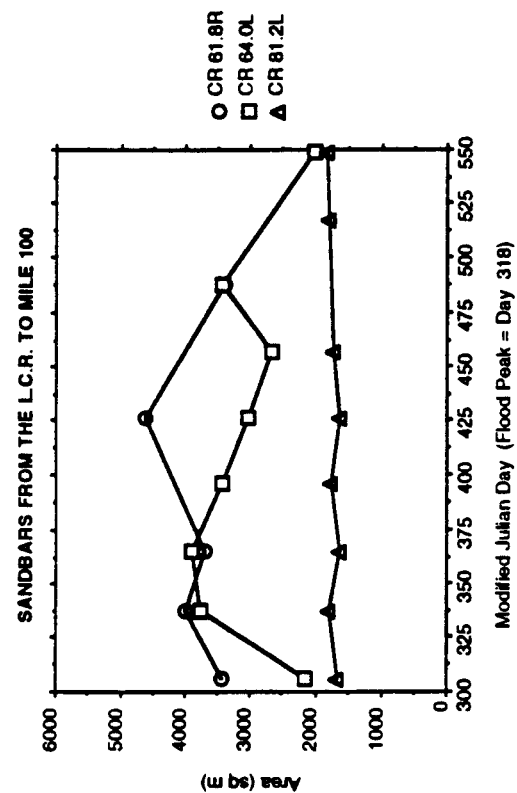


Fig. 93. Details of sandbar area response to the flood on the Little Colorado River, January 1993.

This is the highest sustained discharge in the mainstem during the interim flow period, exceeding the maximum dam release by 13,000 cfs (42%). The period of time that mainstem discharge exceeded 20,000 cfs was 17 days. The responses of the sandbars downstream of the LCR during and following this natural flood provide indications of how a habitat building or habitat maintenance release might modify sandbars. Perhaps more importantly, it provided an opportunity to measure the longevity of those modifications.

The first sandbar downstream of the LCR is study site 61.8R. It responded to the flood with rapid aggradation, particularly in the eddy zone and along the separation deposit (Figures 18 through 22). Area increased approximately 900 m² in two months during January and February 1993. Area decreased dramatically in March to approximately 450 m² less than the pre-flood area. The site was under water for most of this period so it is not known if degradation occurred rapidly or gradually. However, aggradation resumed, and by April the area had increased 260 m² over that measured in February. Area decreased by approximately 1200 m² in June because the eddy bar was completely eroded. The record is poor throughout July, August and September, but increased area measured in October shows the eddy bar completely redeposited and enlarged from its prior maximum size measured in April. The sandbar enlarged in response to the increased discharges and presumed high sediment load of the LCR flood combined with mainstem discharge. Area continued to increase long after the LCR flood had passed. It is particularly interesting that the sandbar was very dynamic during the aggradational period and apparently underwent at least two periods of aggradation followed by wholesale degradation of the eddy bar. Beginning in October 1993 degradation began and continued until the end of record in December. At that time, area was approximately 1000 m² greater than before the LCR flood.

The next sandbar downstream of the LCR is 64.0L. This site responded similarly to 61.8R in that aggradation was measured coincident with the LCR flood but degradation followed within two months (Figure 67 and 93). Aggradation resumed when mainstem discharges reached summer maximums and the greatest area was measured in September 1993.

As discharge maximum decreased in the fall 1993, area of the sandbar decreased rapidly during an event of 552 m² followed by prolonged degradation. By the end of the year, area was reduced to within the range of fluctuation measured prior to the LCR flood.

81.2L, Grapevine Camp, is the next sandbar downstream in our sample. Area increased slightly during the LCR flood and immediately decreased the following month. However, it is important to point out that field observations as well as the daily photographs indicated that the surface of the bar was higher following the flood. This morphologic change, at a site with steep slopes, is not represented by measurements taken in plan area. These results may conflict with volumetric results for the same period.

Downstream of the inner gorge, direct responses to the LCR flood, that is, area increases that clearly exceed the normal range prior to the flood, are not evident from the data. Field observations in summer 1993 did indicate that thin bands of sand were deposited at elevations approximately 1m above interim flow high stage throughout the canyon downstream of the LCR. By July or August 1993 there remained only the slightest evidence of sand deposition at higher than normal elevations.

Although the LCR flood was an aggradational event at many sandbars downstream in the Colorado River, erosion of the enlarged sites began immediately after passage of the flood. Within two weeks of the second flood peak, still on the receding limb, large scale erosional events occurred at five sites downstream (Figure 90). Erosional events occurred at four additional downstream sites within 10 weeks. Following a 10 week period of relative quiescence, repeating erosional events resumed with return periods similar to those before the LCR flood. By the end of the year, all sites downstream had eroded to approximately their pre-LCR flood size except 61.8R which retained about 1,000 m² additional area.

Sub-Annual Cycles

As noted above, a pronounced seasonal variation in sandbar areas is related to discharge and does not necessarily reflect erosional loss or depositional gain in the resulting area. This seasonal cycle is repeated every six months (Table 8) and also shows up as a positive six month lag peak in many of the correlograms in Figure 80 (43.1L, 44.65L, 119.0R, 122.7L, 136.6L, 172.3L and 211.3L).

In addition to the six month lag, several sandbars show positive direction autocorrelation peaks at three months (122.3R, 122.7L, 136.6L, 172.3L), four months (44.6L, 64.0L, 119.0R, 212.9L), five months (122.3R, 145.5L), seven months (60.1R, 64.0L, 172.2L), eight months (119.0R), and nine months (44.6L, 136.6L, 172.3L). The higher order lags (six, eight and nine month) may receive harmonic reinforcement from even-multiple lower order lags (three and four month).

With the exception of the six month lag, we may use these correlogram lags to infer periodic return intervals of associated sandbar area. Results of this technique compare favorably to longer observed return intervals, i.e. 110 days. Shorter return intervals are not resolved using the monthly time intervals of the autocorrelated data. The six month lag should not be included, as it contains a significant area change signature from the bi-annual discharge fluctuation. Sparse and missing data limit the confidence we place in these correlograms. For now, the best interpretation of their pattern is that cycles do appear in the area measurements. The cycle frequency is in agreement with observed return intervals of erosion events.

Annual Time Scales

Results from averaging the measurements from twenty rectified sandbars over 600 days of record (Table 5) indicate that overall, the average change was a 5% (s.d. 29) reduction in area. The extremes are represented by 60.1L gaining 91% of its initial area and 44.6L losing 53% of its initial area.

It is significant to note that only two sandbars (122.3R, 136.7L) began or ended the study period with a maximum or minimum area. All other sandbars achieve maximum areas greater than the beginning value and achieve minimum areas less than the ending areas sometime during the study period.

Within the study period, sandbars are highly dynamic as we have demonstrated above. Comparing the minimum and maximum areas achieved by individual sandbars, the largest relative change was found at 2.6L with a difference of 78% and the smallest relative change was found at 81.2L with a difference of 19%. The coefficient of variability (c.v.) is one of the best comparative indicators of sandbar activity. It is derived by dividing the standard deviation by the mean area which normalizes the amount of change removing the effect of deposit size. Sandbar 60.1L displays the largest c.v. (0.41) while 81.2L displays the lowest c.v. (0.06). Figure 55, a Tukey box and whisker plot (Tukey 1988), is useful in obtaining a quick appraisal of area and variability of all 20 sandbars. Attempts to relate these conclusions in a systematic way follow.

Spatial & Geomorphic Trends

Distance Downriver

An attempt to relate sandbar characteristics and dynamics to simple downriver distance was largely unsuccessful. The only parameter which shows even a small relation is the coefficient of variability. Given the non-normal distribution of sandbar area, we used non-parametric methods. The Spearman correlation coefficient (Spearman's Rho) was $-.314$ which suggests that sandbar area becomes less variable downstream.

Comparison to Reach Type

A slightly more productive approach to systematizing the overall results spatially is to relate sandbar characteristics and dynamics to geomorphology.

We have done a crude analysis of this relationship by classifying general inner canyon widths at each study sandbar into one of three ordinal classes (1 = narrow, 2 = medium, 3 = wide). Again, given the non-normal distribution of sandbar properties and given the ordinal nature of the geomorphic data, we used non-parametric methods. Comparing width to mean sandbar area yields a Spearman's Rho of .360. Comparing width to coefficients of variability yields a Rho of .462. Comparing width to event size yields a Rho of .329 but number of events yields a Rho of only -.006. It appears that the morphometry of the inner canyon and of the channel itself will need to be developed more quantitatively in order to pursue this promising approach further.

Spatial and Temporal Relationships

One hypothesis addressed in the proposal was that daily area records from a large number of sandbars could document spatial and temporal trends. This would improve our understanding of the processes that cause rapid erosional events. This could also provide management alternatives to reduce erosional rates and display potential prolonged benefits of interim flows. Spatial and temporal trends are evident in the 22 month record at 20 sites (Figure 89). Some observations on spatial and temporal trends are described below. During September 1992, eight erosional events occurred at seven sites. The sites were: 2.6L; 43.1L; 136.6L; 172.3L; 211.3L; and 212.9L. Synchronously, three sandbars eroded on January 30, 1993; - 145.5L, 172.2L, and 172.5L. On several occasions two sites eroded on the same day (Figure 90).

Erosional events are not evenly distributed with respect to either space or time. When synchronous erosional events occur at sites that are within certain spatial proximity, it suggests that localized channel processes such as the movement of sediment pulses may trigger rapid erosional events. On the other hand, when spatially separate but temporally synchronous events occur, it suggests that a more global change such as discharge pattern may be the triggering mechanism. An interesting spatial/temporal trend is evident at the sandbars 172.2L and 172.3L, a separation and eddy/reattachment complex in a riffle-pool unit.

On five occasions the separation sandbar was eroded 1-3 days prior to erosion of the reattachment sandbar (see Figures 94 and 95 for examples). These observations are described in detail in the Processes of Adjustment section.

Cumulative Effects

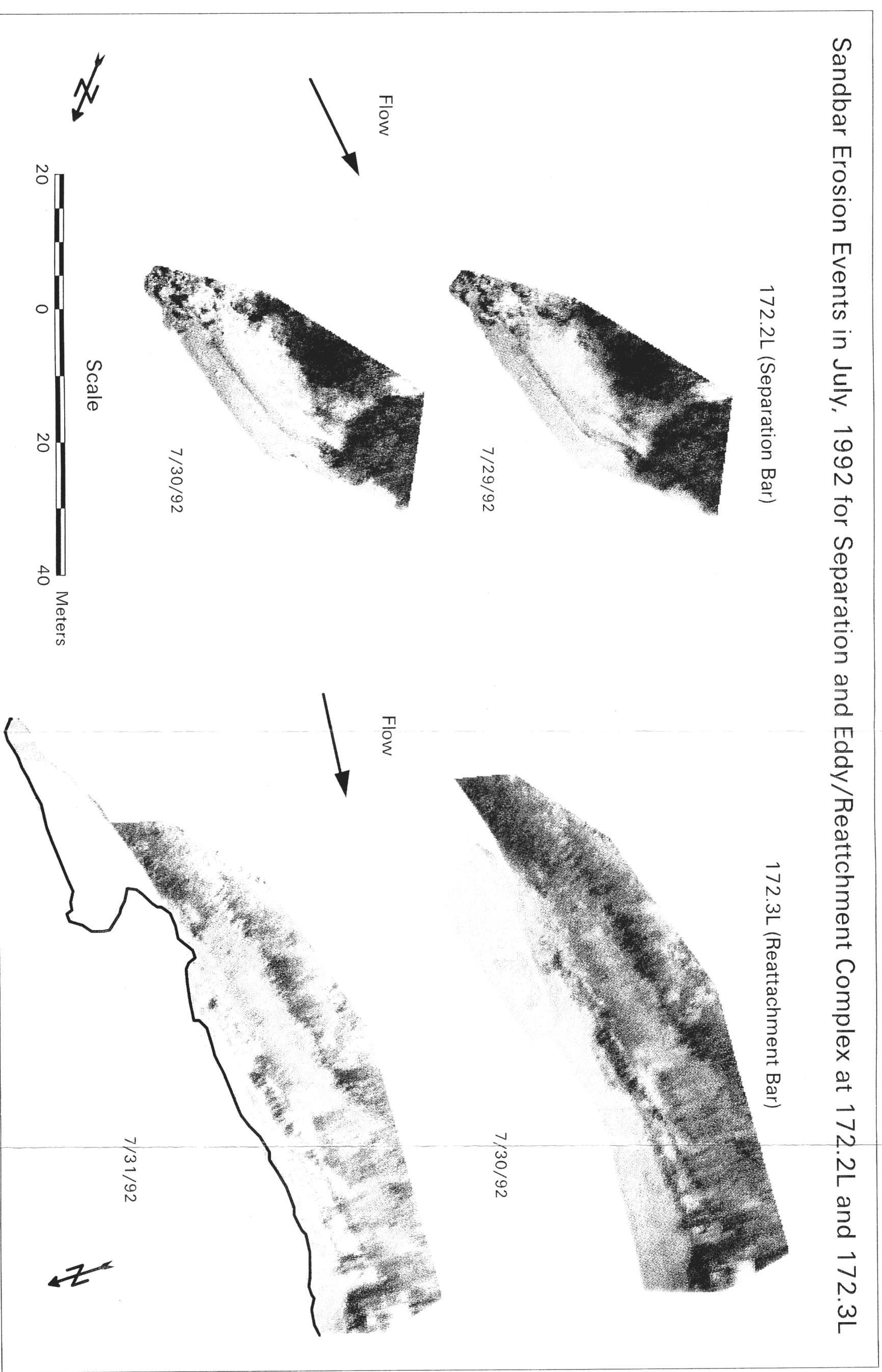
Sandbars with deposits at elevations greater than the maximum river stage suffer a cumulative effect of erosional events. This qualification includes all camping sandbars and most others. Where erosional events repeat, each event results in incremental retreat of cutbanks, or headward migration of steep slopes. This progressive loss of high elevation sediment is irretrievable until the river experiences a discharge that overtops and renews the affected sandbar. Because erosional events continued during the range limited interim flow period, the headward migration/erosion process continued to operate. The result during interim flows has been the progressive erosion of sandbars at elevations corresponding to pre-interim flow discharges. Erosion of a sandbar, stable since the 1980's floods, has occurred at least once; the reattachment bar 172.3L. During the July 1993 erosional event, *baccaris* with up to eight growth rings were found scoured from the higher elevation portions of the reattachment surface.

Processes of Adjustment

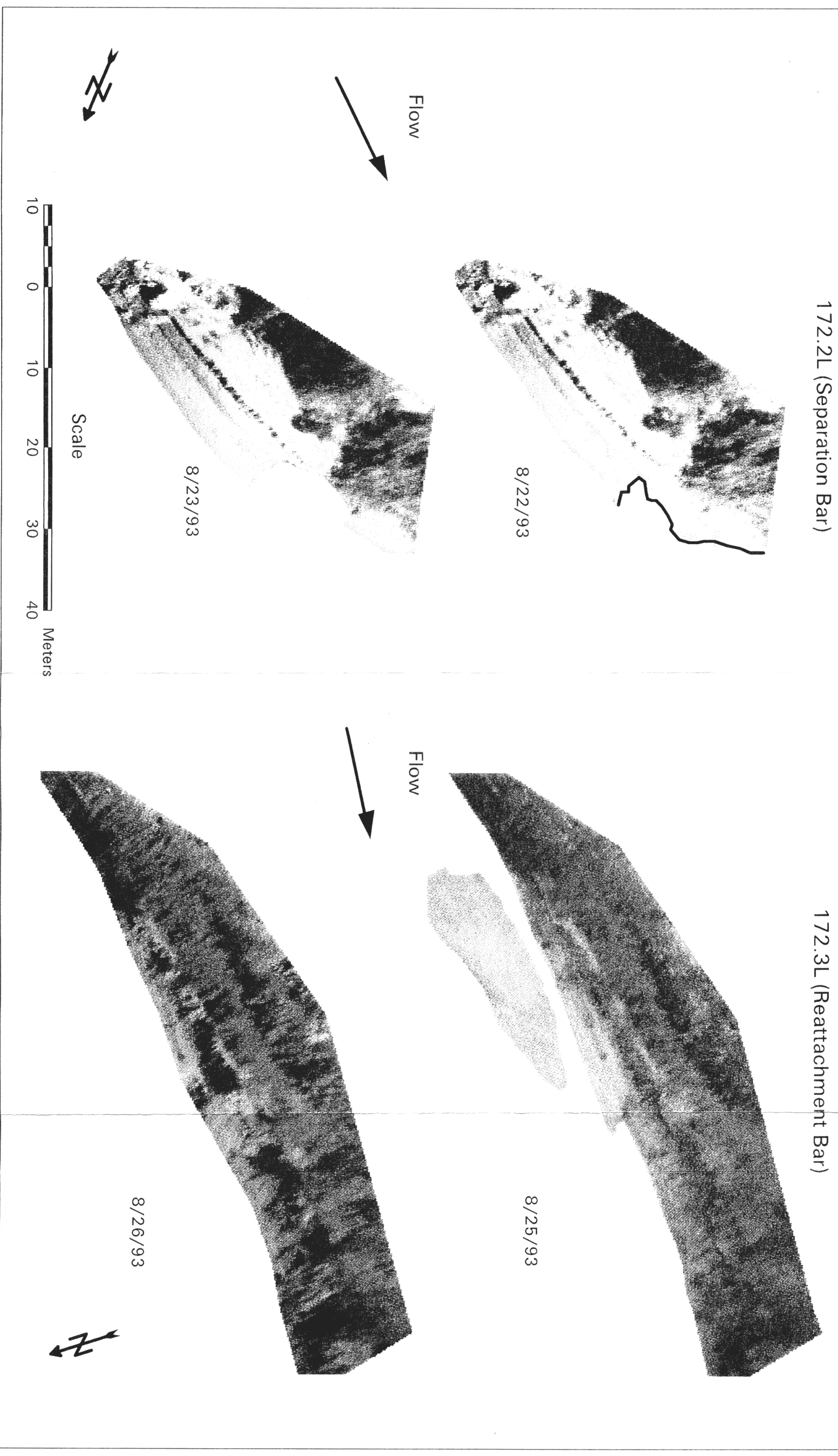
Although the exact size and detailed morphology of sandbars is unique between almost any two periods of measurement, general patterns repeated each time an erosion/deposition event occurred. Short time step repeat photographs reveal the incremental patterns by which sandbars adjust to variations in discharge (see Figures 81 through 88). The other less quantified and more variable forces and parameters within the fluvial system, such as sediment loading and routing are also displayed. The adjustment patterns that repeated during the study are discussed below.

Fig. 94.
Erosion at Mile 172, 7-92.

Sandbar Erosion Events in July, 1992 for Separation and Eddy/Reattachment Complex at 172.2L and 172.3L



Sandbar Erosion Events in August, 1993 for Separation and Eddy/Reattachment Complex at 172.2L and 172.3L



APPENDIX A: SANDBAR AREA DATA SET

Sandbar	Date	Areas (sq. M)	Fail Area	Slope Area		Comments
				Index*		
2.6L	920315	1529		S.I.=1		
Mean=	920419	1646				
1844.43	920509	1423				
STD=	920511 thru 920527					no data
595.28	920621	1770				
VAR=	920719	1391				
354362.08	920823	1493				
RMS=	920907	* (pre-failure)	1575			
3.83	920908	** (failure)	633	942		
	920920		1677			deposition
	921012	8000cfs	2365			
	921105		2210			
	921122		2840			
	921220		2357			
	930117		2700			
	930207		2885			
	930212 thru 930319					no data
	930320 thru 930425					camera flash on
	930516		2341			
	930531	8000cfs	2608			
	930629	*	1805			
	930630	**	1332	473		
	930711		1441			
	930714 thru 930815					high H2O on roll
	930831 thru 931005					blurry film
	931017		1954			
	931114		1402			
	931213		1045			
16.4L	920315	1064		S.I.=2		
Mean=	920419	1222				
1139.55	920510	1202				
STD=	920614	1251				
190.83	920719	1072				
VAR=	920823	1432				
36417.21	920912					high H2O
RMS=	921011	8000cfs	1448			
5.38	921018		1565			
	921023	*	1316			
	921024	**	1260	56		
	921115		1259			
	921206		1174			
	930117		1083			
	930203	*	1068			
	930204	**	964	104		
	930207		1040			
	930212 thru 930320					no data
	930320	*	1017			
	930321	**	987	30		
	930418		883			
	930516					corrupt (lost image in data transfer)
	930531	8000cfs	837			
	930620					high H2O
	930716 thru 930820					blurry film
	930821 thru 931112					no data
	931113		991			
	931212		935			
43.1L	911020	3058		S.I.=3		
Mean=	911110					blurry image
2752.07	911215	2857				

				Slope Area	
Sandbar	Date	Areas (sq. M)	Fail Area	Index*	Comments
STD=	920119	2704			
212.66	920216	3023			
VAR=	920315	2946			
45225.78	920419	3121			
RMS=	920510	2892			
3.81	920614	2948			
	920719	2710			
	920816	2598			
	920824	2509			*
	920825	2427	82		**
	920920	2579			
	920924	2837			*
	920925	2802	35		**
	921011	8000cfs	2527		
	921019	2894			
	921026	2548			*
	921027	2495	53		**
	921115	2856			
	921213 thru 930107				no data
	930117	2376			
	930221	2404			
	930321	2645			
	930418	2714			
	930516	2891			
	930531	8000 cfs	2969		
	930613				blurry image
	930619 thru 930901				no data
	930920				blurry image
	931017	2975			
	931121	2900			
	931211	2605			
44.6L	920315	876		S.I.=3	
Mean=	920419	794			
661.05	920516	678			
STD=	920614	751			
147.98	920719	505			
VAR=	920816	406			
21898.94	920913	616			
RMS=	921012	8000cfs	782		
3.27	921112	658			
	921211 thru 930107				no data
	930117	460			
	930220	519			
	930314	748			
	930418	819			
	930531	8000cfs	652		
	930601 thru 930714				no data
	930718	620			
	930815				high H2O on roll
	930912	709			
	931016	898			
	931114	658			
	931219	411			
44.65L	920315	5288		S.I.=2	
Mean=	920412	4993			
4644.00	920510	4870			
STD=	920614	4732			
707.41	920712	3362			
VAR=	920816	3303			

Sandbar	Date	Areas (sq. M)	Slope Area		Comments
			Fail Area	Index*	
500435	920920	4770			
	921011	8000cfs	5580		
RMS=	921018		5733		
3.56	921115		5190		
	921213 thru 930107				no data
	930120	*	3824		
	930121	**	3623	201	
	930207		4017		
	930314		4890		
	930418				blurry image
	930516		4640		
	930531	8000 cfs	4748		
	930602 thru 930714				no data
	930718				blurry image
	930815				blurry image
	930919				blurry image
	931017		5279		
	931114		4640		
	931212		4754		
60.1R	920315	809		S.I.=1	
Mean=	920418	750			
1378.70	920517	1002			
STD=	920614	977			
566.61	920719	676			
VAR=	920809	620			
321045.27	920920	1634			
RMS=	921013	8000cfs	1797		
6.50	921118		1282		
	921213		1433		
	930117		718		
	930314		1023		
	930418		1039		
	930531	8000cfs	2262		
	930613		2460		
	930718		1682		
	930715 thru 930819				blurry film
	930820 thru 930901				no data
	930919		1959		
	931017		1861		
	931121		2039		
	931219		1551		
61.8R	920315	3247		S.I.=2	
Mean=	920412	3335			
3804.85	920510	3220			
STD=	920614	3568			
764.77	920719	2331			
VAR=	920816	2461			
584877.02	920905	*	3563		
RMS=	920907	**	3527	36	
2.77	920913		3874		
	921001	*	3860		
	921002	**	3832	28	
	921012	8000cfs	3753		
	921018		3640		
	921109		3441		
	921115		3396		
	921212		3443		
	930117		4006		
	930214		4362		

Sandbar	Date	Areas (sq. M)	Fail Area	Slope Area	
				Index*	Comments
	930314	3055			
	930418	4628			
	930422 thru 930611				no data
	930612 thru 930714				blurry roll
	930607	3418			
	930715 thru 930817				blurry roll
	930818 thru 930902				no data
	930903 thru 931008				blurry roll
	931017	5245			
	931024	5127			*
	931025	5056	71		**
	931114	5016			
	931212	4522			
64.0L	920315	3277		S.I.=1	
Mean=	920419	3677			
3455.43	920517	3831			
STD=	920518 thru 920711				no data
948.28	920719	2767			
VAR=	920815	2261			
899227.35	920913	3208			
RMS=	921011	3427			* 8000cfs
3.91	921013	3027	400		** 8000cfs
	921114	2642			
	921211	2153			
	930115	3757			
	930214	3895			
	930315	3454			
	930411	3043			
	930531	2678			8000cfs
	930613	3431			
	930715 thru 930819				blurry roll
	930820 thru 930903				no data
	930815	2018			
	930912 thru 931008				blurry roll
	930912	5662			
	930916	5578			*
	930917	5026	552		**
	931017	3747			
	931114	3510			
	931226	3406			
81.2L	920316	1896		S.I.=3	
Mean=	920413				corrupt (lost image in data transfer)
1819.73	920518	1890			
STD=	920615	1917			
106.05	920720	1910			
VAR=	920817	1890			
11245.73	920923	1820			
RMS=	921012	1947			8000cfs
3.88	921111	1753			
	921214	1686			
	930125	1787			
	930215	1650			
	930315	1757			
	930407	1770			
	930418	1611			
	930515	1666			
	930531	1740			8000cfs
	930614				blurry image
	930712	1807			

Sandbar	Date	Areas (sq. M)	Fail Area	Slope Area	
				Index*	Comments
	921013	8000cfs	1678		
	921116		1689		
	921214		2021		
	930130	*	2021		
	930131	**	1822	199	
	930215		1476		
	930315		1643		
	930331	*	1705		
	930401	**	1527	178	
	930419		1612		
	930517		1566		
	930531	8000cfs	1647		
	930621				burry image
	930710	*	1508		
	930711	**	1304	204	
	930719				burry image
	930727	*	1700		
	930728	**	1250	450	
	930816		1253		
	930825	*	1387		
	930826	**	1208	179	
	930920				burry image
	931007	*	2089		
	931008	**	1610	479	
	931011				burry image
	931115		1493		
	931213		1560		
173.1R	920317		1433		S.I.=2
Mean=	920421		1393		
1584.83	920518		1291		
STD=	920616		1305		
214.49	920713		1254		
VAR=	920817		1522		
46007.56	920921		1844		
RMS=	921012	8000cfs	1977		
1.86	921116		1471		
	921117 thru 921222				camera flash on
	921223 thru 930121				no data
	930125		1832		
	930215		1701		
	930315		1791		
	930401 thru 930502				no data
	930517		1741		
	930601	8000 cfs	1676		
	930608 thru 930617				no data
	930618 thru 930722				blurry roll
	930816		1653		
	930909 thru 931014				blurry roll
	931025		1623		
	931115		1657		
	931220		1363		
211.3L	911022		3938		S.I.=2
Mean=	911119		4121		
3707.48	911224		3813		
STD=	920121		3700		
373.36	920218		3876		
VAR=	920324		4013		
139397.32	920421		3718		
RMS=	920519		4404		

Sandbar	Date	Areas (sq. M)	Fail Area	Slope Area	
				Index*	Comments
RMS=	921114				corrupt (lost image in data transfer)
6.37	921213	2638			
	930125				high H2O
	930222				very high H2O
	930315	2491			
	930327 thru 930502				camera flash on
	930503	2721			
	930601	8000cfs	2800		
	930617 thru 930722				blurry roll
	930821				High H2O
	930907 thru 931012				blurry roll
	931025	3196			
	931122	2719			
	931213	2025			
145.5L	920316	907		S.I.=3	
Mean=	920413	861			
869.83	920518	919			
STD=	920615	897			
69.80	920720	873			
VAR=	920824	*	882		
4872.22	920825	**	845		
RMS=	920826	**	809		
7.11	920827	**	775		
	920828	**	745	137	
	920921		912		
	921013	8000 cfs	929		
	921015	*	948		
	921016	**	945	3	
	921120		799		
	921215		895		
	930130	*	762		
	930131	**	749	13	
	930215		752		
	930315		933		
	930415		946		
	930531	8000cfs	931		
	930621				blurry image
	930719				blurry image
	930816		809		
	930820	*	862		
	930821	**	822	40	
	930920				blurry image
	931010				blurry image
	931025	*	965		
	931026	**	956	9	
	931115		932		
	931231		865		
172.2L	920316	770		S.I.=3	
Mean=	920413	761			
727.69	920518	796			
STD=	920615	801			
60.19	920713	714			
VAR=	920729	*	694		
3622.87	920730	**	689	5	
RMS=	920814	*	698		
5.95	920815	**	677	21	
	920817		694		
	920820	*	688		

		Slope Area			
Sandbar	Date	Areas (sq. M)	Fail Area	Index*	Comments
	930816	1842			
	930913				exposure on film was too dark
	931018	1987			
	931023	1904			
	931115	1953			
	931213	1851			
119.0R	920316	3953		S.I.=3	
Mean=	920413	3776			
3775.80	920518	3912			
STD=	920615	3893			
315.44	920706	3768			
VAR=					no data 920711 thru 920924
99500.92	920928	3961			
RMS=	921012	8000cfs	3394		
8.78	921019				corrupt (lost image in data transfer)
	921116	4056			
	921214	3723			
	930125	3924			
	930203	*	3912		
	930204	**	3677	235	
	930221		3470		
	930225	*	3470		
	930226	**	3379	91	
	930303	*	4124		
	930304	**	4011	113	
	930322		3829		
	930419		3568		
	930517		4168		
	930531	8000cfs	3996		
	930621				blurry image
	930712				blurry image
	930816	2811			
	930920				blurry image
	931018	4069			
	931122	4112			
	931219	3439			
122.3R	920316	5429		S.I.=2	
Mean=	920420	4152			
4331.22	920518	4798			
STD=	920615	4598			
609.37	920711 thru 920924				no data
VAR=	920928	4334			
371334.18	921012	8000cfs	4824		
RMS=	921116		3985		
3.78	921214		3842		
	930124	*	3846		
	930125	**	3450	396	
	930215		4343		
	930322		5032		
	930419		3261		
	930517		4834		
	930531	8000cfs	4653		
	930621		4917		
	930712		3421		
	930816				high H2O
	930906 thru 931011				blurry roll
	931018				corrupt (lost image in data transfer)
	931122	4243			
	931220				corrupt (lost image in data transfer)

Sandbar	Date	Areas (sq. M)	Fail Area	Slope Area	
				Index*	Comments
122.7L	920315	3162		S.I.=2	
Mean=	920420	3692			
3431.95	920518	3672			
STD=	920622				corrupt (lost image in data transfer)
446.48	920706	3363			
VAR=	920711 thru 921016				no data
199341.52	921012	8000 cfs			no data
	921019	4149			
RMS=	921109	3822			
1.27	921113 thru 921218				exposure on film was too dark
	921219 thru 930120				no data
	930125	2983			
	930215	3255			
	930225	3255	*		
	930226	3211	**	44	
	930315	3335			
	930418	4113			
	930517	3565			
	930531	8000 cfs	3553		
	930614	3817			
	930712	2736			
	930816	2297			
	930906 thru 931017				blurry roll
	931018	3708			
	931122	3698			
	931213	3253			
136.6L	920316	1220		S.I.=3	
Mean=	920413	1202			
1192.38	920420	1212			
STD=	920511	1264			
120.02	920615	1289			
VAR=	920705	1152			
14405.15	920825	1155			
RMS=	920921	1190			
2.22	921012	8000cfs	1326		
	921115	1314			
	921213	1241			
	930124	843			
	930214	1042			
	930314	1278			
	930418	1023			
	930518	1232			
	930531	8000cfs	1264		
	930617 thru 930722				blurry roll
	930621				blurry image
	930726	1054			
	930823				high H2O
	931022	1347			
	931115	1240			
	931220	1152			
136.7L	920315	2861		S.I.=2	
Mean=	920412	2454			
2663.54	920517	2781			
STD=	920614	2555			
283.03	920711 thru 920926				no data
VAR=	920927	2464			
80103.77	921011	8000cfs	2921		

APPENDIX B: SANDBAR AREA STATISTICS

X₁: CR 2.6L

Mean:	Std. Dev.:	Std. Error:	Variance:	Coef. Var.:	Count:
1844.435	595.283	124.125	354362.075	32.275	23
Minimum:	Maximum:	Range:	Sum:	Sum of Sqr.:	# Missing:
633	2885	2252	42422	86040578	635
t 95%:	95% Lower:	95% Upper:	# < 10th %:	10th %:	25th %:
257.42	1587.015	2101.855	2	1274.6	1427.5
50th %:	75th %:	90th %:	# > 90th %:	Mode:	Geo. Mean:
1677	2353	2728	2	•	1744.804
Har. Mean:	Kurtosis:	Skewness:			
1632.482	-.709	.172			

X₂: CR 16.4L

Mean:	Std. Dev.:	Std. Error:	Variance:	Coef. Var.:	Count:
1139.545	190.833	40.686	36417.212	16.746	22
Minimum:	Maximum:	Range:	Sum:	Sum of Sqr.:	# Missing:
837	1565	728	25070	29333166	636
t 95%:	95% Lower:	95% Upper:	# < 10th %:	10th %:	25th %:
84.611	1054.935	1224.156	2	919.4	991
50th %:	75th %:	90th %:	# > 90th %:	Mode:	Geo. Mean:
1077.5	1259	1436.8	2	•	1124.774
Har. Mean:	Kurtosis:	Skewness:			
1110.511	-.458	.512			

X₃: CR 43.1L

Mean:	Std. Dev.:	Std. Error:	Variance:	Coef. Var.:	Count:
2726.72	211.142	42.228	44580.793	7.743	25
Minimum:	Maximum:	Range:	Sum:	Sum of Sqr.:	# Missing:
2376	3121	745	68168	186944988	633
t 95%:	95% Lower:	95% Upper:	# < 10th %:	10th %:	25th %:
87.155	2639.565	2813.875	2	2427	2542.75
50th %:	75th %:	90th %:	# > 90th %:	Mode:	Geo. Mean:
2714	2895.5	2969	2	•	2718.819
Har. Mean:	Kurtosis:	Skewness:			
2710.882	-1.197	-.058			

APPENDIX B: SANDBAR AREA STATISTICS

X4: CR 44.6L					
Mean:	Std. Dev.:	Std. Error:	Variance:	Coef. Var.:	Count:
661.053	147.983	33.95	21898.942	22.386	19
Minimum:	Maximum:	Range:	Sum:	Sum of Sqr.:	# Missing:
406	898	492	12560	8697002	639
t 95%:	95% Lower:	95% Upper:	# < 10th %:	10th %:	25th %:
71.325	589.727	732.378	2	430.6	543.25
50th %:	75th %:	90th %:	# > 90th %:	Mode:	Geo. Mean:
658	774.25	853.2	2	658	644.073
Har. Mean:	Kurtosis:	Skewness:			
625.932	-.879	-.253			

X5: CR 44.65L					
Mean:	Std. Dev.:	Std. Error:	Variance:	Coef. Var.:	Count:
4644	707.414	162.292	500435	15.233	19
Minimum:	Maximum:	Range:	Sum:	Sum of Sqr.:	# Missing:
3303	5733	2430	88236	418775814	639
t 95%:	95% Lower:	95% Upper:	# < 10th %:	10th %:	25th %:
340.963	4303.037	4984.963	2	3466.4	4172.75
50th %:	75th %:	90th %:	# > 90th %:	Mode:	Geo. Mean:
4754	5140.75	5463.2	2	4640	4588.859
Har. Mean:	Kurtosis:	Skewness:			
4529.63	-.6	-.566			

X6: CR 60.1R					
Mean:	Std. Dev.:	Std. Error:	Variance:	Coef. Var.:	Count:
1378.7	566.609	126.698	321045.274	41.097	20
Minimum:	Maximum:	Range:	Sum:	Sum of Sqr.:	# Missing:
620	2460	1840	27574	44116134	638
t 95%:	95% Lower:	95% Upper:	# < 10th %:	10th %:	25th %:
265.181	1113.519	1643.881	2	697	893
50th %:	75th %:	90th %:	# > 90th %:	Mode:	Geo. Mean:
1357.5	1829	2150.5	2	•	1265.279
Har. Mean:	Kurtosis:	Skewness:			
1156.847	-1.129	.286			

APPENDIX B: SANDBAR AREA STATISTICS

X7: CR 61.8R

Mean:	Std. Dev.:	Std. Error:	Variance:	Coef. Var.:	Count:
3804.846	764.773	149.984	584877.015	20.1	26
Minimum:	Maximum:	Range:	Sum:	Sum of Sqr.:	# Missing:
2331	5245	2914	98926	391020136	632
t 95%:	95% Lower:	95% Upper:	# < 10th %:	10th %:	25th %:
308.898	3495.948	4113.744	3	3071.5	3396
50th %:	75th %:	90th %:	# > 90th %:	Mode:	Geo. Mean:
3604	4362	5052	3	•	3730.735
Har. Mean:	Kurtosis:	Skewness:			
3655.85	-.393	.304			

Xg: CR 64.0L

Mean:	Std. Dev.:	Std. Error:	Variance:	Coef. Var.:	Count:
3455.435	948.276	197.729	899227.348	27.443	23
Minimum:	Maximum:	Range:	Sum:	Sum of Sqr.:	# Missing:
2018	5662	3644	79475	294403681	635
t 95%:	95% Lower:	95% Upper:	# < 10th %:	10th %:	25th %:
410.065	3045.369	3865.5	2	2239.4	2832
50th %:	75th %:	90th %:	# > 90th %:	Mode:	Geo. Mean:
3427	3754.5	5136.4	2	•	3339.529
Har. Mean:	Kurtosis:	Skewness:			
3230.163	.552	.872			

Xg: CR 81.2L

Mean:	Std. Dev.:	Std. Error:	Variance:	Coef. Var.:	Count:
1819.727	106.046	22.609	11245.732	5.828	22
Minimum:	Maximum:	Range:	Sum:	Sum of Sqr.:	# Missing:
1611	1987	376	40034	73087122	636
t 95%:	95% Lower:	95% Upper:	# < 10th %:	10th %:	25th %:
47.018	1772.709	1866.745	2	1661.2	1753
50th %:	75th %:	90th %:	# > 90th %:	Mode:	Geo. Mean:
1831	1904	1948.8	2	1890	1816.73
Har. Mean:	Kurtosis:	Skewness:			
1813.687	-.893	-.355			

APPENDIX B: SANDBAR AREA STATISTICS

X10: CR 119.0R					
Mean:	Std. Dev.:	Std. Error:	Variance:	Coef. Var.:	Count:
3775.8	315.438	63.088	99500.917	8.354	25
Minimum:	Maximum:	Range:	Sum:	Sum of Sqr.:	# Missing:
2811	4168	1357	94395	358804663	633
t 95%:	95% Lower:	95% Upper:	# < 10th %:	10th %:	25th %:
130.206	3645.594	3906.006	2	3394	3543.5
50th %:	75th %:	90th %:	# > 90th %:	Mode:	Geo. Mean:
3893	3999.75	4112	2	•	3762.114
Har. Mean:	Kurtosis:	Skewness:			
3747.248	1.465	-1.204			

X11: CR 122.3R					
Mean:	Std. Dev.:	Std. Error:	Variance:	Coef. Var.:	Count:
4331.222	609.372	143.63	371334.183	14.069	18
Minimum:	Maximum:	Range:	Sum:	Sum of Sqr.:	# Missing:
3261	5429	2168	77962	343983428	640
t 95%:	95% Lower:	95% Upper:	# < 10th %:	10th %:	25th %:
303.034	4028.189	4634.256	2	3429.7	3846
50th %:	75th %:	90th %:	# > 90th %:	Mode:	Geo. Mean:
4338.5	4824	4997.5	2	•	4289.414
Har. Mean:	Kurtosis:	Skewness:			
4246.425	-.865	-.18			

X12: CR 122.7L					
Mean:	Std. Dev.:	Std. Error:	Variance:	Coef. Var.:	Count:
3431.95	446.477	99.835	199341.524	13.009	20
Minimum:	Maximum:	Range:	Sum:	Sum of Sqr.:	# Missing:
2297	4149	1852	68639	239353105	638
t 95%:	95% Lower:	95% Upper:	# < 10th %:	10th %:	25th %:
208.958	3222.992	3640.908	2	2859.5	3232
50th %:	75th %:	90th %:	# > 90th %:	Mode:	Geo. Mean:
3458	3703	3967.5	2	3255	3402.038
Har. Mean:	Kurtosis:	Skewness:			
3369.359	.47	-.644			

APPENDIX B: SANDBAR AREA STATISTICS

X13: CR 136.6L					
Mean:	Std. Dev.:	Std. Error:	Variance:	Coef. Var.:	Count:
1192.381	120.021	26.191	14405.148	10.066	21
Minimum:	Maximum:	Range:	Sum:	Sum of Sqr.:	# Missing:
843	1347	504	25040	30145322	637
t 95%:	95% Lower:	95% Upper:	# < 10th %:	10th %:	25th %:
54.633	1137.748	1247.014	2	1034.4	1152
50th %:	75th %:	90th %:	# > 90th %:	Mode:	Geo. Mean:
1220	1267.5	1318.8	2	•	1186.003
Har. Mean:	Kurtosis:	Skewness:			
1178.899	1.535	-1.283			

X14: CR 136.7L					
Mean:	Std. Dev.:	Std. Error:	Variance:	Coef. Var.:	Count:
2663.538	283.026	78.497	80103.769	10.626	13
Minimum:	Maximum:	Range:	Sum:	Sum of Sqr.:	# Missing:
2025	3196	1171	34626	93188928	645
t 95%:	95% Lower:	95% Upper:	# < 10th %:	10th %:	25th %:
171.031	2492.508	2834.569	1	2368.2	2484.25
50th %:	75th %:	90th %:	# > 90th %:	Mode:	Geo. Mean:
2719	2815.25	2976	1	•	2649.032
Har. Mean:	Kurtosis:	Skewness:			
2633.783	.625	-.397			

X15: CR 145.5L					
Mean:	Std. Dev.:	Std. Error:	Variance:	Coef. Var.:	Count:
869.828	69.801	12.962	4872.219	8.025	29
Minimum:	Maximum:	Range:	Sum:	Sum of Sqr.:	# Missing:
745	965	220	25225	22077823	629
t 95%:	95% Lower:	95% Upper:	# < 10th %:	10th %:	25th %:
26.551	843.277	896.379	3	756	809
50th %:	75th %:	90th %:	# > 90th %:	Mode:	Geo. Mean:
882	931.25	947.2	3	809	867.045
Har. Mean:	Kurtosis:	Skewness:			
864.189	-1.08	-.462			

APPENDIX B: SANDBAR AREA STATISTICS

X16: CR 172.2L					
Mean:	Std. Dev.:	Std. Error:	Variance:	Coef. Var.:	Count:
727.688	60.19	10.64	3622.867	8.271	32
Minimum:	Maximum:	Range:	Sum:	Sum of Sqr.:	# Missing:
590	851	261	23286	17057240	626
t 95%:	95% Lower:	95% Upper:	# < 10th %:	10th %:	25th %:
21.701	705.987	749.388	3	657.8	691
50th %:	75th %:	90th %:	# > 90th %:	Mode:	Geo. Mean:
728	766.5	805.2	3	694	725.25
Har. Mean:	Kurtosis:	Skewness:			
722.784	-.223	-.051			

X17: CR 172.3L					
Mean:	Std. Dev.:	Std. Error:	Variance:	Coef. Var.:	Count:
1626.906	266.939	47.189	71256.281	16.408	32
Minimum:	Maximum:	Range:	Sum:	Sum of Sqr.:	# Missing:
1024	2136	1112	52061	86907311	626
t 95%:	95% Lower:	95% Upper:	# < 10th %:	10th %:	25th %:
96.242	1530.665	1723.148	3	1252.1	1500.5
50th %:	75th %:	90th %:	# > 90th %:	Mode:	Geo. Mean:
1625	1730.5	2041.4	3	•	1605.141
Har. Mean:	Kurtosis:	Skewness:			
1582.617	-.056	.078			

X18: CR 173.1R					
Mean:	Std. Dev.:	Std. Error:	Variance:	Coef. Var.:	Count:
1584.833	214.494	50.557	46007.559	13.534	18
Minimum:	Maximum:	Range:	Sum:	Sum of Sqr.:	# Missing:
1254	1977	723	28527	45992669	640
t 95%:	95% Lower:	95% Upper:	# < 10th %:	10th %:	25th %:
106.665	1478.168	1691.499	2	1295.2	1393
50th %:	75th %:	90th %:	# > 90th %:	Mode:	Geo. Mean:
1638	1741	1840.4	2	•	1570.972
Har. Mean:	Kurtosis:	Skewness:			
1557.039	-1.097	.011			

APPENDIX B: SANDBAR AREA STATISTICS

X19: CR 211.3L					
Mean:	Std. Dev.:	Std. Error:	Variance:	Coef. Var.:	Count:
3674.964	392.871	74.246	154347.517	10.69	28
Minimum:	Maximum:	Range:	Sum:	Sum of Sqr.:	# Missing:
3115	4839	1724	102899	382317533	630
t 95%:	95% Lower:	95% Upper:	# < 10th %:	10th %:	25th %:
152.339	3522.625	3827.304	3	3196.2	3403
50th %:	75th %:	90th %:	# > 90th %:	Mode:	Geo. Mean:
3597	3951	4104.7	3	•	3655.782
Har. Mean:	Kurtosis:	Skewness:			
3637.571	1.046	.988			

X20: CR 212.9L					
Mean:	Std. Dev.:	Std. Error:	Variance:	Coef. Var.:	Count:
2145.059	441.987	107.198	195352.184	20.605	17
Minimum:	Maximum:	Range:	Sum:	Sum of Sqr.:	# Missing:
1442	2911	1469	36466	81347350	641
t 95%:	95% Lower:	95% Upper:	# < 10th %:	10th %:	25th %:
227.249	1917.81	2372.307	2	1521.8	1706.5
50th %:	75th %:	90th %:	# > 90th %:	Mode:	Geo. Mean:
2249	2531	2592	2	•	2100.08
Har. Mean:	Kurtosis:	Skewness:			
2053.602	-1.114	-.148			

APPENDIX C: COMPARATIVE SANDBAR STATISTICS

X1: BEGIN					
Mean:	Std. Dev.:	Std. Error:	Variance:	Coef. Var.:	Count:
2420.15	1459.527	326.36	2130220.345	60.307	20
Minimum:	Maximum:	Range:	Sum:	Sum of Sqr.:	# Missing:
770	5429	4659	48403	157616707	0
t 95%:	95% Lower:	95% Upper:	# < 10th %:	10th %:	25th %:
683.08	1737.07	3103.23	2	842.5	1142
50th %:	75th %:	90th %:	# > 90th %:	Mode:	Geo. Mean:
2072.5	3262	4620.5	2	•	2011.701
Har. Mean:	Kurtosis:	Skewness:			
1665.767	-.624	.647			

X2: END					
Mean:	Std. Dev.:	Std. Error:	Variance:	Coef. Var.:	Count:
2249.35	1339.959	299.624	1795490.766	59.571	20
Minimum:	Maximum:	Range:	Sum:	Sum of Sqr.:	# Missing:
411	4754	4343	44987	135305833	0
t 95%:	95% Lower:	95% Upper:	# < 10th %:	10th %:	25th %:
627.12	1622.23	2876.47	2	805.5	1098.5
50th %:	75th %:	90th %:	# > 90th %:	Mode:	Geo. Mean:
1938	3329.5	4382.5	2	•	1850.071
Har. Mean:	Kurtosis:	Skewness:			
1468.753	-1.019	.481			

X3: % CHOT					
Mean:	Std. Dev.:	Std. Error:	Variance:	Coef. Var.:	Count:
-4.579	28.816	6.443	830.366	-629.309	20
Minimum:	Maximum:	Range:	Sum:	Sum of Sqr.:	# Missing:
-53.08	91.72	144.8	-91.58	16196.304	0
t 95%:	95% Lower:	95% Upper:	# < 10th %:	10th %:	25th %:
13.486	-18.065	8.907	2	-30.435	-15.985
50th %:	75th %:	90th %:	# > 90th %:	Mode:	Geo. Mean:
-6.765	-.83	21.605	2	•	•
Har. Mean:	Kurtosis:	Skewness:			
•	4.737	1.85			

APPENDIX C: COMPARATIVE SANDBAR STATISTICS

X4: MAX					
Mean:	Std. Dev.:	Std. Error:	Variance:	Coef. Var.:	Count:
3076.2	1663.862	372.051	2768435.642	54.088	20
Minimum:	Maximum:	Range:	Sum:	Sum of Sqr.:	# Missing:
851	5733	4882	61524	241860406	0
t 95%:	95% Lower:	95% Upper:	# < 10th %:	10th %:	25th %:
778.711	2297.489	3854.911	2	931.5	1771
50th %:	75th %:	90th %:	# > 90th %:	Mode:	Geo. Mean:
2898	4503.5	5545.5	2	•	2605.52
Har. Mean:	Kurtosis:	Skewness:			
2144.309	-1.232	.284			

X5: MIN					
Mean:	Std. Dev.:	Std. Error:	Variance:	Coef. Var.:	Count:
1677.1	972.888	217.544	946511.989	58.01	20
Minimum:	Maximum:	Range:	Sum:	Sum of Sqr.:	# Missing:
406	3303	2897	33542	74237016	0
t 95%:	95% Lower:	95% Upper:	# < 10th %:	10th %:	25th %:
455.326	1221.774	2132.426	2	605	791
50th %:	75th %:	90th %:	# > 90th %:	Mode:	Geo. Mean:
1526.5	2353.5	3188	2	•	1389.795
Har. Mean:	Kurtosis:	Skewness:			
1128.482	-1.256	.33			

X6: % TDIF					
Mean:	Std. Dev.:	Std. Error:	Variance:	Coef. Var.:	Count:
43.933	16.093	3.599	258.989	36.631	20
Minimum:	Maximum:	Range:	Sum:	Sum of Sqr.:	# Missing:
18.92	78.06	59.14	878.65	43522.077	0
t 95%:	95% Lower:	95% Upper:	# < 10th %:	10th %:	25th %:
7.532	36.401	51.464	2	23.335	34.095
50th %:	75th %:	90th %:	# > 90th %:	Mode:	Geo. Mean:
41.16	53.425	69.58	2	•	41.152
Har. Mean:	Kurtosis:	Skewness:			
38.397	-.283	.553			

APPENDIX C: COMPARATIVE SANDBAR STATISTICS

X7: MEAN					
Mean:	Std. Dev.:	Std. Error:	Variance:	Coef. Var.:	Count:
2374.95	1273.64	284.795	1622158.892	53.628	20
Minimum:	Maximum:	Range:	Sum:	Sum of Sqr.:	# Missing:
661	4644	3983	47499	143628769	0
t 95%:	95% Lower:	95% Upper:	# < 10th %:	10th %:	25th %:
596.082	1778.868	2971.032	2	799	1285.5
50th %:	75th %:	90th %:	# > 90th %:	Mode:	Geo. Mean:
1994.5	3565	4068	2	•	2024.057
Har. Mean:	Kurtosis:	Skewness:			
1687.808	-1.275	.284			

X8: ST. DEV.					
Mean:	Std. Dev.:	Std. Error:	Variance:	Coef. Var.:	Count:
372.85	254.641	56.94	64842.134	68.296	20
Minimum:	Maximum:	Range:	Sum:	Sum of Sqr.:	# Missing:
60	948	888	7457	4012343	0
t 95%:	95% Lower:	95% Upper:	# < 10th %:	10th %:	25th %:
119.176	253.674	492.026	2	88	169.5
50th %:	75th %:	90th %:	# > 90th %:	Mode:	Geo. Mean:
299	581	736	2	•	285.828
Har. Mean:	Kurtosis:	Skewness:			
207.276	-.564	.65			

X9: CV					
Mean:	Std. Dev.:	Std. Error:	Variance:	Coef. Var.:	Count:
.161	.091	.02	.008	56.476	20
Minimum:	Maximum:	Range:	Sum:	Sum of Sqr.:	# Missing:
.058	.411	.353	3.223	.677	0
t 95%:	95% Lower:	95% Upper:	# < 10th %:	10th %:	25th %:
.043	.119	.204	2	.078	.092
50th %:	75th %:	90th %:	# > 90th %:	Mode:	Geo. Mean:
.138	.204	.299	2	•	.141
Har. Mean:	Kurtosis:	Skewness:			
.125	1.105	1.28			

APPENDIX D: DAM DISCHARGE STATISTICS

X1: MINIMUM					
Mean:	Std. Dev.:	Std. Error:	Variance:	Coef. Var.:	Count:
8225.51	1619.451	63.181	2622620.509	19.688	657
Minimum:	Maximum:	Range:	Sum:	Sum of Sqr.:	# Missing:
5040	14010	8970	5404160	4.617E10	1
t 95%:	95% Lower:	95% Upper:	# < 10th %:	10th %:	25th %:
124.061	8101.449	8349.571	65	6340	6880
50th %:	75th %:	90th %:	# > 90th %:	Mode:	Geo. Mean:
8000	9352.5	10680	65	8000	8071.865
Har. Mean:	Kurtosis:	Skewness:			
7924.329	-.335	.533			

X2: MEAN					
Mean:	Std. Dev.:	Std. Error:	Variance:	Coef. Var.:	Count:
11293.886	2180.031	85.051	4752536.818	19.303	657
Minimum:	Maximum:	Range:	Sum:	Sum of Sqr.:	# Missing:
6539	17093	10554	7420083	8.692E10	1
t 95%:	95% Lower:	95% Upper:	# < 10th %:	10th %:	25th %:
167.005	11126.881	11460.891	66	8658.6	9810.5
50th %:	75th %:	90th %:	# > 90th %:	Mode:	Geo. Mean:
10855	12700	14809.8	66	•	11089.481
Har. Mean:	Kurtosis:	Skewness:			
10891.087	-.504	.474			

X3: MAXIMUM					
Mean:	Std. Dev.:	Std. Error:	Variance:	Coef. Var.:	Count:
13975.586	2770.317	108.08	7674653.962	19.823	657
Minimum:	Maximum:	Range:	Sum:	Sum of Sqr.:	# Missing:
7770	20760	12990	9181960	1.334E11	1
t 95%:	95% Lower:	95% Upper:	# < 10th %:	10th %:	25th %:
212.225	13763.361	14187.811	66	10546	12230
50th %:	75th %:	90th %:	# > 90th %:	Mode:	Geo. Mean:
13540	15695	18558	66	•	13703.763
Har. Mean:	Kurtosis:	Skewness:			
13433.897	-.526	.354			

APPENDIX E: AREA VALUES FOR SYNTHETIC SANDBAR

Synthetic Normal Sandbar	
1	2300
2	2100
3	1480
4	2200
5	1705
6	1793
7	1832
8	1861
9	1905
10	1943
11	1993
12	1944
13	2032
14	2120
15	2221
16	2189
17	2005
18	1850
19	2031
20	2333
21	2415
22	2516
23	2605
24	2717
25	1600
26	2100
27	2120
28	2095
29	2310
30	2010
31	2201
32	2205
33	2290
34	2287
35	2350

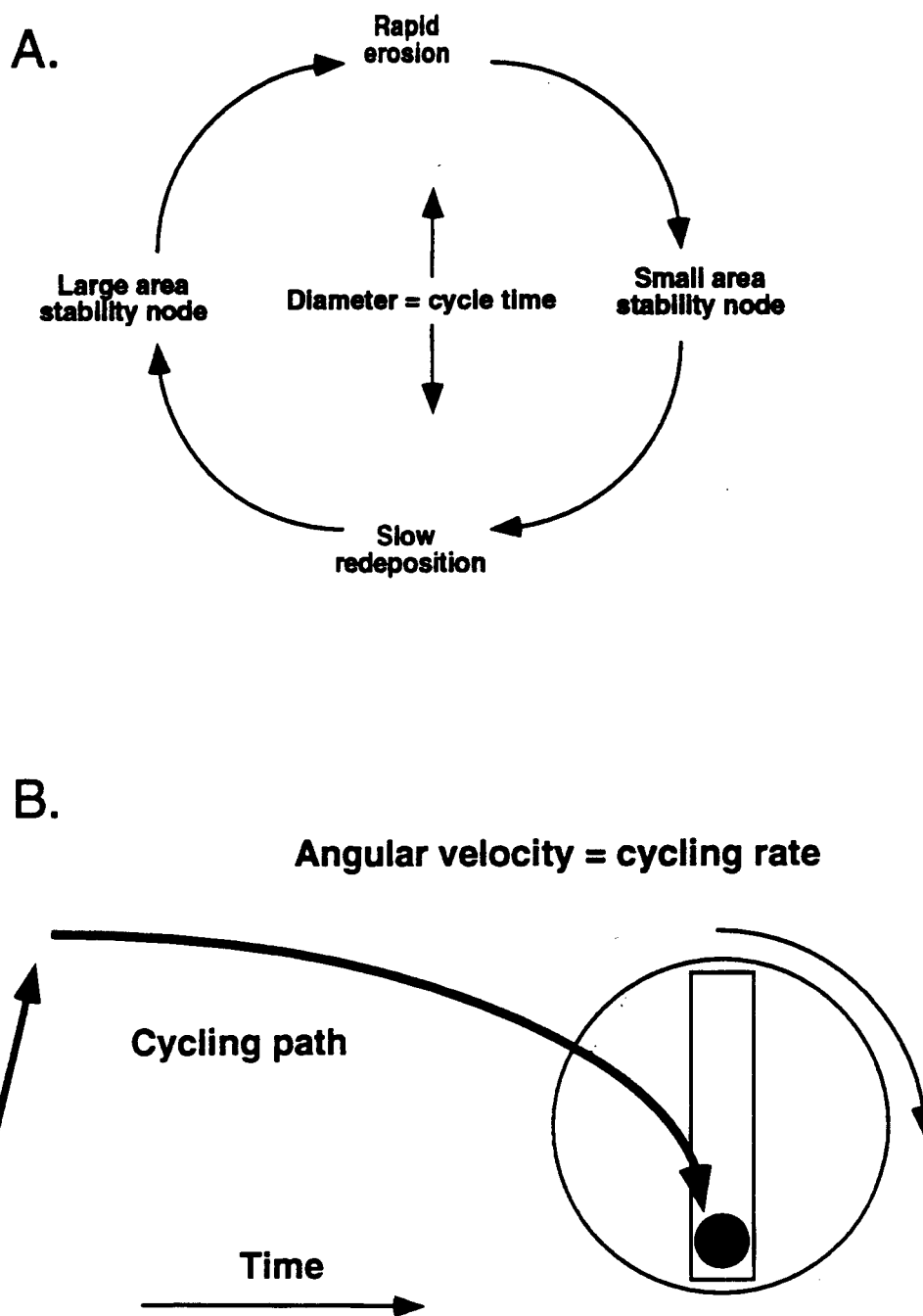


Fig. 96. Conceptual analog models of sandbar dynamics principles as suggested by this research. Panel A illustrates rapid erosion cycling and slow redeposition separated by quasi-stable area nodes. Panel B is a mechanical analog simulating erosional cycling by the path described by an axle moving within the slot of a rolling wheel (see text for details).

On March 16, 1992 a camera began monitoring area changes at the adjacent separation deposit 172.2L (that forms the eddy and reattachment deposits called 172.3L). Multiple erosional events were also documented during the period of record which began March 16, 1992. The timing of these events with respect to the events that occurred on the adjacent eddy bar suggests a definite process linkage between the sandbars that reside within one riffle-pool unit. On four separate occasions failure of the separation bar preceded failure of the eddy bar by two days, and by one day on one occasion (Figure 90).

One such event was observed in the field in July 1993. At noon on July 25, 1993 during daily low stage, a semi-circular area on the downstream face of the separation bar began eroding. The driving force appeared to be a secondary vortex with sufficient spatial and temporal stability to scour sand from submerged as well as subaerial portions of the deposit. The vortex persisted for about 2-3 h and eroded an area about 50 m² with an estimated volume of 50 m³. Erosion ceased as daily stage increased and no additional erosion was observed. During the following discharge fluctuation, approximately 15 cm of sand were evenly deposited over the top of the eddy bar. About 5 cm of sand were deposited on top of the eddy bar during high stage on July 26. As stage increased on July 27, erosion was initiated about 8:30 PM along the river facing side of the eddy bar in a fashion much like that observed on April 17, 1991. Within about three hours the eddy deposit was completely eroded by high velocity currents and retreat of the bank along vertical faces.

The same style of sandbar size adjustment was observed at 61.8R in three separate events. One camera covers the separation and eddy deposits, and thus allows for combined area change measurements. Area degradation in the separation bar region was followed by area aggradation in the eddy bar region on three occasions. The measured area changes were not particularly large but that is because areas eroded from the separation bar were compensated for by areas deposited on the eddy bar. The individual area changes could be best depicted by separating the two measurements. At this site there is not an obvious break between the deposits.

Consequently, it appears that processes very similar to those observed at the separation bar 172.2L and eddy/reattachment bar 172.3L operate at 61.8R as well.

The sequence of events that occur during large scale adjustments of sandbar size and morphology indicates a strong linkage between processes by which separation bars erode and eddy bars deposit. Both processes culminate in stripping large quantities of sand from the eddy. A simple conceptual model was devised to facilitate visualization of these processes (Figure 96). An axle within an eccentric bearing on a wheel rolling along a path scribes a repeating pattern of deposition and erosion. Deposition is initially rapid, diminishing with time, and culminates with an instantaneous erosional event. A sandbar at maximum size is stable but close to a threshold where a perturbation in the daily flow pattern, or a sudden increase in sediment supply cause wholesale erosion of the eddy. Aggradation ensues immediately following degradation. This cycle repeats. The wheel diameter relates to the weekly range of discharge. The velocity of rotation relates to the supply of sediment and other local variables such as channel geometry (See Figures 86, 87 and 88 for field examples).

Documenting the timing and sequence of erosion and deposition within the geomorphic unit of the riffle-pool is valuable for several reasons. It provides an increased understanding of the processes involved in the adjustment of sandbar size and morphology. It illustrates how sands interchange between bank storage and the channel. Finally, it provides a conceptual model of disjunct sediment routing. This includes repeated cycles of sandbar aggradation with variable length but temporary storage and infrequent but voluminous erosion, mobilization and transport. These processes are the subject of detailed investigation by Cluer.

Success of the Interim Flows

The interim flow prescription was designed to reduce adverse impact to all the resources downstream using the best available information. This was done by reducing the maximum discharge, daily range, and ramping rates which were believed to induce seepage erosion. This study had developed a database from seven sandbars during the GCES Phase II test flow program.

Comparisons of sandbar areas and dynamics during the test flow and interim flow periods were made in order to assess the success of the interim flow prescription (see Table 12). By combining the results of photography and photogrammetry from this investigation and an earlier pilot project (Cluer 1992), the records for seven selected sandbars are extended from August 1990 to December 1993. Photos from 172.3L obtained during the test flow period were rectified by methods described in this report. For the other sites in the pilot study, photographs were used in original oblique view form for the purpose of determining event timing, qualitative assessments of morphological change, and semi-quantitative estimation of size change. The results are summarized in Table 12.

Erosional events occurred at all sites during the period of record. Erosional events were documented at five of seven sites during the latter part of the test flow period. During the interim flow period until December 1993, erosional events were documented at six of seven sites. The overall mean return period for erosional events during the test flow period was 32.4 days, and 25.8 days during the interim flow period. The period between erosional events decreased at 43.1L, 172.3L, and 215.8R and increased at 51.7L, and 211.3L. Little change in event periodicity was found at sandbar 68.3R where daily photography began August 8, 1990. During the interim flow period, the 613 day record documented 12 erosional events. The annual event frequency is 6.8 for the test flow period and 7.1 for the interim flow period. The mean time interval between erosional events is 63 days for both periods, or every nine weeks.

Image geometry prevents rectification at 68.3R. Visual estimates rank the areas of erosional events very similar in the test flow and interim flow periods. Rectified image maps of erosional events at 172.3L were made for both time periods. The mean area eroded during test flow events was 227.7 m² and 320.1 m² for events during the interim flow period.

There were opposing changes in mean event area and frequency at individual sites. Therefore, the annual sediment cycling rate might serve as an indicator of the relative dynamic activities during the test flow and interim flow periods. Annual cycling rates were calculated for individual sites as the product of the mean erosional event area and the annual event frequency. Data are available to compare the periods at site 172.3L. The respective rates are 1836 m² and 1773 m², representing a 3% reduction that is probably insignificant given gaps in the record and the accuracy of area measurements. Consequently, it appears that the interim flow prescription was not successful in reducing the dynamic activity of sandbars. Because erosional events continued at similar frequencies and magnitudes, seepage as an important erosional process was probably overestimated.

Summary: Uniformitarianism or Catastrophism ?

The concepts of uniformitarianism versus catastrophism have dominated the philosophical developments in geology for centuries. Uniformitarianism describes the belief that much of the erosional and depositional work performed at the earth's surface is gradual and very slow but progressive. Over long periods of time great landscapes such as the Grand Canyon are developed. Alternatively, catastrophism is the philosophy that over long periods of time, little or no erosion or depositional work is performed. Most work is performed during very short periods that are often recorded in the geologic record as catastrophes. These two philosophies are also familiar to the science of hydrology. Copious literature on the topic of channel formation and maintenance centers on the debate is whether frequent but small discharges are ultimately more powerful than are infrequent but large flood discharges.

We feel that the varying time-scales applied to monitoring sandbars in the Grand Canyon illustrates the two philosophies of uniformity and catastrophe by the sampling intervals employed. If one's philosophy is that sandbars are resistant to the changes imposed by upstream impoundment, then one would design a monitoring program that measures sandbars at long time steps i.e. annually or longer. This scale of reevaluation was proposed by Howard and Dolan (1979) and implemented by various investigators for nearly two decades. This philosophy assumes that sandbars have a uniform response in time and space. The response can be measured in order to determine trends in erosion and predict the ultimate fate of Grand Canyon sandbars.

Results from the investigation presented here show that sandbar size is rarely at a median value. Sandbars are ephemeral features, constantly adjusting through erosion or deposition as cyclic processes repeat several times each year. This suggests that the philosophy of catastrophe is the more conservative in an era of monitoring sandbar responses with the hope of operating dams to minimize adverse impacts. A philosophy of catastrophism applied to research and monitoring leads one to evaluate sandbars at intervals that are similar to those over which discharge fluctuates.

Recommendations

Value of the Technique

Documentation of the processes of sandbar adjustment is unique to this study. Earlier studies documented changes in size and morphology, but over temporal periods that were too long to document details. Consequently, this is the first sandbar monitoring investigation to utilize a sampling interval that closely matches the adjustment interval of the very dynamic subject. It is also the first to report the effects of dam operations and fluvial processes observed at the time-scale within which the adjustments occur.

The technology developed in this study was designed to solve a particular problem. As is true with any new technology development, it is not unexpected that the time-lapse photographic monitoring technique has certain strengths as well as limitations. In this study we have made plan area measurements of sandbars above water level. Consequently, the greatest limitation in this application is a function of inconsistent water levels at consistent time intervals. Water level is controlled by dam operations with the complexities of flow routing downstream. Because dam operations are not consistent on a daily basis, the effect is a change in the exposed areas of sandbars when monitored at consistent but very brief times.

The effect of inconsistent stage was minimized in two ways. First, by selecting images for the analysis processes that were taken during times of lower than average daily low stage (e.g. weekends). Secondly, by taking advantage of windows of constant 8,000 cfs release during the programmed aerial photography missions. However, these selection processes did not completely eliminate the effects of inconsistent stage because most weekends have unique discharge patterns resulting in unique stage levels. The stage versus exposed area relationship is not only temporally variable but also has differing spatial effects depending on sandbar geometry. Sandbars with broad, low angle areas are more affected by the same change in stage than are sandbars with steep angle shores. The elevation-area site rating system partially addresses this variability and results were presented with this variability in mind (Table 3 and Appendix A).

Stage/area limitations were encountered in previous sandbar studies that compared aerial photographs taken at different discharges (i.e. Howard and Dolan 1979; Schmidt and Graf 1990). Various compensating techniques were used. This study, using oblique photographs, has the distinct advantage of good representation of the vertical image component. Consequently, we feel that the limitations created by differing stage on exposed area can be greatly reduced. This can be achieved in subsequent analysis by surveying elevations on prominent immobile features that are visible at all stages. With this information, stage/area relationships can be developed for each sandbar.

Measurements made at stages higher than low stage can be adjusted accordingly. This technique can be applied to all prior and subsequent photographs.

The advantages far outnumber the limitations of daily time-lapse photography as a technique for monitoring changes in environmental conditions. The technique is relatively non-obtrusive in the highly sensitive wilderness setting of the Grand Canyon compared to the traditional techniques of land surveying and aerial photography. The greatest advantage is the option of short time step evaluation not available in other investigation techniques. It is remarkable the changes that became apparent when different time steps of evaluation were utilized. It was not that short time step changes did not occur before, but that there was little knowledge and no documentation of the time scales of change.

This is illustrated by the ironic progression of observations and results on sandbar dynamics. The shortest time step evaluation interval ever applied to monitor Grand Canyon sandbars (daily, this report) has documented the greatest changes in sandbar sizes and morphologies. It was results from the next shortest time step study, the bimonthly surveys (Beus and Avery 1991), that prompted the daily evaluation interval. Unexpected results from a project monitoring ground water levels in sandbars at 20-minute intervals (Carpenter and others 1991) show that some of the more dramatic changes documented with daily photography occurred in periods of time shorter than an hour. This is supported by multiple field observations (Cluer 1991; Cluer and others 1993).

Other advantages to this technique are inherent in the film recording medium itself. Virtually any object or attribute visible in an image can be measured, in temporal and/or spatial terms. Processes we have observed in the Grand Canyon images range from thermal fracturing of boulders on talus slopes to willow colonization of newly deposited sandbars. We have photographed debris fan deposition, snow at river level, ducks feeding in eddies, bighorn sheep grazing sandbars, beaver pruning willows as well as tamarisk, and collared lizards peeking into camera boxes. All of these observations are from a fraction of a second each day. One wonders what we miss the rest of the day.

Management of the Sediment Resource

Our results indicate that the reduced fluctuation range of the interim flow prescription not decrease the dynamic activity of sandbars. Erosion continued at similar rates because it occurs from the bottom of deposits through poorly understood processes of rapid erosion and bank collapse. The reduced maximum stages of the interim flows simply reduced the elevations that deposition could achieve. The general result was that the interim flows shifted sandbars to lower elevations commensurate to the stage reductions.

There are at least two approaches to managing the sediment resources along the Colorado River in Grand Canyon.

The first approach is to attempt to deposit sandbars at high elevations and ignore the subsequent erosional processes caused by dam operations. With this approach, the hope would be that benefits have longevity allowing a positive sediment balance. The second approach is to attempt to manage erosional processes so that existing sandbars or new sandbars following depositional events are optimally prolonged. We believe there is greater promise to the latter approach. It provides the opportunity to balance the sediment budget. It would also increase sediment storage over a period of years as a buffer for prolonged droughts or unexpected mainstem flood. This approach requires timely and reliable results from process studies in order to isolate and define particular dam operations that cause erosion of sandbars. Our results suggest that the elimination of weekend low discharges would prolong the time that sandbars exist at their maximum size. However, other aspects of the river ecosystem may derive benefits from the dynamic activity of sandbars. Therefore, we encourage riparian and aquatic disciplines to address this hypothesis.

Monitoring Time Scales

Results from this investigation illustrate that sandbars are cyclically dynamic over temporal scales that are considerably shorter than the traditional annual monitoring time scale. This is significant in that it suggests some reinterpretation of past investigations is needed. It also indicates that plans for future monitoring need to account for short time step dynamic activity not detectable in more traditional long time step evaluation methods. We feel that the appropriate time interval for monitoring sandbars in the Grand Canyon is daily or at least weekly. This is in deference to recent recommendations for continued annual monitoring (Patten 1993).

Acknowledgments

We wish to thank the National Park Service for funding support. We also thank Dave Wegner and others on the Glen Canyon Environmental Studies staff for direct and in kind support of this project. Peer reviews of the Draft Final Report were provided by Larry Martin and Bill Werrell, both from the National Park Service Water Resources Division, and an anonymous reviewer from the National Academy of Sciences. Their helpful comments and suggestions were incorporated in the Final Report.

The listing of specific brand names of equipment or software are in no way official endorsements of those products.

Literature Cited

- Andrews, E. D. 1991. Sediment transport in the Colorado River Basin. Pages 54-74 in *Colorado River Ecology and Dam Management: Proceedings of a Symposium, May 24-25, 1990, Santa Fe, New Mexico*. National Academy Press, Washington, D. C.
- Beus, S.S., and C.C. Avery, 1992. The influence of variable discharge regimes on Colorado River sandbars below Glen Canyon Dam. Final report. Glen Canyon Environmental Studies, Flagstaff, Arizona.
- Beus, S. S. 1992. Colorado River Investigations, Northern Arizona University, Flagstaff, Arizona.
- Budhu, M.R. 1992. Mechanisms of erosion and a model to predict seepage-driven erosion due to transient flow. Chapter 2, pages 1-75 in Beus, S. and C. Avery, editors. *The influence of variable discharge regimes on Colorado River sandbars below Glen Canyon Dam*. Final report. Glen Canyon Environmental Studies, Flagstaff, Arizona.
- Carpenter, M.C., R.L. Carruth, and B.L. Cluer, 1991. Beach erosion and deformation caused by outward flowing bank storage associated with fluctuating flows along the Colorado River in the Grand Canyon. *EOS (Trans. Am. Geophys. Union)*, v.72, p.222.
- Cluer, B.L. 1991. Catastrophic erosional events and rapid deposition of sandbars on the Colorado River, the Grand Canyon, Arizona. *EOS (Trans. Am. Geophys. Union)*, v.72, p.222.
- Cluer, B.L. 1992. Daily responses of Colorado River sand bars to releases from Glen Canyon Dam, 1990-1991: instantaneous erosion and dependent deposition. Chapter 5, pages 1-47 in Beus, S. and C. Avery, editors. *The influence of variable discharge regimes on Colorado River sandbars below Glen Canyon Dam*. Final report. Glen Canyon Environmental Studies, Flagstaff, Arizona.
- Cluer, B.L., M.C. Carpenter, L.J. Martin, M.A. Wondzell, L.R. Dexter, and M.F. Manone, 1993. Rapid erosion and slow redeposition of sand bars along the regulated Colorado River in the Grand Canyon. *EOS (Trans. Am. Geophys. Union)*, v.74, p.321.
- Committee to Review the Glen Canyon Environmental Studies. 1987. *River and Dam Management: A Review of the Bureau of Reclamation's Glen Canyon Environmental Studies*. National Academy of Science, Washington, D. C. 152 pp.

- Dawdy, D. R. 1991. Hydrology of Glen Canyon and Grand Canyon. Pages 40-53 in *Colorado River Ecology and Dam Management: Proceedings of a Symposium, May 24-25, 1990, Santa Fe, New Mexico*. National Academy Press, Washington, D. C.
- Dolan, R., A. D. Howard, and A. Gallenson. 1974. Man's impact on the Colorado River in Grand Canyon. *American Scientist* 62:393-401.
- ERDAS Inc. 1992. P.C. ERDAS V.7.5 software, users guide and technical manuals. ERDAS, Inc., Atlanta, Georgia.
- Howard, A.D. 1975. Establishment of benchmark study sites along the Colorado River in Grand Canyon National Park for monitoring of beach erosion caused by natural forces and human impact. University of Virginia Grand Canyon Study, Technical Report 1, 182p.
- Howard, A. D., and R. Dolan. 1979. Changes in the fluvial sandbars of the Colorado River in the Grand Canyon caused by Glen Canyon Dam. Pages 845-851 in *Proceedings of the First Conference on Scientific Research in the National Parks, v. 2, New Orleans, Louisiana, November 9-12, 1976*, National Park Service Transactions and Proceedings Series no. 5.
- Howard, A.D., and R. Dolan. 1981. Geomorphology of the Colorado River in the Grand Canyon. *Journal of Geology*, 89. pp. 269-298.
- Ingram, H., D. A. Tarlock, and C. R. Oggins. 1991. The law and politics of the operation of Glen Canyon Dam. Pages 10-27 in *Colorado River Ecology and Dam Management: Proceedings of a Symposium, May 24-25, 1990, Santa Fe, New Mexico*. National Academy Press, Washington, D. C.
- Kieffer, S.W. 1985. The 1983 hydraulic jump in Crystal Rapid: implications for river-running and geomorphic evolution in the Grand Canyon. *Journal of Geology*, 93(4). pp. 385-406.
- Johnson, R. R. 1991. Historic changes in vegetation along the Colorado River in Grand Canyon. Pages 178-206 in *Colorado River Ecology and Dam Management: Proceedings of a Symposium, May 24-25, 1990, Santa Fe, New Mexico*. National Academy Press, Washington, D. C.
- Patten, D.T. 1993. Long-term monitoring in Glen and Grand Canyon: response to operations of Glen Canyon Dam. Pages A1-A25 in *Operation of Glen Canyon Dam, Draft Environmental Impact Statement, Appendices*. U.S. Bureau of Reclamation.

- Schmidt, J.C. 1990. Recirculating flow and sedimentation in the Colorado River in Grand Canyon, Arizona. *Journal of Geology*, 98. pp. 704-724.
- Schmidt, J.C., and J.B. Graf. 1990. Aggradation and degradation of alluvial sand deposits, 1965 to 1986, Colorado River, Grand Canyon National Park, Arizona. U.S. Geological Survey Professional Paper 1493, 74p.
- Smillie, G.M., W.L. Jackson, and D. Tucker. 1993. Colorado River sand budget: Lees Ferry to Little Colorado River, National Park Service Technical Report NPS/NRWRD/NRTR-92/12, 11p.
- Tukey, J. W. 1977. *Exploratory Data Analysis*. Addison-Wesley Publishing Co., Reading, Massachusetts. 688p.
- Webb, R.H. in press. A century of environmental change in Grand Canyon: repeat photography of the 1889-90 Stanton expedition on the Colorado River. University of Arizona Press.
- Valdez, R. A., and R. D. Williams. 1993. Ichthyofauna of the Colorado and Green Rivers in Canyonlands National Park. Pages 2-22 in *Proceedings of the First Biennial Conference on Research in Colorado Plateau National Parks*, Flagstaff, Arizona, 22-25 July 1991. Transactions and Proceedings Series NPS/NRNAU/NRTP-93/10. U.S.N.P.S., U.S.D.I., Denver, Co.